AFIT/GCS/ENG/97D-14

A MAMMOGRAPHIC REGISTRATION METHOD BASED ON OPTICAL FLOW AND MULTIRESOLUTION COMPUTING

THESIS
Kevin A. Lee
Major, USAF

AFIT/GCS/ENG/97D-14

The views expressed in this thesis are those of the author and do not reflect the official policy or position of the Department of Defense or the United States Government.

AFIT/GCS/ENG/97D-14

A MAMMOGRAPHIC REGISTRATION METHOD BASED ON OPTICAL FLOW AND MULTIRESOLUTION COMPUTING

THESIS

Presented to the Faculty of the School of Engineering
of the Air Force Institute of Technology
Air University
In Partial Fulfillment of the
Requirements for the Degree of
Master of Science in Computer Science

Kevin A. Lee, B.S. M.S.S.M
Major, USAF

December, 1997

AFIT/GCS/ENG/97D-14

A MAMMOGRAPHIC REGISTRATION METHOD BASED ON OPTICAL FLOW AND MULTIRESOLUTION COMPUTING

Kevin A. Lee, B.S. M.S.S.M

Major, USAF

Approved:

Dr. Martin DeSimio Thesis Advisor	6 Nov 97 Date
Dr. Steven Rogers Committee Member	6 Nov 97 Date
Dr. Matthew Kabrisky Committee Member	6 NOV 97 Date
Dr. Henry Potoczny Committee Member	6 Nov. 97 Date

Acknowledgements

The last eighteen months have been a journey, sometimes perilous, often exhilarating, in pursuit of higher education. This odyssey would not have been possible—nor as meaningful—were it not for the support of many people. I am truly indebted to my wonderful wife Deana for her unbounded love, unselfish devotion, and unwaivering support throughout the arduous AFIT experience. Keeping a bustling household running smoothly was certainly as demanding and stressful, it not more, than keeping up with projects, exams, and research. Thanks for being there. You're the best! Would a cruise around the Carribean help express my gratitude? Special thanks to my little guy Eric for his understanding when Dad was too busy for that special time together we both enjoy so much.

I was very fortunate for the opportunity to learn from an all-star cast of gifted and devoted educators. I appreciate my committee members, Dr. Steve Rogers, Dr. Martin DeSimio, Dr. Matthew Kabrisky, and Dr. Henry Potoczny, and my sponsor, Maj Jeff Hoffmeister, for their enthusiasm, accessibility and sense of humor. I thank Dr. Rogers for getting me fired up about neural networks and information processing models a la biology and Dr. DeSimio for his constant encouragement and patience when I went charging off to explore something new. I'm thankful to John Keller, Randy Broussard, Lem Myers, and Amy Magnus for the many fruitful discussions and helpful comments. I'm grateful to my lab mates Fred Baier, Don Cournoyer, Ed Fitzgerald, and Brian Reid for making the many hours in front of the computer more enjoyable. Many thanks to Jill Leighner for the superb support getting me the mammograms I needed for my research. Special thanks to Larry Hutson for his self-appointed role as class social engineer. Last, but certainly not least, I would like to thank Dan Zambon and Dave Dauk for the superb computer support and their patience when I chewed up way too much disk space. Thanks one and all!

Kevin A. Lee

Table of Contents

List of Figures

List of Tables

Abstract

Breast cancer is second only to lung cancer as the most prevalent form of cancer to afflict women—remaining the leading cause of cancer death in women between the ages of 40 and 55. Mammography is a potent weapon in the fight against this lethal disease, due in large part to its widespread availability and low cost. Despite the fact that mammography can detect small lesions as early as two years before they become palpable on physical exam, between 10 and 30 percent of cancerous lesions go undetected during evaluation by the radiologist. One approach to improving detection rates involves comparing mammograms of the same breast from successive years. Since most forms of breast cancer develop slowly, multiple-view techniques might be able to detect subtle changes indicative of cancerous growth. This thesis proposes a computer-aided system designed to bring two images into correspondence, or alignment, so that they can be compared and evaluated for possible abnormalities. The system estimates a mapping between two images by calculating the optical flow, or apparent intensity change, between a source and target mammogram. The efficiency of the proposed registration system is enhanced by utilizing a multiresolution approach whereby images are compared at more than one scale. In contrast to other registration attempts which match sets of morphological features, this system does not require the identification of any control points at all. This advantage permits the system to perform well even when the two images differ significantly from one another. Preliminary results suggest the potential usefulness of this system as part of a clinical computer-aided detection (CADx) system.

A MAMMOGRAPHIC REGISTRATION METHOD BASED ON OPTICAL FLOW AND MULTIRESOLUTION COMPUTING

I. Introduction

1.1 Introduction

1.1.1 Background. According to the American Cancer Society, breast cancer is second only to lung cancer as the most prevalent form of cancer to afflict women, but remains the leading cause of cancer death in women between the ages of 40 and 55. To put this problem in perspective, this year approximately 180,000 women will be diagnosed with breast cancer, while in the same period some 44,000 more women will lose the fight against this deadly disease (60). Computer-aided detection (CADx) technologies hold great promise in the effort to improve early detection of breast cancer. This thesis explores the potential of analyzing mammograms taken at different times to identify changes which may be the harbingers of cancerous growth.

1.1.2 Problem Statement. Radiologists typically compare the current mammogram with x-ray images taken previously in hopes of detecting changes indicating possible cancerous tissue growths. Figure 1 shows a sequence of two mammograms taken at screenings two years apart. Today practitioners rely, for the most part, on visual inspection to detect possible abnormal growth patterns. Locating a region on one image corresponding to a region of interest on another image is essentially a judgment call. This subjective practice is both time consuming and error prone.

A system able to perform autonomous image-to-image matching would free the radiologist to concentrate on the most important tasks—image analysis and

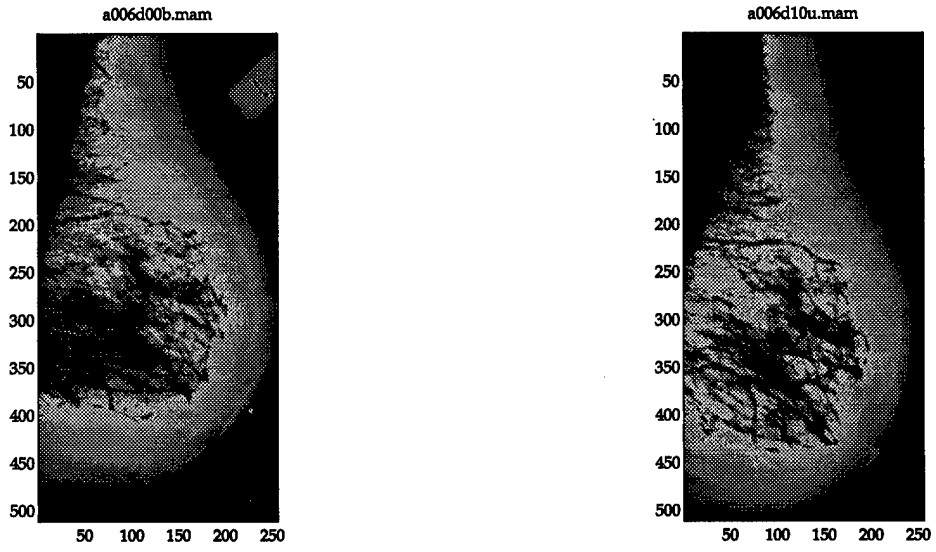

(a) (b)

Figure 1 Time sequence of mammograms. (a) Previous screening (b) current screening.

interpretation. It could suggest the best match and let the radiologist decide the acceptability of the match. The ultimate goal, of course, is to make the system smart enough to participate in the change detection process itself, improving the radiologist's ability to catch the cancer at a very early stage.

1.1.3 Scope. This thesis will develop an accurate, reliable method for registering a time series of mammograms. Although in principle any number of images can be brought into a common alignment, this thesis will concentrate on a sequence of two images. Specifically, the matching will be constrained to two images of the same breast taken at different times. The registration method will not support bi-lateral comparisons of the left and right breasts. The algorithm will be based solely on optical flow approaches.

The registration scheme will interface seamlessly with other image analysis activities. The registration procedure is not an end in itself; rather, it is merely one of many preprocessing activities. The driving force behind the development of

registration techniques is the need to detect cancer-induced tissue changes as early as possible. Comparing mammograms from the current and previous screenings has the potential to detect warning signs long before they would be discovered by single-image analysis. With this goal in mind, the registration technique should enhance post-registration mammogram analysis as much as possible.

1.1.4 Methodology. Although a series of mammograms taken from the same view (i.e. craniocaudal or mediolateral) exhibit many similarities over time, the images may also appear quite different. Certain types of distortion may be traced to the imaging equipment, while others can be attributed to the image-taking procedure itself. An example of equipment-based distortion is variation in background illumination, causing one image to appear brighter than the other. Differences in breast compression from one session to the next cause its overall shape to appear different. Although care is taken during the mammography session to ensure proper alignment of the breast, there is very little the technician can do to ensure exact positioning of the breast.

The complexity of the task makes it clear that there is no silver bullet solution. Instead, the synergistic effect of several techniques may make the solution more tractable. The method developed here is based on a series of processing stages, each trying to further constrain the problem. In particular, the method follows a coarse-to-fine approach in which global matching precedes—and indeed enables—matching at finer and finer levels of resolution. This approach mitigates the potential for the solution to be less than acceptable.

1.1.4.1 Global Alignment. The first problem encountered has to do with the orientation problem discussed above. Clearly, the two breasts in the mammograms must first be aligned to the same relative position and orientation before any serious attempt can be made to correspond regions within the breast structure. A simple and effective way to ensure optimal alignment involves identifying

an appropriate affine transformation from one image to the other. An affine transformation can be considered a parametric estimate of global, linear differences with respect to rotation, translation, and scale (25). The method proposed here solves for an optimal set of parameters using a genetic algorithm and realigns the source image to the target image based on these values.

1.1.4.2 Regional Deformation. The affine transformation carried out in the previous step does not correct nonlinear deformations such as compression and dilation. The approach taken here involves identifying the apparent motion (directional change in intensity) between the source and target images. The proposed method uses the optical flow as a measure of change between images. The inter-image velocity information is then used to deform the source image into an intermediate form more closely resembling the target image. The transformation is carried out by an appropriate interpolation function.

1.1.4.3 Local Similarity Assessment. During the registration process, a similarity measure between the transformed source image and the target image must be evaluated. In this system, a neural network approach based on the Kohonen Self-Organizing Map (SOM) is taken to develop a problem-dependent similarity metric. The network learns to segment an image by partitioning it into homogeneous regions based on the spatial distribution of image intensity values. A traditional subtraction method is also used to measure the similarity between two images.

1.1.5 Overview. The remaining chapters are organized as follows. Chapter II discusses previous and on-going work in the area of image registration. Chapter III describes the proposed mammogram registration system. Experimental results and conclusions are discussed in Chapters IV and V, respectively.

II. Background

This chapter first motivates the need for registering mammograms from a health care perspective. It then discusses several technical aspects of image processing relevant to the registration problem. Finally, the major issues involved in registration are discussed, highlighting key research in each area.

2.1 Breast Cancer

Breast cancer is second only to lung cancer as the leading form of cancer to strike women (63). While mammography has proven to be a highly effective tool in the early detection of breast cancer, between 10 and 30 percent of cases diagnosed as cancer had negative mammogram interpretations.

2.2 Computer-Aided Diagnosis (CADx)

Considerable effort is being devoted to the development of automated systems capable of assisting the radiologist in mammogram analysis and interpretation (50, 37, 61). A typical CADx system uses sophisticated image processing techniques to detect either microcalcifications or masses which might otherwise go unnoticed. It is important to note that these computer-based systems are designed to assist—not replace—the trained radiologist.

Due to the complexity of mammogram interpretation, radiologists base their decisions on all available information. In practice, this means comparing all four views (craniocaudal and mediolateral oblique for each breast) from the current screening and prior screenings. Since most forms of breast cancer develop slowly, comparison of mammograms taken at different times can provide evidence of a growth not previously detected (40, 77).

Although most CADx implementations currently under development or in clinical test are limited to single image analysis, attempts are underway to develop

multi-view capable systems (50). Dinten et al. (18) propose a system which combines analysis from single mammograms with a bilateral comparison between left and right mammograms. The primary stumbling stock to the development of these CADx systems is the need to register two images before they can be compared and analyzed. The variation between two same-breast mammograms taken at different times can be enormous, rendering the registration task impractical. For example, differences in breast positioning and compression can result in appreciable distortion. Until these complications have been resolved, progress in multi-view CADx system development will remain slow.

2.3 Image Processing Methods

Image processing is often divided into three stages: preprocessing, feature extraction, and classification (59). Preprocessing consists of low-level techniques designed to transform the input data into a form useful to the other stages. Feature extraction identifies and isolates characteristics (patterns) in the preprocessed data based on semantic merit. Finally, extracted features are combined and manipulated so that the original problem can be solved. The following subsections examine some representative image processing methods most important to solving the registration problem.

2.3.1 Noise Reduction. The useful information conveyed by images is partially degraded by unwanted signals in the form of noise. Origins of noise include the image capturing device (e.g. mammography unit), the subsequent film development process, and the digitization of this film for computer analysis. The presence of noise may corrupt the image and lessen the radiologist's ability to detect an abnormality in the mammogram (39).

Noise reduction is most often achieved by smoothing the image with one or more filters (28). Although Gaussian filters have found wide support in the image

analysis community, they have the undesirable property of smoothing over discontinuous as well as continuous areas, possibly removing valuable boundary information in the process (2). Saint-Marc et al. propose an adaptive smoothing technique designed to retain the benefits of Gaussian smoothing while preserving discontinuities (60).

2.3.2 Image Segmentation. Segmentation refers to the process of partitioning an image into homogeneous regions based on texture, intensity, or any other problem-dependent measure. Techniques for segmenting an image can be grouped into three general classes: edge detection, thresholding, and region growing (25). An important application of this technique involves extracting the breast structure from the background image (5, 13, 34, 48, 53, 69).

2.4 Registration Methods

Registration is the process of establishing the best possible correspondence between two objects—images in this case. Brown provides an exhaustive survey of registration techniques and offers an excellent taxonomy for making sense of the many approaches available (9). The following discussion on registration methods and characteristics will follow Brown's organizational framework.

2.4.1 Correlation. Correlation-based, sometimes called block matching, techniques attempt to register two images using similarity measures. As Brown points out, correlation matching is more a similarity metric than a registration method unto its own. Combined with template matching, cross-correlation can provide a useful measure of how well a region in the source image spatially matches a region in the target image. In the standard block matching method given by

$$E(\{u_i, v_i\}) = \sum_{p \in R} \|I(p, t_1) - I(p + d, t_2)\|^2 \quad (1)$$

the error $E(\{u_i, v_i\})$ is minimized over a small image region where $\{u_i, v_i\}$ represents the optimum displacement vector (25).

Correlation is particularly useful when spatial structure remains relatively constant between two images. For example, two different aerial photographs taken of the same land area fit this criterion. A translational shift in one image relative to the other will have no effect on the structure of a given region. However, a relative difference in scale between the two images will introduce considerable noise (error) into the correlation measurement. Caves (12) demonstrates the effectiveness of template matching in registering two land mass images taken by Synthetic Aperture Radar (SAR).

2.4.2 Fourier Methods. Whereas correlation is based on spatial characteristics, Fourier methods operate in the frequency domain. Calway (11) presents a multiresolution Fourier Analysis approach to the problem of estimating disparity and motion in image registration. This method is appropriate if the frequency components of the image correspond to the actual disparity.

2.4.3 Point Mapping. Mapping a set of points in a source image to its counterpart in a target image is a very powerful registration method if stable correspondence points can be extracted from each image (54). However, significant variations between the two images can make these fiducial markers, or control points, very difficult to identify.

This approach has recently been applied to the registration of two mammograms with considerable success (72). It should be noted that the images presented in (72) have easily identifiable fiducial markers—an exception rather than the rule for most mammogram comparisons. Bookstein (8) has shown how this point-to-point mapping can be decomposed into its constituent linear and nonlinear components. This type of analysis is useful in understanding the displacement forces responsible for transforming one image into the other.

2.4.4 Deformable Models. Deformable models are attracting considerable attention in many areas of image processing and computer analysis. Durbin (20) demonstrated the power of elastic nets by finding a good solution to the NP-complete Traveling Salesman Problem. Also known as snakes, elastic nets, and active contour models, these versatile tools offer a fresh perspective to long-standing challenges such as scene segmentation, boundary extraction, and image registration. Many of the approaches under investigation can trace their roots to the snake model developed by Kass et al. (36). These investigators used this one-dimensional deformable model to seek out curves in images. The snake is really a spline which reaches its desired configuration by minimizing a three-component energy function:

$$E_{snake} = \int_0^1 E_{snake}(v(s))ds = \int_0^1 E_{int}(v(s)) + E_{image}(v(s)) + E_{con}(v(s))ds \qquad (2)$$

The first component, the internal energy term, represents the energy stored in the deformable model due to bending. The second term, the external energy, corresponds to image features. The third component of the energy function allow the user to add additional constraints to the solution.

A number of investigators have applied deformable models to difficult problems in medical image analysis. Lobregt et al. (45) use an active contour model to locate arteries in vascular x-ray images and tumors in MR images. Ranganath (55), Cohen et al (14), and Coppini et al. (15) apply similar approaches to the automatic extraction of left ventricle boundaries from cardiac imagery. Yue et al. (75) detect rib borders with a snake. A deformable surface model is used by Sandor et al. to match MR brain images with a brain atlas. Davatzikos and Prince (16) developed a technique for mapping the outer cortex in brain images using deformable ribbons.

2.5 Registration Considerations

2.5.1 Feature Selection. The image features selected to guide the registration process can dramatically affect the final outcome. Simply stated, features which represent the image well should produce a more accurate registration result than features less representative of the images. Features can be categorized as either structural and statistical in nature. Structural features represent morphological aspects of the image, such as edges and landmarks. Statistical features, on the other hand, capture textural properties of the image in the form of intensity variance, moments, etc. Structural features are sometimes called intrinsic features because they are derived directly from the image.

2.5.2 Similarity Measure. Closely related to feature selection is the decision of how to measure the similarity between two images. Anandan (1) uses a simple sum of squared difference (SSD) measure, given by the equation

$$E(\{u_i, v_i\}) = \sum_t [I_1(x_i + u_i, y_i + v_i) - I_0(x_i, y_i)]^2 \tag{3}$$

to measure the difference between two image frames. This optimization equation can be readily solved by a least squares or other iterative numerical method.

Rogowska (56) uses the normalized cross-correlation equation

$$NCOR_{ij} = \frac{(A_{ij} - \mu_{Aij}) \bullet (R - \mu_R)}{\sqrt{[(A_{ij} - \mu_{Aij}) \bullet (A_{ij} - \mu_{Aij})][(R - \mu_R) \bullet (R - \mu_R)]}} \tag{4}$$

to perform a type of dynamic image analysis called similarity mapping between two consecutive frames of a dynamic MRI temporal sequence. The author presents evidence that this technique can identify different image structures having clinical interest.

2.5.3 Search Models. Having selected a set of features and similarity measure, a search strategy appropriate to the type of registration problem must be identified. Specifically, the a transformation model appropriate to the registration problem at hand must be selected. The model should match the expected transformation as closely as possible. Transformation models typically used by registration procedures are fall into one of four families: rigid, affine, projective, or curved (70).

2.5.3.1 Affine Transformations. The simplest types of transformations are affine. An affine transformation is restricted to changes resulting from translation, rotation, and shear. Therefore, lines parallel before the transformation will remain parallel in the transformed image. The parametric affine model defined mathematically by

$$u(x,y;a) = \begin{bmatrix} s_x cos\theta_x & -s_y sin\theta_y \\ s_x sin\theta_x & s_y cos\theta_y \end{bmatrix} \begin{bmatrix} x \\ y \end{bmatrix} + \begin{bmatrix} d_x \\ d_y \end{bmatrix} \quad (5)$$

will transform each point in the source image to its corresponding location in the target image. Fuh (25) use an affine model to estimate the velocity field between two frames of an aerial image sequence.

2.5.4 Search Strategy. The final component to make the registration system complete is the search strategy. This decision is critical because it will decide important issues such as registration accuracy and computational resource requirements.

2.5.4.1 Algorithm-based. Many traditional search strategies are based on well-defined algorithms. If the registration problem can be subdivided into smaller and smaller subproblems, the matching problem may be amenable to a dynamic programming approach. However, the exhaustive nature of dynamic programming

algorithms can cause computation time and resource requirements to become prohibitive.

2.5.4.2 Relaxation-based. Several researchers have developed optimization approaches to solve the registration problem. Relaxation methods are typically used to propagate local information throughout the system, enabling a more accurate global solution. In general, these methods search for an optimal solution by minimizing an objective energy function. Comprehensive discussions on relaxation techniques and their application to image processing can be found in (32, 57, 58).

2.5.4.3 Deterministic Relaxation. Numerical analysis theory offers a number of techniques to solve optimization problems through deterministic relaxation (47). Iterative methods, such as the Jacobi, Gauss-Seidel, and simultaneous over-relaxation (SOR) variants, gradually converge to a stable minimum (under the appropriate conditions). Recently, the Hopfield network has been used to perform the optimization task (13, 17, 32, 41, 43, 53, 54, 68, 78). The Hopfield network is a fully-connected single-layer neural network which can minimize a cost function representing the problem at hand. This architecture lends itself to parallel computer implementations.

2.5.4.4 Stochastic Relaxation. Complementing deterministic relaxation techniques are those based on stochastic processes (24, 26, 49, 69). Geman and Geman (26) demonstrate how image restoration problems can be addressed with a probabilistic relaxation technique called simulated annealing. This approach can avoid local minima by allowing states to be accepted that actually increase the system's energy. The probability that such an energy-increasing state will be tolerated is determined by an annealing schedule. Initially set to a high value, the acceptance probability (based on a Gibbs distribution) is gradually lowered until finally only energy-decreasing states are allowed. Although very effective at reaching an opti-

mal global minimum, simulated annealing methods generally suffer from very slow convergence rates compared to other deterministic relaxation methods.

2.5.4.5 Genetic Algorithms. Genetic algorithms offer a biologically-motivated alternative to traditional search approaches. Patterned after DNA replication in living creatures, genetic algorithms conduct global searches with the help of mutation and crossover of chromosomes (27, 30). These artificial chromosomes represent partial solutions to the larger problem to be solved. Over the course of several generations, these building blocks are combined so as to evolve an optimal solution. Genetic algorithms thrive on search spaces too messy to be solved by more structured search strategies.

2.6 Optical Flow

The analysis of image sequences requires an understanding of how they differ from one another. In the context of image registration, we wish to map a set of features in the source image to the corresponding set of features in the target image. These features can be intrinsic image structures like contours, or they can be statistical measures such as contrast, moments, etc. Although several techniques exist to estimate this interimage mapping, one approach which has proven extremely useful is based on the estimation of optical flow. Luettgen et al. define optical flow as the "apparent velocity vector field corresponding to the observed motion of brightness patterns in successive image frames" (46).

Barron et al. (3) provide a comprehensive survey of optical flow approaches and assess nine of the most popular methods in use today. The authors place optical flow estimation techniques into four categories: differential, region-based matching, energy-based, and phase-based. Differential methods use spatio-temporal derivatives to estimate a dense velocity field relating the source image to the target image. Region-based techniques, on the other hand, rely on similarity measures between

features in the image sequence to derive a sparse optical flow field. The third category, energy-based optical flow techniques, apply velocity-tuned filters to produce a flow estimate. In a similar vein, phase-based techniques use the outputs of band-pass filters to derive the flow estimate.

2.6.1 Horn and Schunck Method. In many types of image matching, this set of consistent features is difficult, if not impossible, to identify. Horn and Schunck (31) established the basis for the development of homogeneous differential optical flow methods based on image gradient information. Their method is predicated on the brightness constancy equation

$$\frac{dE}{dt} = E_x u + E_y v + E_t = 0 \tag{6}$$

where

$$E_x = \frac{\partial E(x,y,t)}{\partial x}, E_y = \frac{\partial E(x,y,t)}{\partial y}, E_t = \frac{\partial E(x,y,t)}{\partial t} \tag{7}$$

represent the image spatial and temporal intensity derivatives and

$$(u, v) = (dx/dt, dy/dt) \tag{8}$$

denotes the derived optical flow. The brightness constraint assumes that "changes in image brightness are due only to motion in the image frame" (46).

This single linear equation in two unknowns results in an ill-posed problem, requiring more information for an acceptable solution (4). An ill-posed problem denotes a solution that is in general neither unique nor stable (76). One well-established technique to condition this type of underconstrained problem is to add a regularization term. Poggio et al. (52) describe how regularization techniques can be used to tame a variety of difficult problems, including optical flow calculations. The

regularization term is not constrained to assume a particular form; it simply needs to add sufficient information to make the problem well-posed. Horn and Schunck (31) attack the problem by incorporating a smoothness constraint, resulting in a minimization problem of the form

$$\Phi = \int\int_{Image} (E_x u + E_y v + E_t)^2 + \alpha^2 (u_x^2 + u_y^2 + v_x^2 + v_y^2) dx dy \tag{9}$$

where α represents the regularization parameter (smoothness, in this case).

This quadratic variational functional can be recast into a set of Euler-Lagrange equations of the form

$$(E_x u + E_y v + E_t) E_x = \alpha^2 \Delta u (E_x u + E_y v + E_t) E_y = \alpha^2 \Delta v \tag{10}$$

2.6.2 Alternative Methods. Several researchers have proposed modifications to the basic Horn and Schunck framework in an attempt to improve accuracy of the optical flow calculation. Black et al. (6, 7) propose a robust estimation framework designed to minimize the negative effect of violations to the basic assumptions—brightness constancy and spatial smoothness. Specifically, they incorporate ρ-functions, such as the Lorentzian and Geman-McClure variants, to attenuate the influence of outlying measurements on the solution. Optical flow is then estimated by minimizing the objective function

$$\sum_x \left[\lambda_D \rho((\nabla I(x) u(x) + I_t(x)), \sigma_D) + \frac{\lambda_S}{|\mathcal{G}(x)|} \sum_{z \in \mathcal{G}(x)} \rho(\|u(x) - u(z)\|, \sigma_S) \right] \tag{11}$$

The first term enforces fidelity to image intensity values as determined by the control parameter σ_D, while the second term regulates smoothness as determined by another control parameter σ_S and serves as the regularization parameter.

Fleet (23) uses local phase information to calculate optical flow, while Fuh (25) extracts regional optical flow estimates from the observed affine transformation in each region. Nagel and Enkelmann provide an excellent discussion on the role of smoothness constraints in optical flow formulations (51). Fan et al. (22) describe an image motion estimation method based on the Expectation-Maximization (EM) technique and affine transformations. Verri (71) also gives a good discussion on motion fields and optical flow computation. Zhang and Hanauer (76) apply the concepts of mean field theory to address the optical flow problem.

2.7 Multiscale Methods

The notion of multiresolution image analysis is not new. Research efforts into new analysis approaches integrating information generated on more than one scale have been reported since the mid 1970's (58). Burt (10) introduced the idea of a Laplacian pyramid to create a compact image code. Although he developed this technique to improve data transmission performance, this multiscale analysis tool has found application in the image analysis realm and has been applied to hyperspectral image data fusion (73). The Gaussian kernel is generally preferred because "it is the only kernel that leads to monotonic destruction of detail under repeated blurring...no new details will appear at a given scale s that did not exist at smaller scales" (44). Repeated blurring of the source image defines a continuously-generated family of images referred to as scale space.

Multiscale methods offer levels of analysis and manipulation not generally available using single-scale methods. Specifically, they employ coarse-to-fine strategies which decompose an image (or sequence of images) into more than one level of resolution. This method is extremely useful in image registration because motion,

or intensity change between two images, will often be present to different degrees. In other words, there might be rapid change at the breast edge along with much smaller local change from region to region. Simple optical flow methods (e.g. Horn and Schunck) assume a linear intensity change within the measurement area, but this assumption is often violated.

Multiscale methods address this well-known "aperture problem" by looking at the problem from different levels of resolution. Using this approach, small intensity changes can be investigated at fine levels while larger intensity changes can be explored at an appropriate level of resolution. For the purpose of optical flow calculations, we look for the level at which a given intensity change is linear. This hierarchical decomposition ensures that all degrees of motion are analyzed at the level appropriate to their magnitude.

Several investigators have developed optical flow estimation methods based on this multiresolution approach (4, 21, 33, 62, 65, 66, 64, 67, 74). Szeliski et al. (65, 66, 64) base their methods on a hierarchical family of splines. Battiti et al. (4) address the shortcomings of homogeneous differential methods (e.g. Horn and Schunck) by estimating the relative error associated with each optical flow calculation. An optical flow measurement with error exceeding a specified threshold will be recalculated at the next finer level, while those below the threshold (high confidence estimates) are retained. In a similar vein, Enkelmann (21) and Hwang (33) also estimate the relative error; their approach incorporates the error estimate directly into the next calculation iteration. Hwang and Lee (33) apply multigrid techniques to their multiresolution pyramid with excellent results. Luettgen et al (46) develop a multiscale regularization approach for robust optical flow estimation. The performance of such multiresolution frameworks can be dramatically improved by incorporating true multigrid algorithms that make explicit use of interlevel residual errors to speed up the relaxation process. Douglas and Terzopoulos (19, 67) present a comprehensive discussion of multigrid techniques for improving convergence rates.

2.8 Summary

Mammography has proven to be a powerful tool in the fight against breast cancer. When interpreting mammograms, radiologists normally compare the current mammogram set with those taken previously. Researchers are actively developing computer-aided detection (CADx) systems capable of helping the radiologist make more informed decisions. Much of today's CADx research, however, still focuses on the analysis of one image at a time. Although single-view analysis is extremely important, a sequence of mammograms contains information about the growth of cancer over time. Since most types of breast cancers grow slowly, the simultaneous analysis of mammograms spanning more than one year may significantly improve the detection of cancers too difficult to identify on a single image.

A key technology in multiple-image processing is registration—matching locations on one image with the corresponding locations on the other. The significant differences typically encountered between two images often make registration very difficult. In the case of mammography, it's a non-linear problem requiring a non-linear solution. Using optical flow techniques to estimate the disparity between two images and facilitate registration is not a new idea. However, these powerful techniques have not as yet been applied to the registration of mammograms. Optical flow techniques offer a potentially powerful approach to this complex problem. This thesis develops a registration method based on optical flow and explores both the advantages and disadvantages of this approach.

III. Methodology

This chapter describes the proposed mammogram registration system.

3.1 System Overview

The mammogram registration system developed in this thesis consists of several modules each designed to perform a specific function. It relies on both analytical techniques, such as iterative relaxation, where appropriate, and appeals to biologically-motivated methods, such as genetic algorithms and neural networks, where they outperform the traditional approaches. It is based on a multiresolution hierarchy to facilitate analysis at more than one scale. This approach enables the system to deal with registration and tumor detection at the most appropriate level(s) of resolution. From a philosophical standpoint, this system is designed to be an integrated approach to both mammogram registration and tumor detection. Specifically, the proposed system uses velocity field estimates between two images to simultaneously bring two images into correspondence and identify potential tumor growth areas. Figure 2 gives a bird's-eye view of the entire registration system. Figure 3 displays a time series of four mammograms for the same woman taken during different screenings. The registration system must align these images to help the radiologist compare corresponding regions in hopes of detecting a growth if one is present.

The preprocessing module is responsible for low-level data manipulation to ensure both images are as similar as possible. The global alignment module reduces differences in position and orientation prior to estimating intensity differences between two images. The segmentation module extracts each breast structure from the background to help define for the system what to register and what to ignore. The multiscale pyramid generator decomposes each image into a specified number of scales. The number of levels is not fixed and can be adjusted to meet the current

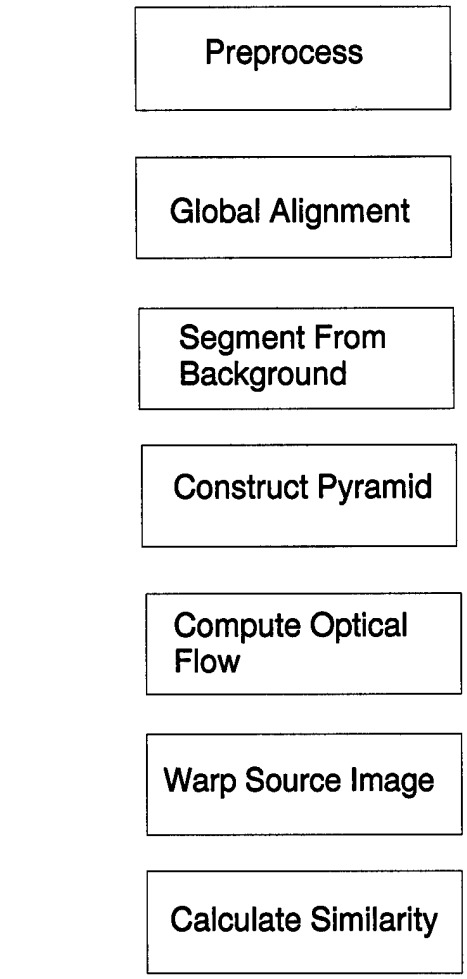

Figure 2 Proposed mammogram registration system.

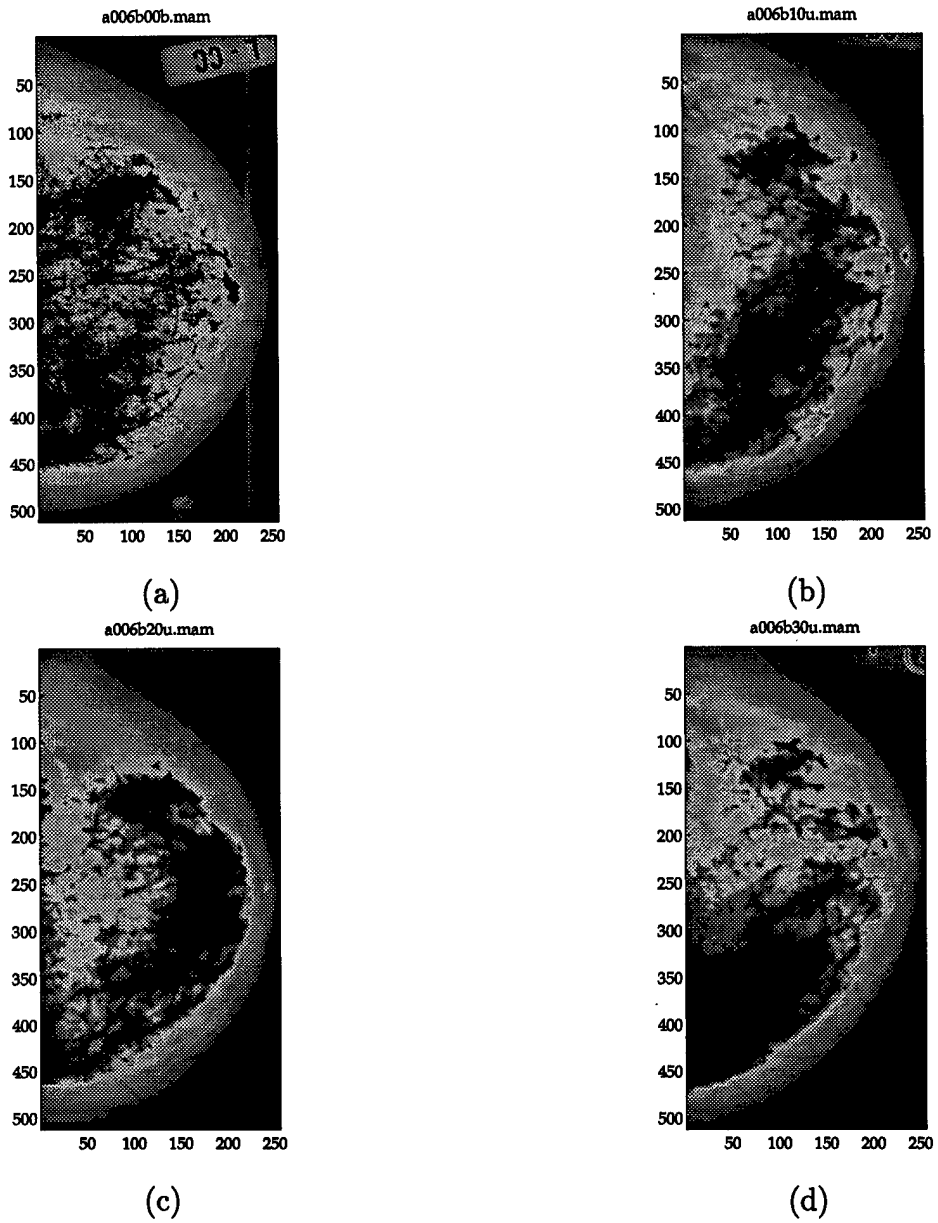

Figure 3 Time sequence of mammograms taken during four consecutive screenings. (a) First screening (b) second screening (c) third screening (d) last screening.

need. The heart of the registration system is the optical flow computation module. This module estimates the apparent difference between the two images being registered. The warping module takes the output from the optical flow computation module and generates a warped image based on the apparent motion from source to target image. Finally, the evaluator module measures the similarity between the warped image and target image and decides whether the sequence must be repeated. The similarity maps generate can be used to evaluate the possibility of abnormal growth in the second mammogram.

3.2 Preprocessing

3.2.1 Noise Reduction. Noise due to film granularity and introduced by the digitization process will always be present in mammogram images. Median filtering has been shown to be an effective tool in removing this type of noise. In this system, images are filtered using a median filter with a 5 x 5 kernel.

3.2.2 Normalization. The first problem encountered by any image registration process is the variety of differences which may be present in the images. Global differences such as background illumination, unequal intensity ranges, and variable contrast can impair the registration process significantly. To minimize the effect of theses factors, the images are first quantized such that all intensity values fall in the range 0 to 255.

3.3 Global Alignment

Although care is taken during the mammography session to ensure proper positioning of the breast, there is very little that can be done to establish the same same alignment between two different mammograms. The registration system will simply have to be prepared to deal with this problem in the course of the alignment procedure.

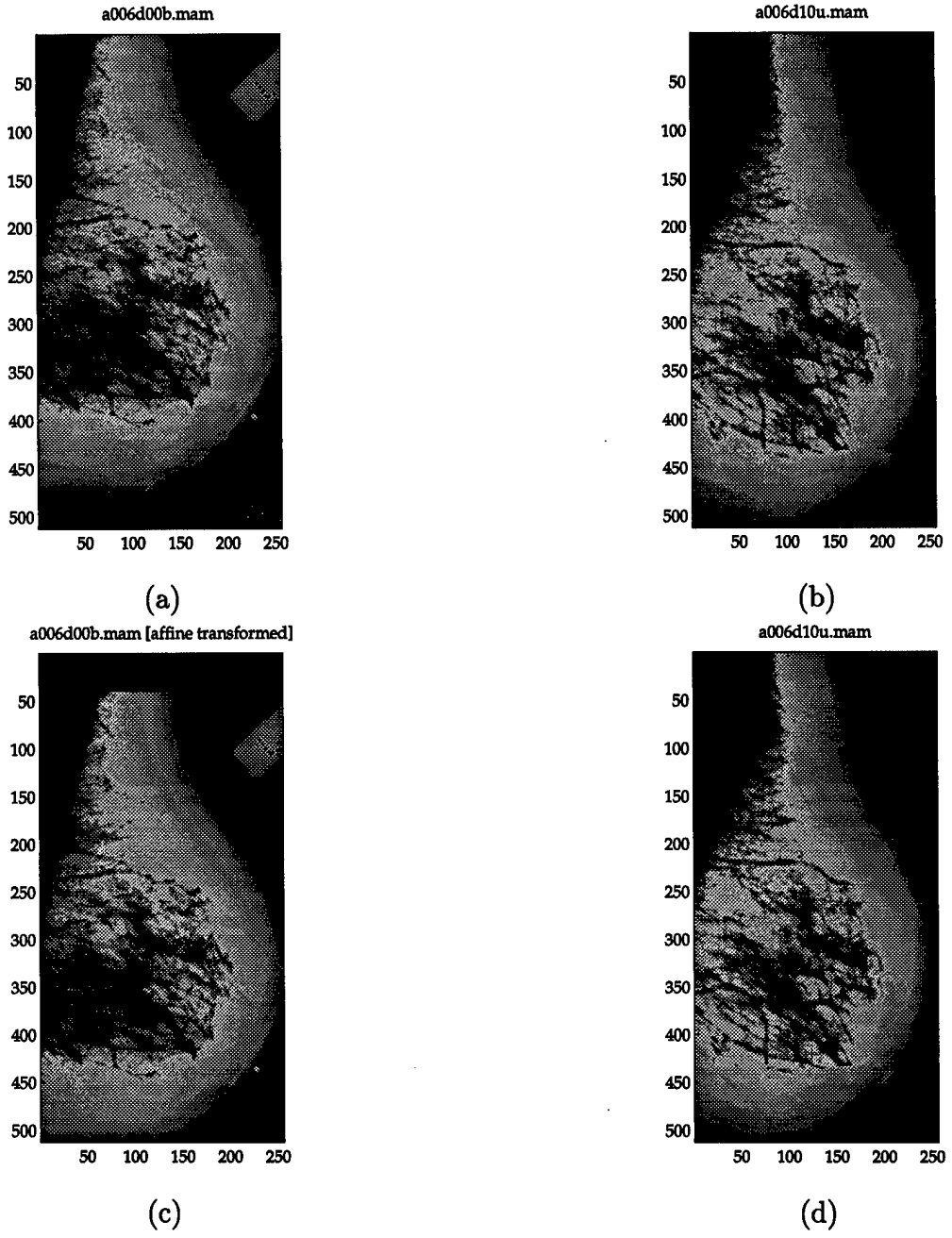

Figure 4 Mammograms of the same breast taken one year apart. Global alignment differences are resolved by applying an affine transformation to the image in the upper left panel. (a) Previous screening (b) Current screening (c) first image after affine adjustment (d) second image unaltered

The images in Figure 4 are mammograms taken of the same breast in two different years. Although they show the same structural features, the breast on the right (b) is positioned lower relative to the breast on the left and is possibly enlarged. It is clear that the two images must be more closely aligned before attempting to correct regional deformations (e.g. compression and expansion due to differences in patient positioning pressure applied by the imaging equipment) .

3.3.1 Key Factors. Analytical techniques, such as least squares fitting, offer one approach to resolving alignment differences (50). Although these methods can perform quite well under most circumstances, they can generate unacceptable solutions if the differences between the two images are too great. They are especially sensitive to outlier measurements—those falling far outside the acceptable range of values. However, it is exactly these types of "messy" situations on which evolutionary approaches thrive. As described in the previous chapter, genetic algorithms excel at searching through landscapes where rules are few and far between (27, 30).

The approach taken here is to model global (mis)alignment as an affine transformation problem. The rationale for this decision is straightforward: attempting to resolve differences due to distortion cannot be done in a meaningful way if the images suffer from translational, rotational, and scale differences. Once these linear differences have been resolved, the nonlinear distortions become manageable.

3.3.2 Implementation. The global alignment subsystem uses a genetic algorithm to search for an optimal set of transformation parameters. The parameters required to specify the affine transformation

$$u(x,y;a) = \begin{bmatrix} s_x cos\theta_x & -s_y sin\theta_y \\ s_x sin\theta_x & s_y cos\theta_y \end{bmatrix} \begin{bmatrix} x \\ y \end{bmatrix} + \begin{bmatrix} d_x \\ d_y \end{bmatrix} \tag{12}$$

determine the transformation are $s_x, s_y, \theta_x, \theta_y, d_x$ and d_y. The four parameters of the rotation matrix, $s_x, s_y, \theta_x, \theta_y$, specify the amount of rotation and scaling that

will be applied, while the d_x and d_y terms represent the amount of translation along the x and y axes, respectively, required.

A family of 25 chromosomes, each encoding the six affine parameters, are allowed to evolve using crossover and mutation operators. At the end of each generation, the genetic algorithm evaluates the fitness of each chromosome using a sum-of-squared difference (SSD) function. Specifically, the parameters from each chromosome are used to create a new image, and the calculated SSD between this image and the target image determine the chromosome's fitness. By minimizing this simple SSD function, the genetic algorithm converges to a specified error goal in less than 20 generations (in most cases). Table 1 details how the affine parameters are encoded in each chromosome, and Table 2 summarizes the genetic algorithm parameters execution used by the alignment module.

Genetic Algorithm Chromosome String		
Parameter	Bits	Description
d_x	5	Translation in Vertical Direction
d_y	5	Translation in Horizontal Direction
s_x	4	Scaling Ratio for Vertical Direction
s_y	4	Scaling Ratio for Horizontal Direction
θ_x	4	Rotation Angle X
θ_y	4	Rotation Angle Y

Table 1 The six affine parameters encoded as genes in each chromosome.

Genetic Algorithm Parameters	
Parameter	Value
Chromosome Length (bits)	26
Population Size	25
Mutation Rate	0.25
Crossover Rate	0.9

Table 2 Genetic algorithm execution parameters.

3.4 Multiscale Decomposition

This registration system relies on a hierarchy of images to achieve the most accurate registration result while minimizing the overall processing requirement. Since intensity differences between image segments can be substantial, more than one level will generally be required. The general rule of thumb states that the interframe velocity should not exceed one pixel per frame for an accurate optical flow measurement (10). This system allows a maximum of six levels, depending upon the degree of variation between the two images. Figure 5 depicts the basic pyramid structure.

The higher levels are all created by smoothing and decimation operations. To obtain a new image at level $k+1$, the image at level k is convolved with the 2-D Gaussian smoothing operator over a 3 x 3 window using the equation

$$I(x,y) = \frac{1}{N} \sum_{i=-1}^{+1} \sum_{j=-1}^{+1} I(x+i, y+j) e^{\frac{-(x^2+y^2)}{2\sigma^2}} \tag{13}$$

where

$$N = \sum_{i=-1}^{+1} \sum_{j=-1}^{+1} I(x+i, y+j) \tag{14}$$

and σ is a scale constant. The smoothed image is then decimated by a factor of two in each dimension, resulting in an image having one fourth the area of the image one level below. Figures 6 and 7 depict a five-tier pyramid generated from the example source and target images, respectively. Each level is magnified to full base size for ease of viewing. The axes show the actual dimensions of each frame.

The full power of a hierarchical representation can be appreciated if we view it as the corresponding Laplacian pyramid. Burt (10) developed the Laplacian pyramid scheme to improve the transmission speed of images. We can convert the Gaussian pyramid described above to its Laplacian counterpart by recursively subtracting from

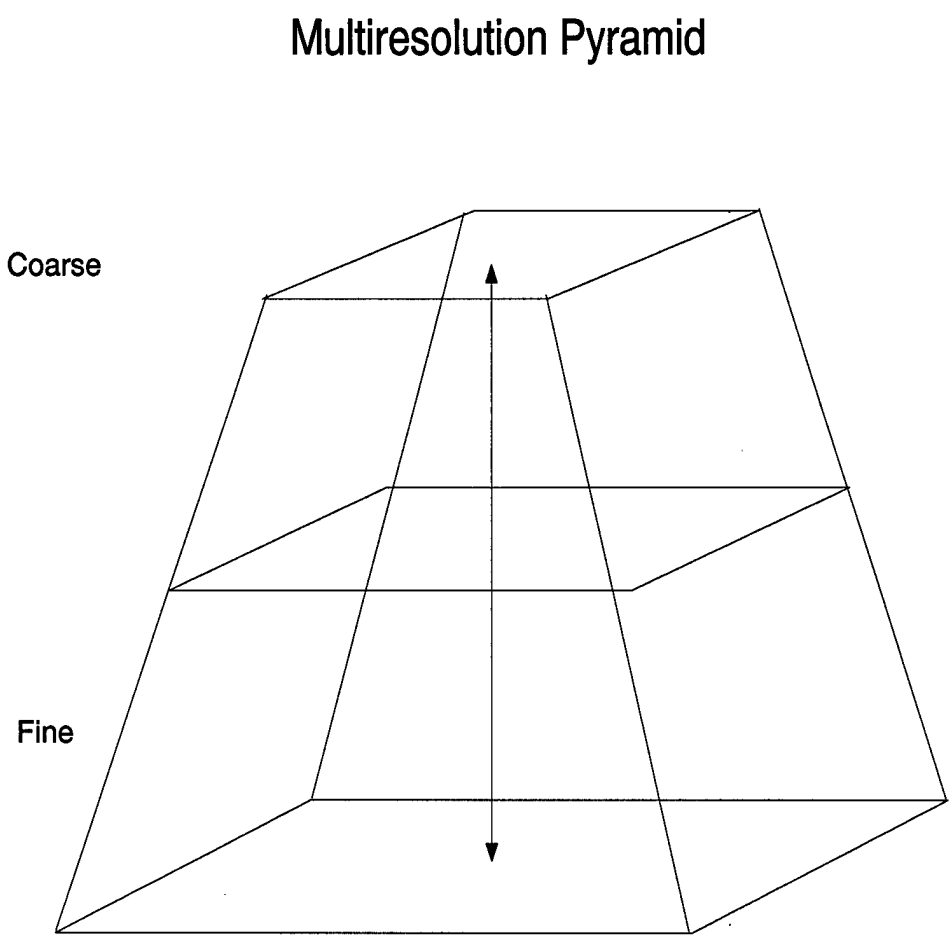

Figure 5 Basic multiresolution pyramid architecture. Levels two and three are created by smoothing and decimating by a factor of two the level below them.

the Gaussian image at level k from the one on the level $k+1$. Figures 8 and 9 show the Laplacian pyramids corresponding to the Gaussian pyramids in Figures 6 and 7, respectively.

Projection operators are needed to transform pixel values to the appropriate values on adjacent levels. This system uses the averaging operator

$$P_k^{k+1} = \frac{1}{16} \begin{bmatrix} 1 & 2 & 1 \\ 2 & 4 & 2 \\ 1 & 2 & 1 \end{bmatrix} \tag{15}$$

and interpolation operator

$$P_{k+1}^{k} = \frac{1}{4} \begin{bmatrix} 1 & 2 & 1 \\ 2 & 4 & 2 \\ 1 & 2 & 1 \end{bmatrix} \tag{16}$$

employed by Hwang and Lee (33) in their three-tier Gaussian pyramid implementation.

3.5 Segmentation

After the two images have been brought into coarse alignment by minimizing the translational, rotational, and scale differences between them and the multiresolution pyramid has been constructed, it useful to segment the images. In this system, two types of segmentation are implemented: breast structure extraction and internal structure partitioning. The first procedure extracts the region of the image belonging to the breast image away from the surrounding background. This step ensures that later processing stages are matching breast tissue rather than attempting to match pixels belonging to the background region.

3.5.1 Rationale. As discussed in Chapter II, the three most common segmentation philosophies are based on either edge detection, region growing or thresholding techniques. The method selected for this system belongs to the second group of methods because it segments the image by clustering similar pixels into homogeneous partitions. Since the segmentation activity should operate without the need for outside intervention, an unsupervised method would seem like the best choice. The Kohonen self-organizing feature map (SOM) is a neural network based on unsupervised learning (38). The SOM uses vector quantization to discover patterns in the input data. The Kohonen SOM is unique among neural networks in that it creates a topographical map of the input space. In other words, patterns close together in the input space will remain close to one another in the feature map as well. The SOM map has many of the same characteristics of maps found in biological information processing systems.

This thesis extends the previous method by introducing a multiresolution component. Each image is transformed into a deck of images smoothed by a different Gaussian scale factor. The pattern vector associated with a given image pixel consists of elements representing the pixel intensity at each scale.

Kohonen Extraction Network	
Parameter	Value
Pattern Vector Length (pixels)	25
Competitive Layer Nodes	2
Iterations	10000
Update Mode	Batch

Table 3 Kohonen extraction network parameters.

3.5.2 Breast Extraction. Lee (42) demonstrated how a Kohonen self-organizing feature map (SOM) can effectively partition a mammogram using a competitive learning paradigm. First, a preprocessing stage extracts small pixel neighborhoods by sliding a 5 x 5 window in raster fashion from left to right, top to bottom. These neighbor pixel regions are small enough to characterize homogeneous areas,

Kohonen Segmentation Network	
Parameter	Value
Pattern Vector Length (pixels)	5
Competitive Layer Nodes	25
Iterations	10000
Update Mode	Batch

Table 4 Kohonen segmentation network parameters.

yet large enough to ensure the data is statistically valid. Figure 10 demonstrates the extraction capability of this segmentation technique. Each of the two nodes in the competitive layer of the network encode either is-breast or is-background based on the neighbor intensity values.

3.5.3 Breast Segmentation. This thesis proposes a novel technique for segmenting the internal structure of mammogram images. As with the breast extraction procedure described above, this method also uses a Kohonen neural network. This method, however, differs from the other in that it uses information from the multiresolution pyramid generated in the previous processing step. Specifically, an n-level image deck is created in which each level is smoothed using a successively larger scale parameter (typically following a geometric progression). Then an n-dimensional feature vector composed of pixel values from each level is defined for each pixel in the original image. Since each successive Gaussian image is a low-pass version of the image below it, pixel values at coarser levels will be more resistant to noise than those on lower levels. A segmentation based on multiple pixel values should in principle produce a partition that identifies more or less homogeneous regions in the image: the addition of more levels to the image deck will increase the smoothness of the partitioning. Figure 11 shows the example source and target images after segmentation by the Kohonen neural segmentation procedure. Figures 12 through 16 compare the performance of the proposed Kohonen-based segmenter with the well-known fuzzy c-means clustering algorithm using successively more pyramid levels. Fuzzy c-means clustering is described in detail in (29, 35).

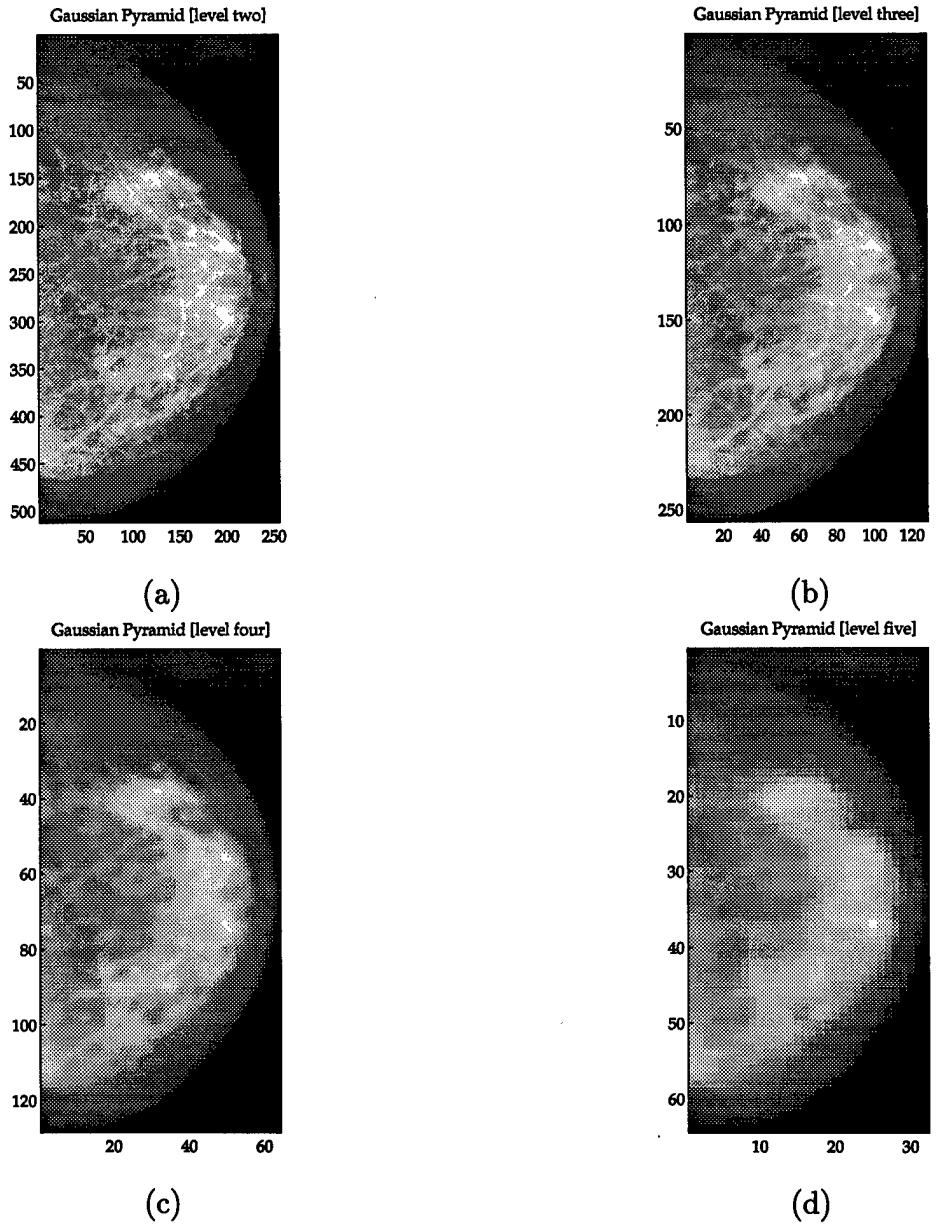

Figure 6 Gaussian pyramid generated for source image in Figure 3 [$\sigma = 1.5$]. (a) Base image decimated X 4 (b) second tier decimated X 8 (c) third tier decimated X 16 (d) fourth tier decimated X 32.

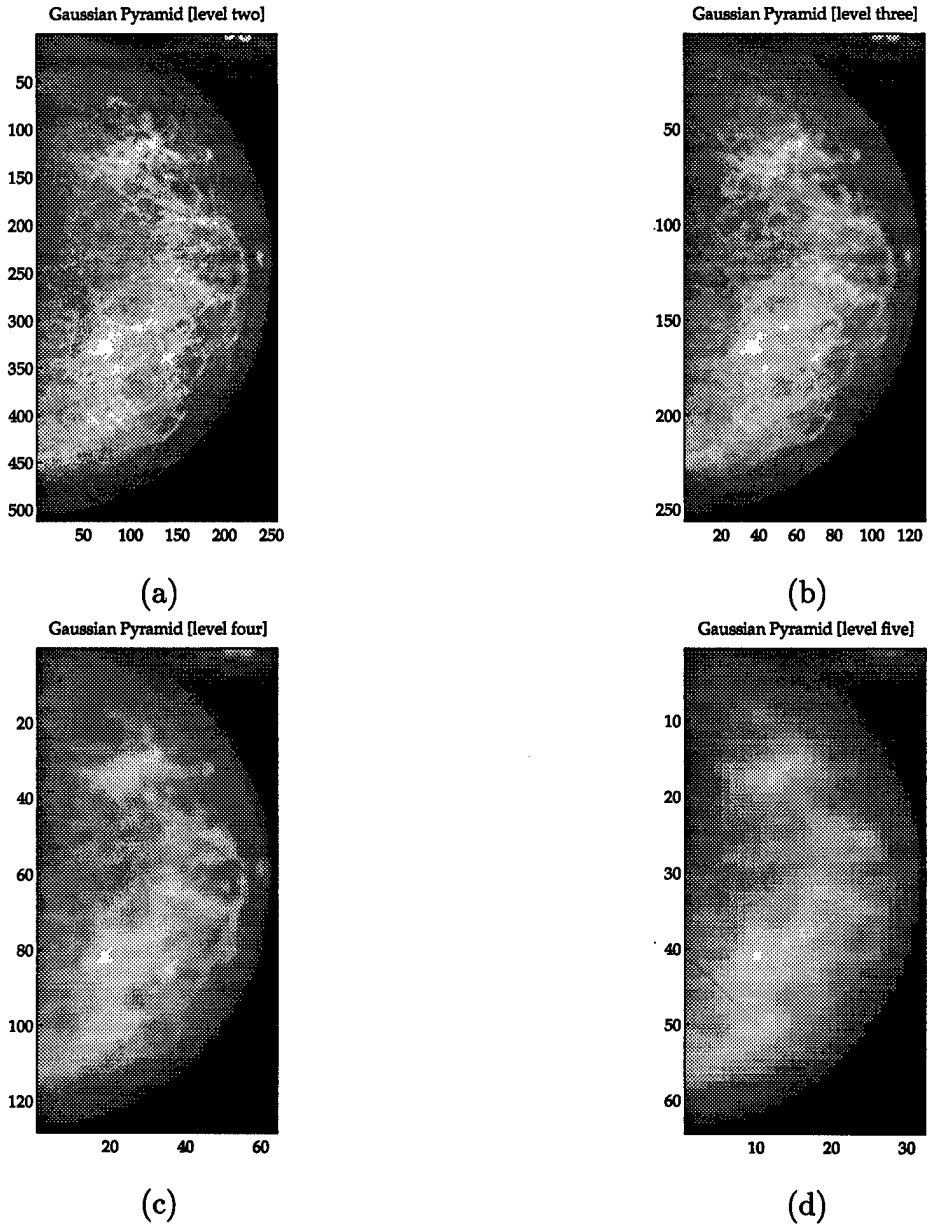

Figure 7 Gaussian pyramid generated for target image Figure 3 [$\sigma = 1.5$]. (a) Base image decimated X 4 (b) second tier decimated X 8 (c) third tier decimated X 16 (d) fourth tier decimated X 32.

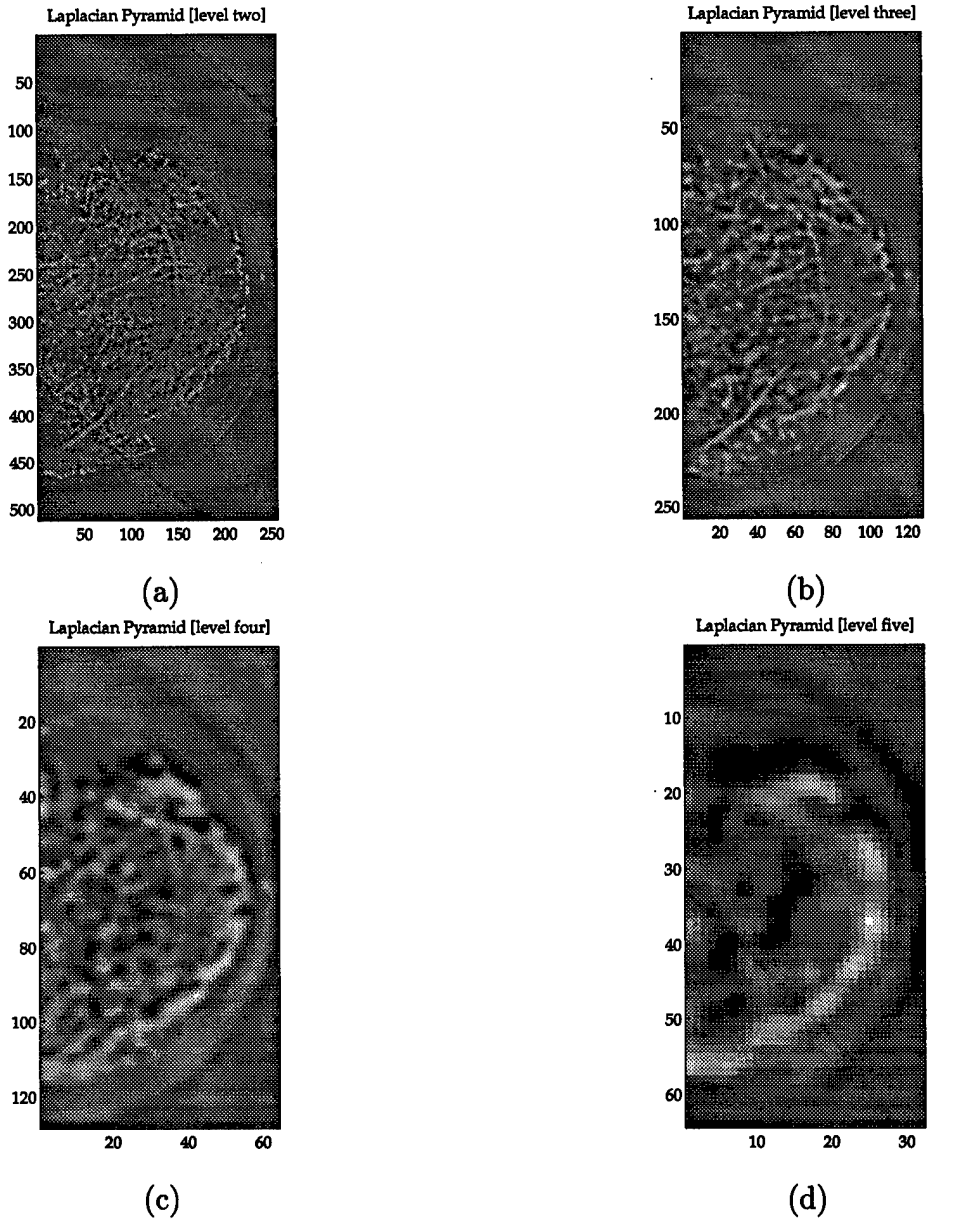

Figure 8 Laplacian pyramid generated for source image Figure 3 [$\sigma = 1.5$]. (a) Base image decimated X 4 (b) second tier decimated X 8 (c) third tier decimated X 16 (d) fourth tier decimated X 32.

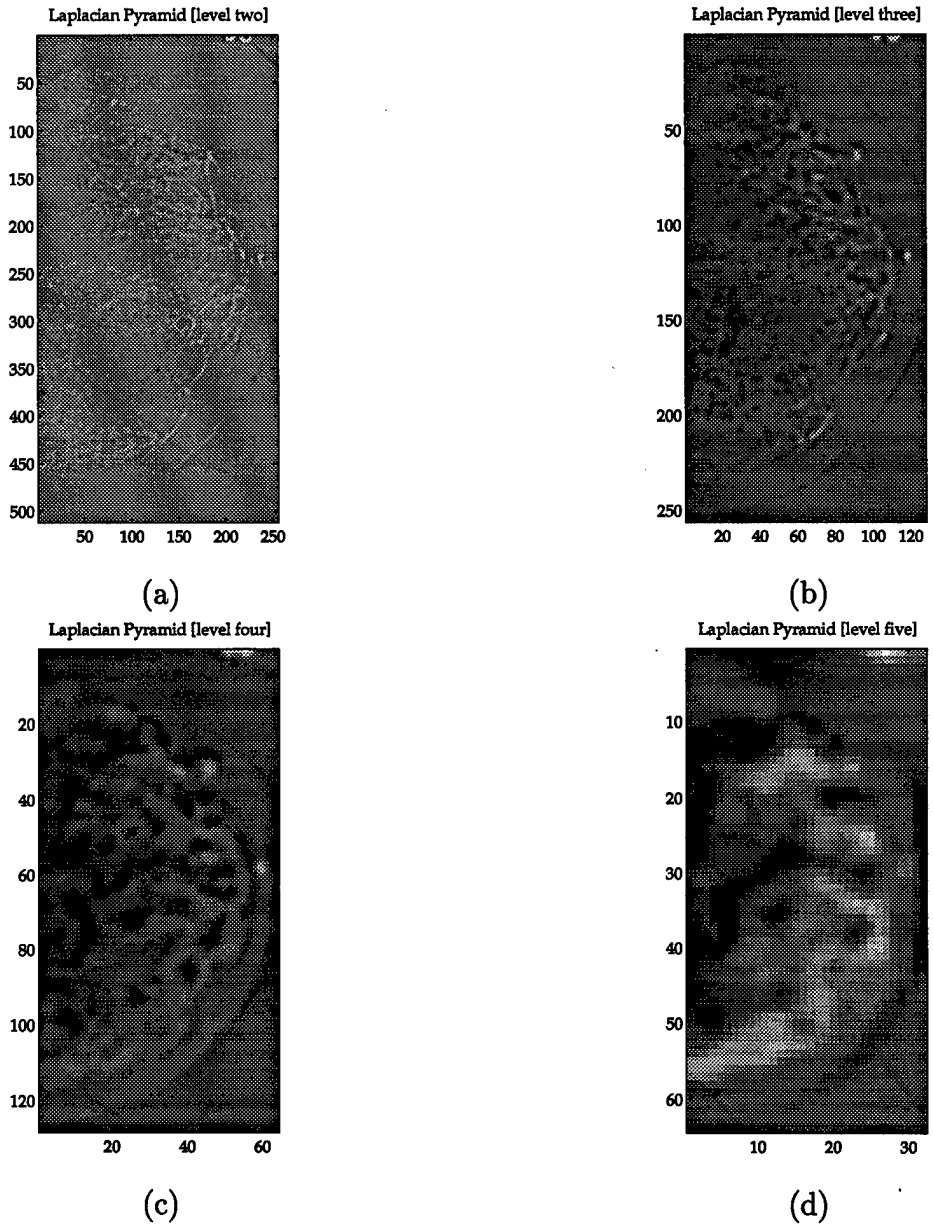

Figure 9 Laplacian pyramid generated for target image Figure 3 [$\sigma = 1.5$]. (a) Base image decimated X 4 (b) second tier decimated X 8 (c) third tier decimated X 16 (d) fourth tier decimated X 32.

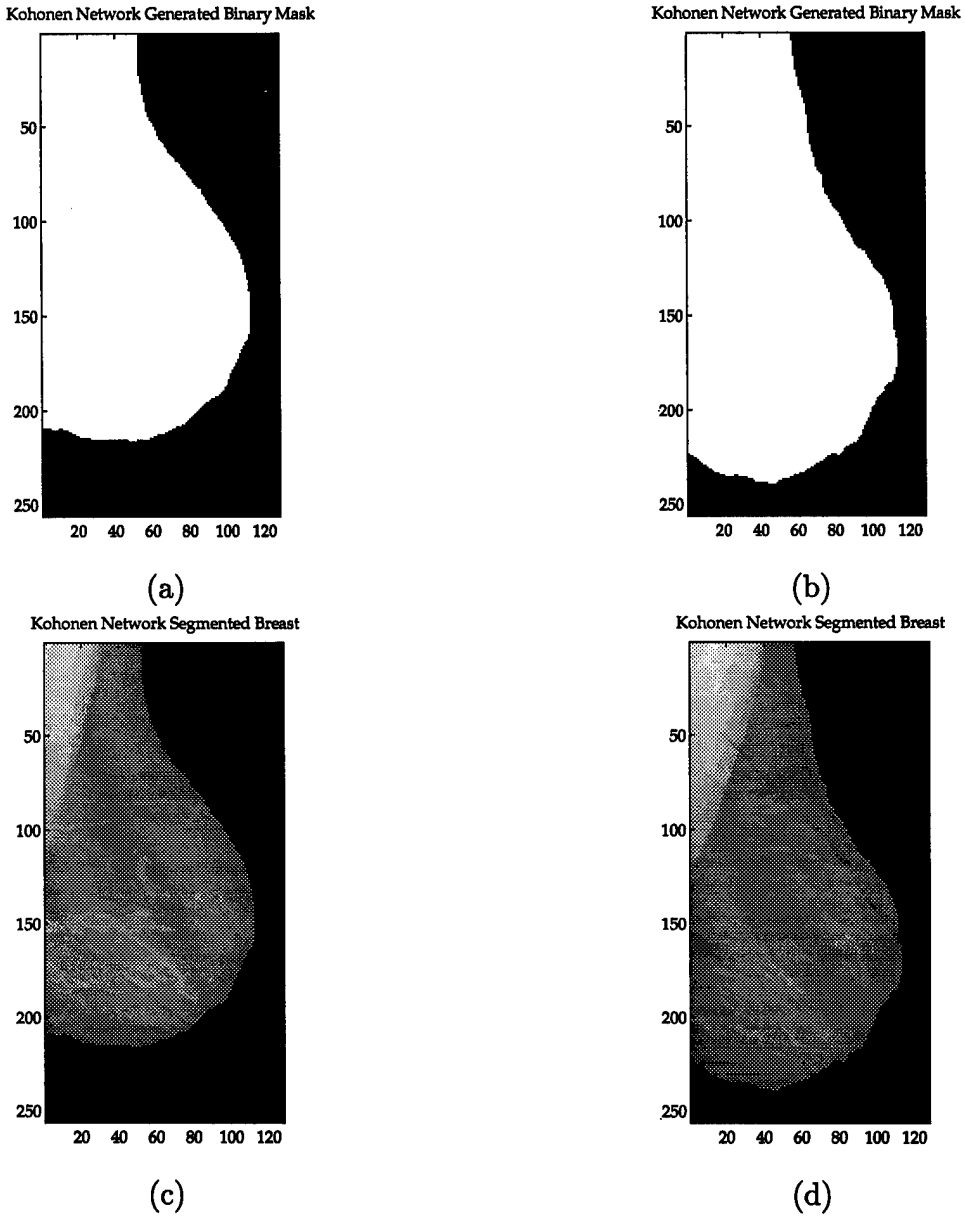

Figure 10 Binary masks and segmented breast images for two different screenings [generated by Kohonen Neural Network]. (a) Binary mask for previous mammogram (b) binary mask for current mammogram (c) previous breast structure extracted from background (d) current breast structure extracted from background.

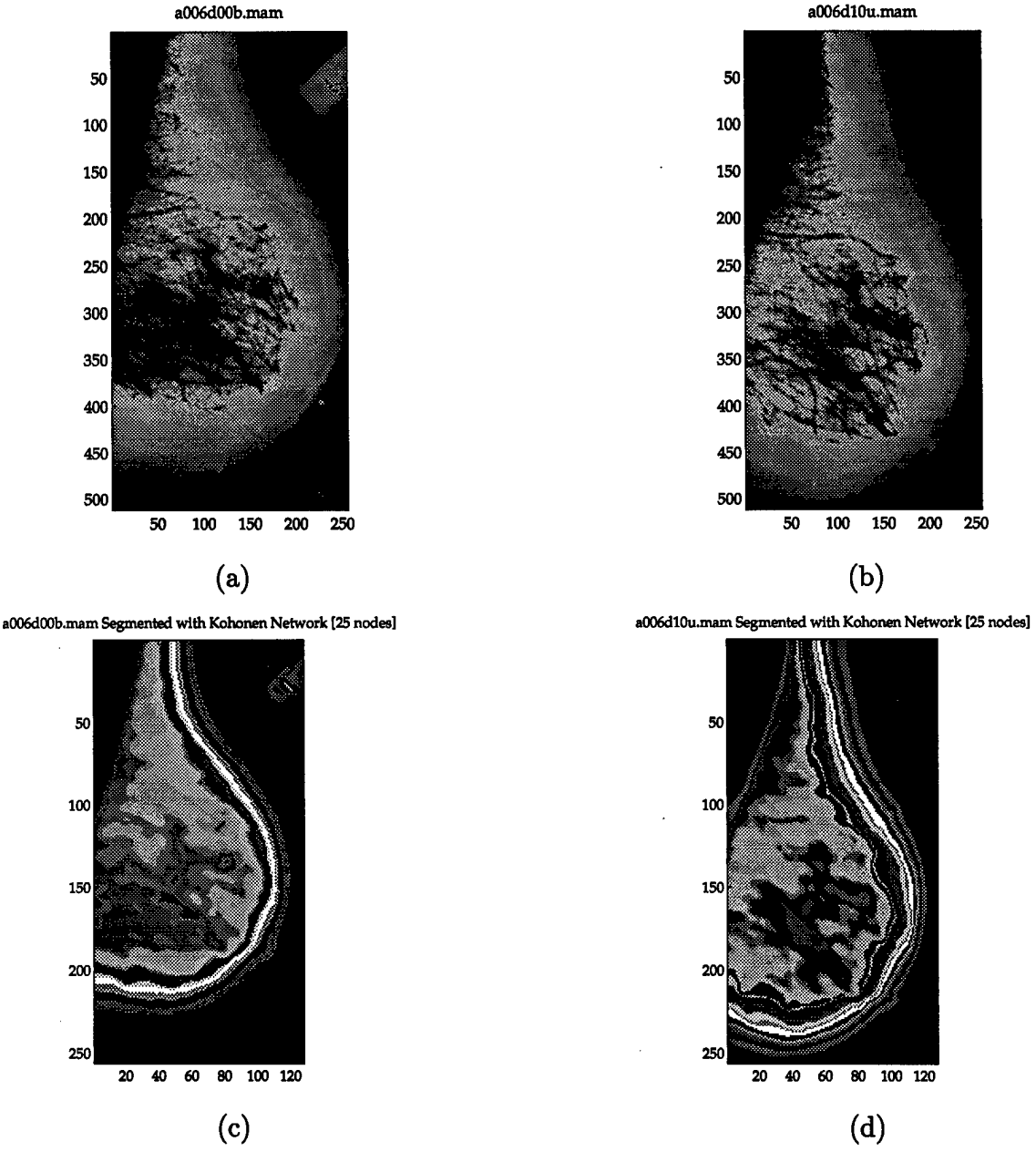

Figure 11 Mammograms segmented using a Kohonen Neural Network with 25 nodes in the competitive layer. Segmentation shows variations in image intensity corresponding to regions of different density (a) Mammogram from previous screening (b) mammogram from current screening (c) segmented version of image in upper left panel (d) segmented version of image in upper right panel.

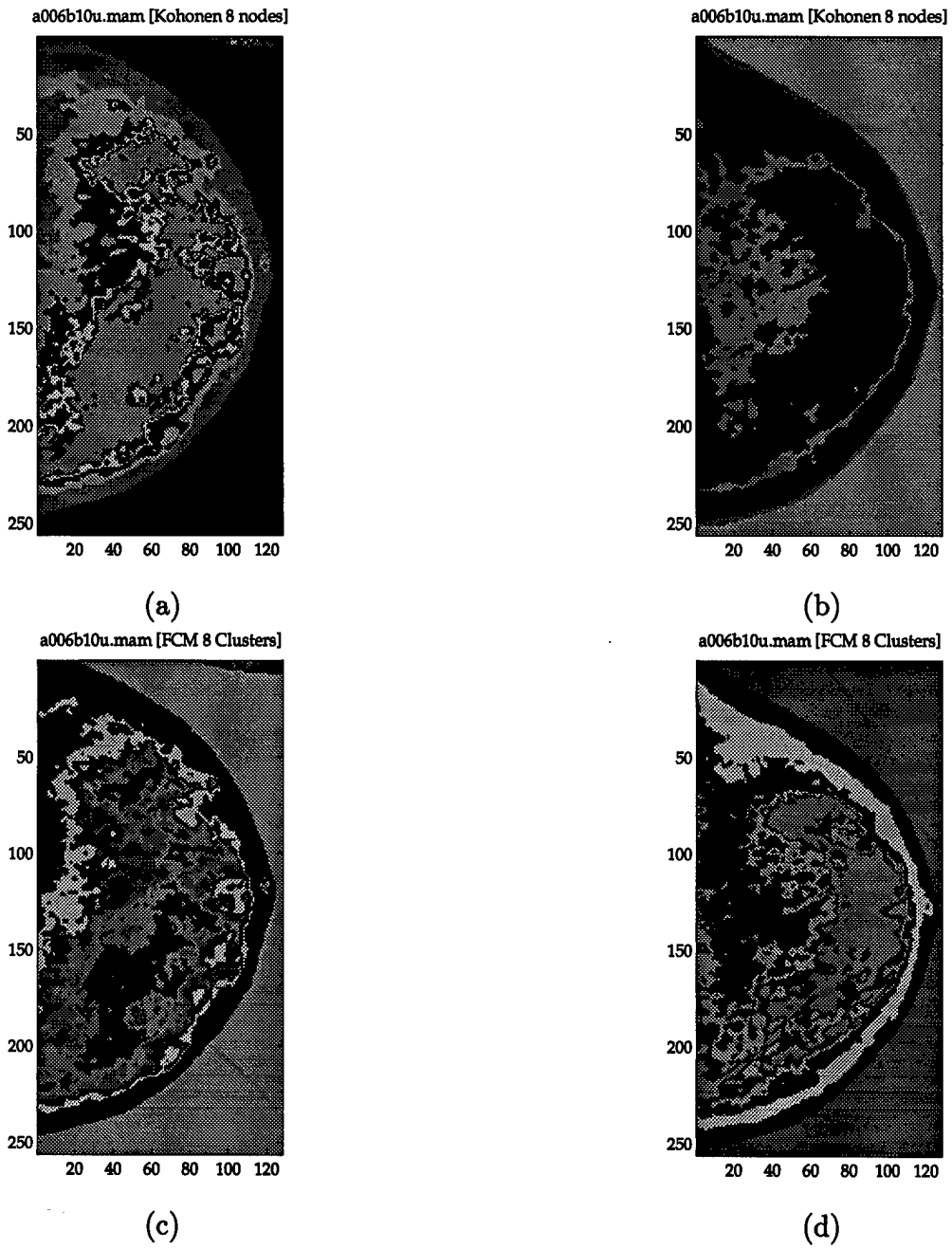

Figure 12 Comparison of Kohonen and Fuzzy C-Means (FCM) segmentation methods. Source and target mammogram images are segmented into 8 regions using single level. (a) Source image segmented with Kohonen method (b) target image segmented with Kohonen method (c) source image segmented with FCM method (d) target image segmented with FCM.

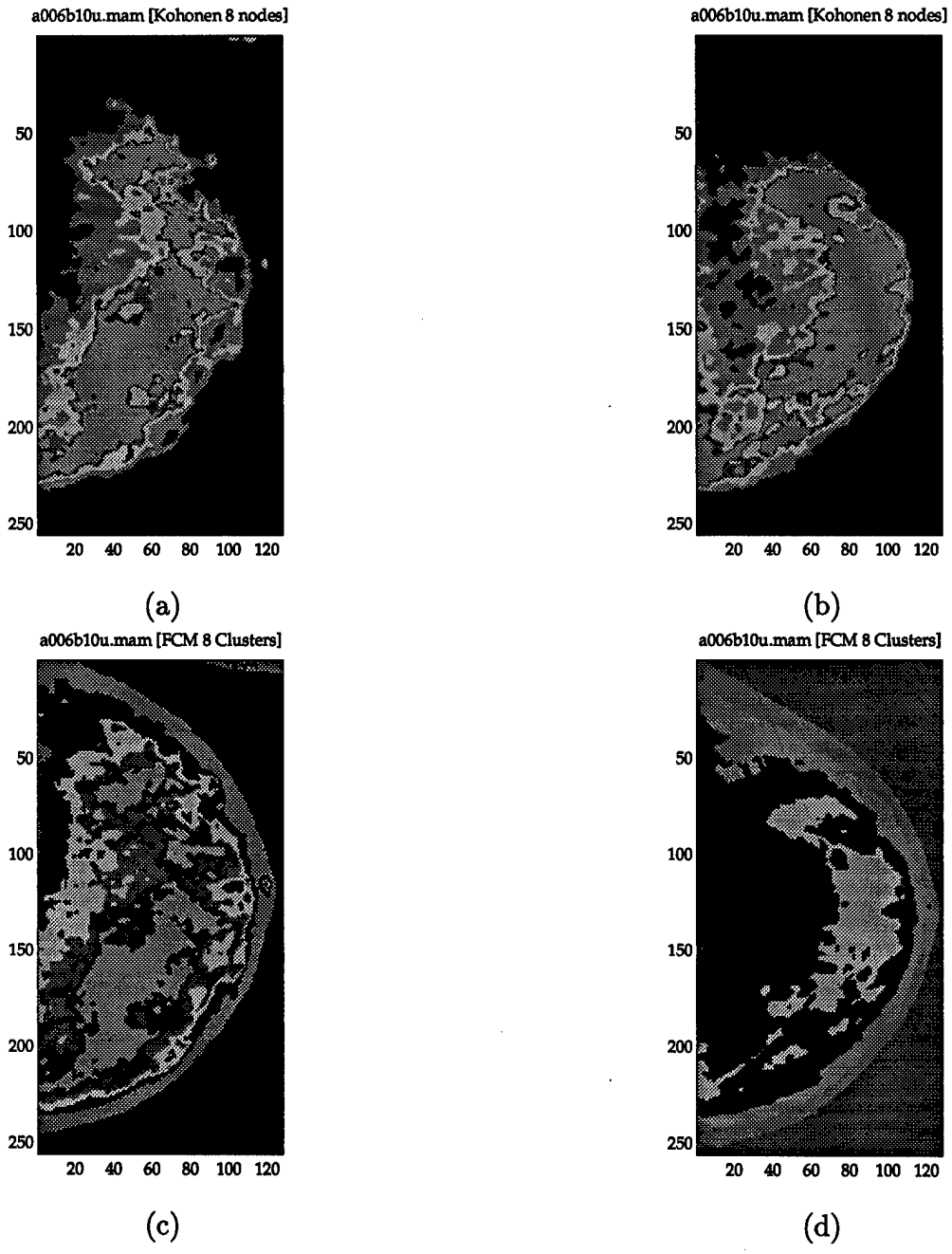

Figure 13 Comparison of Kohonen and Fuzzy C-Means (FCM) segmentation methods. Source and target mammogram images are segmented into 8 regions using two-level pyramid. (a) Source image segmented with Kohonen method (b) target image segmented with Kohonen method (c) source image segmented with FCM method (d) target image segmented with FCM.

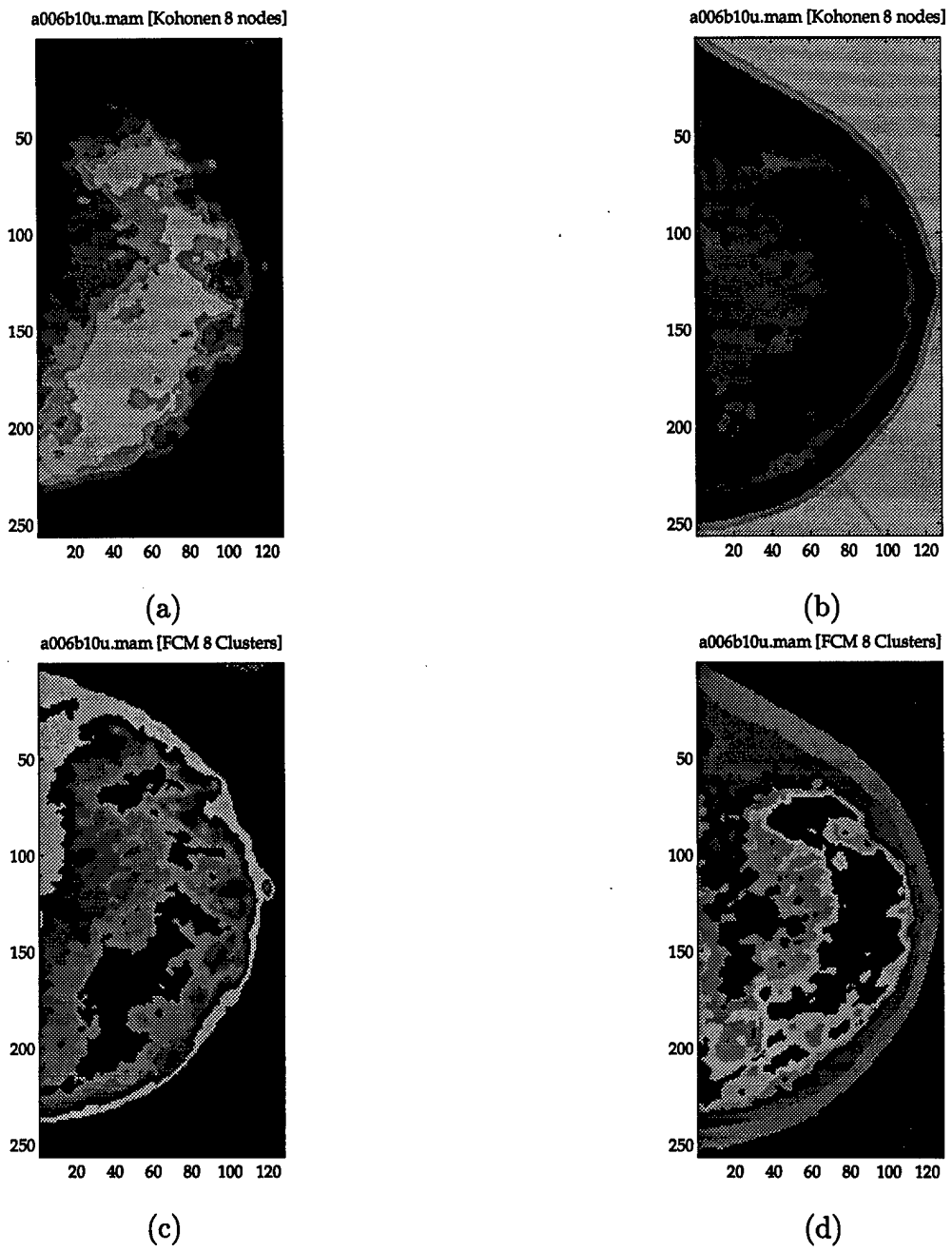

Figure 14 Comparison of Kohonen and Fuzzy C-Means (FCM) segmentation methods. Source and target mammogram images are segmented into 8 regions using three-level pyramid. (a) Source image segmented with Kohonen method (b) target image segmented with Kohonen method (c) source image segmented with FCM method (d) target image segmented with FCM.

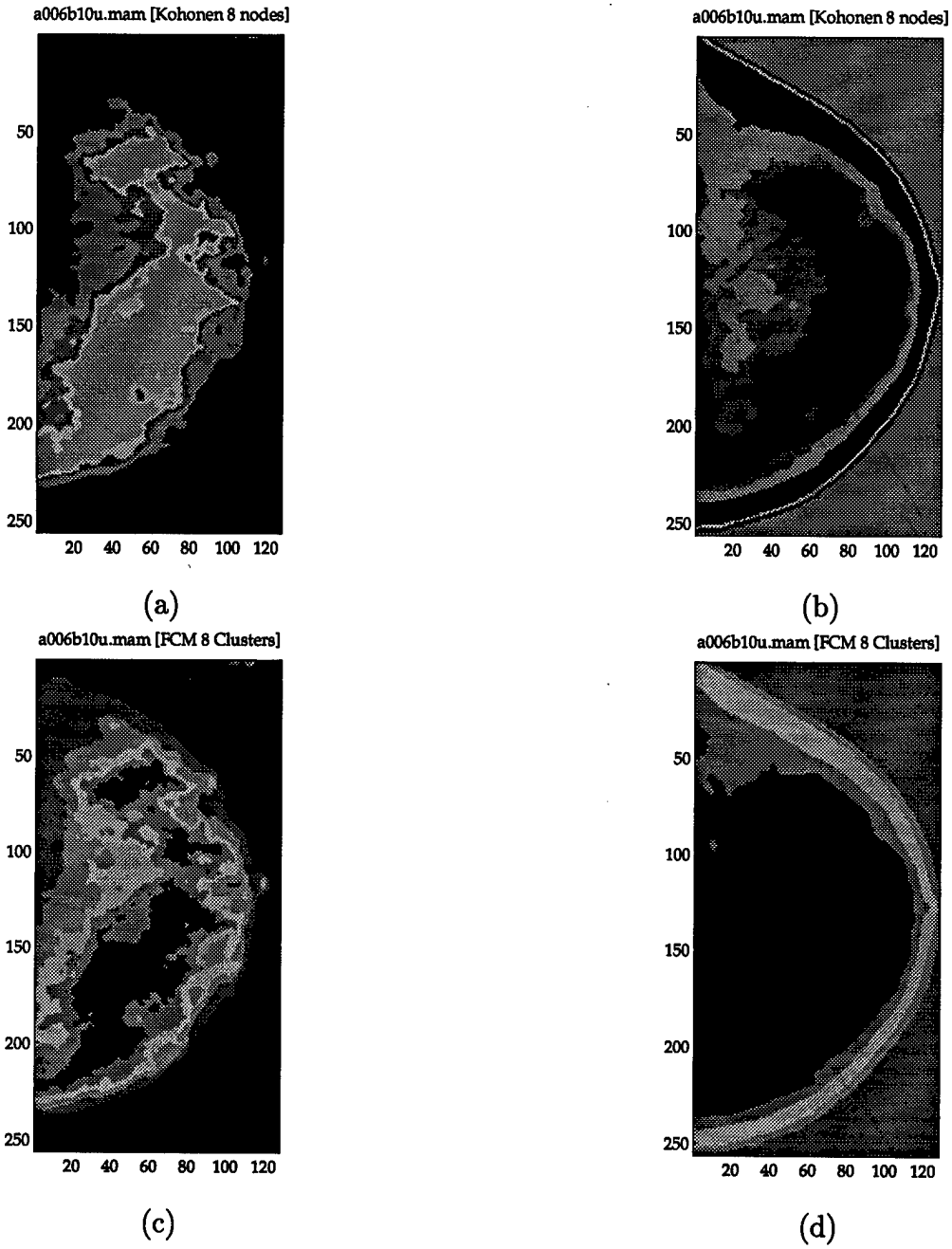

Figure 15 Comparison of Kohonen and Fuzzy C-Means (FCM) segmentation methods. Source and target mammogram images are segmented into 8 regions using four-level pyramid. (a) Source image segmented with Kohonen method (b) target image segmented with Kohonen method (c) source image segmented with FCM method (d) target image segmented with FCM.

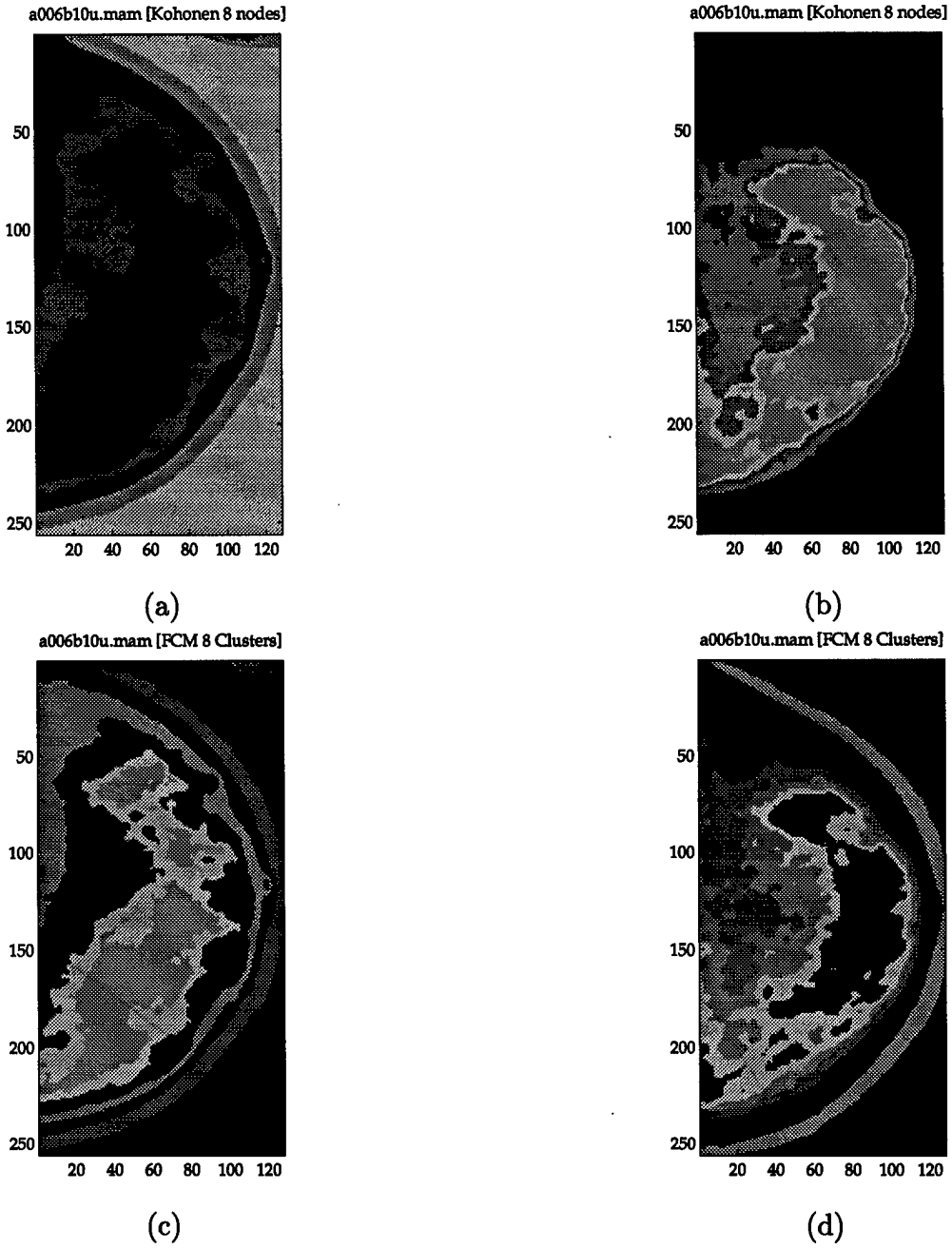

Figure 16 Comparison of Kohonen and Fuzzy C-Means (FCM) segmentation methods. Source and target mammogram images are segmented into 8 regions using five-level pyramid. (a) Source image segmented with Kohonen method (b) target image segmented with Kohonen method (c) source image segmented with FCM method (d) target image segmented with FCM.

3.6 Optical Flow Computation

After the two images have been grossly aligned, expanded into a multiscale representation, and segmented into homogeneous regions, the optical flow between the two images can be more reliably estimated. The approach taken in this thesis is based on a multiscale, cooperative computation paradigm. Since we are dealing with unknown, sometimes significant, inter-image differences, the multiresolution approach should be better able to cope with these challenges than its single-level model counterpart. The information provided by the Laplacian pyramid and that obtained by residual errors further enhance the effectiveness of a hierarchical strategy.

3.6.1 Theoretical Background. As described in the previous chapter, estimating the optical flow vector field can be considered a constrained optimization problem having the general form

$$\Phi = \int\int_{Image} (E_x u + E_y v + E_t)^2 + \alpha^2 (u_x^2 + u_y^2 + v_x^2 + v_y^2) dx dy \qquad (17)$$

where α represents the Lagrange multiplier constant. The spatio-temporal partial derivatives E_x, E_y, and E_t are approximated using the four-point differencing method described in Horn and Schunck's original work (31). This thesis adopts the solution method developed by Hwang and Lee (33) as outlined below.

Since we are using a hierarchical approach, the additional constraint $\alpha^2(u_x^2 + u_y^2 + v_x^2 + v_y^2)dxdy$ can be taken to be the difference between the velocity vector at the current level k and the velocity vector projected from an adjacent level (i.e. $k-1$ or $k+1$). Thus, we can model this constraint as a minimization of

$$C(u^k, v^k) = \sqrt{(((u^{proj} - u^k)^2 + (v^{proj} - v^k)^2))} \qquad (18)$$

where (u^k, v^k) denote the velocity vectors at level k and (u^{proj}, v^{proj}) are the velocity vectors projected from an adjacent level. The minimization equation thus

becomes

$$E(u^k, v^k) = \int\int_{Image} (E_x u + E_y v + E_t)^2 + \alpha^2 \{C(u^k, v^k)\}^2) dx dy \tag{19}$$

which in turn can be formulated as a set of Euler-Lagrange equations of the form

$$\{\alpha^2 + (E_x^k\}u^k + E_x^k E_y^k v^k = \alpha^2 u^{proj} - E_x^k E_t^k \tag{20}$$

$$E_x^k E_y^k u^k + \{\alpha^2 + (E_y^k\}v^k = \alpha^2 v^{proj} - E_y^k E_t^k \tag{21}$$

by setting $E(u^k, v^k)$ equal to 0.

Hwang and Lee use the iterative Gauss-Seidel relaxation technique to solve the minimization equation. The iterative update equations are

$$u^k = u_0 - E_x^k \frac{P}{D} \tag{22}$$

$$v^k = v_0 - E_y^k \frac{P}{D} \tag{23}$$

where

$$P = E_x^k u^{proj} + E_y^k v^{proj} + E_t^k \tag{24}$$

$$D = \alpha^2 + (E_x^k)^2 + (E_y^k)^2 \tag{25}$$

The update variables u^k and v^k are initialized to u^{proj} and v^{proj}, the optical flow vectors computed at the previous level, to provide a good starting point for further refinement.

3.6.2 Algorithm Dynamics. The coarse-to-fine computational strategy used by this system facilitates the progressive refinement of an initial guess. In Hwang and Lee's (33) implementation, the optical flow calculation from the next level above

serves as the regularization parameter required to make the problem well-posed. This design underlies the superior performance of the multiscale approach over Horn and Schunck's (31) single-scale approach. The proposed system can also implement true multigrid processing by projecting the residual from one level to the level above it where it can be used to speed convergence (19). Figure 18 depicts an example of the residual error between the optical flow computed at two different levels of the image pyramid. It represents the high frequency component of the computed flow field. Figure 17 shows the final optical flow fields computed at each level of a four-level image pyramid.

3.7 Image Warping

The optical flow estimate can be used directly to create a warped version of the source image. This non-linear transformation can be accomplished using the equation

$$Image_{warped}(i,j) = Image_{source}(i - \Delta u, j - \Delta v). \tag{26}$$

Since the transformed image coordinates $(i - \Delta u, j - \Delta v)$ will be real-valued and therefore fall outside the standard integer grid, the actual intensity values must be interpolated from the source image. This system uses a standard bilinear interpolation.

3.8 Evaluation

The primary evaluation criterion is the similarity measure between the transformed image and the target image. Although many matching routines use some type of correlation measure to estimate the similarity between two images or image regions, it is not used by this system because it is unreliable when any significant amount of non-rigid motion is present. Instead, the optical flow estimate itself is

used as a measure of the remaining difference between the two images. Since the original motivation behind using optical flow was to have it estimate the inter-image disparity, it seems reasonable that the optical flow residual would likewise be a good estimate of any remaining intensity difference. The lower the post-alignment optical flow, the lower the dissimilarity (i.e. better match) between the two image segments.

Comparison of the two corresponding Laplacian images offers a qualitative sense of how well the images match. As Barron et al. (3) point out in their evaluation of optical flow methods, the Laplacian pyramid "helps to enhance image structure, such as edges, that is often thought to be important". Whereas such features are normally subjected to blurring in a Gaussian pyramid, they can become more prominent in the Laplacian pyramid. If similar structural features can be found in the warped and target images, we can better evaluate the success of the matching procedure.

3.9 Summary

This chapter presented a mammogram registration technique based on optical flow estimates in a multiresolution framework. After preprocessing, the images undergo coarse alignment to eliminate major positional and orientation differences between them. The two breast structures are then segmented from the background image for improved matching accuracy and computational performance. Next, a Gaussian pyramid of four to five levels, depending on the degree of disparity between the images, is constructed. A multiscale algorithm then computes the apparent difference between the images using an iterative coarse-to-fine approach. Optical flow estimates generated at a given level become the starting point for higher resolution estimates at the next level down the pyramid. The computed velocity field is used to transform the source image into one more closely resembling the target image. Finally, the disparity between the warped image and the target is evaluated.

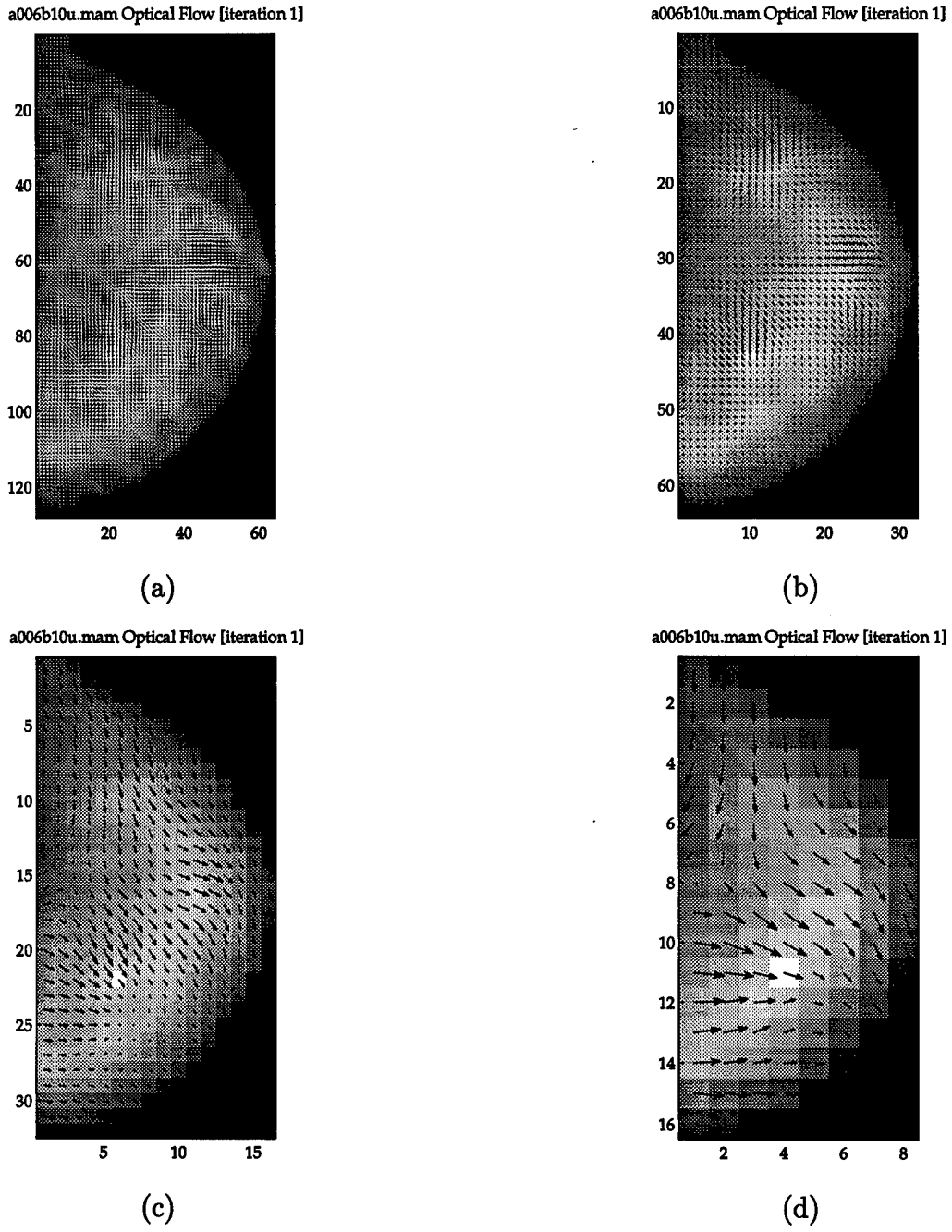

Figure 17 Optical Flow Pyramid: Decomposition of the optical flow estimate into four levels. The calculated flow at level $k+1$ becomes the initial estimate for refining the estimate at level k. (a) Bottom level (finest resolution) (b) second level (c) third level (d) top most level (coarsest resolution).

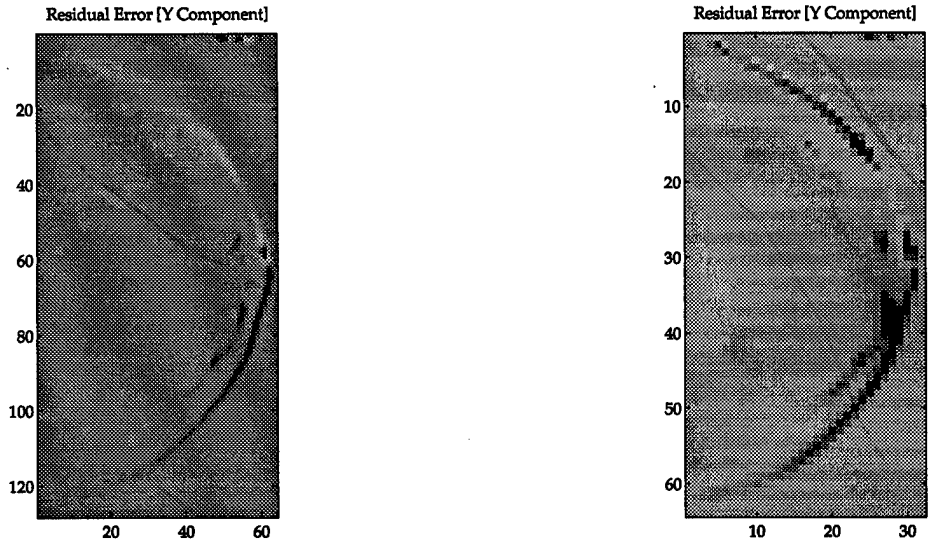

(a) (b)

Figure 18 Residual error at two levels of the Gaussian pyramid [Y component only]. (a) Residual computed at level two (b) residual computed at level three.

IV. Results

This chapter discusses results from applying the proposed mammogram registration system to synthetic and real images.

4.1 System Testing

It's important to evaluate the accuracy of the proposed registration method before relying on matching results using real mammograms. Since it is difficult to precisely determine the expected results, the performance of two different optical flow estimation techniques will be analyzed. Single-level estimation will be tested using the Horn and Schunck (31) method, while the multi-resolution approach will be represented by Hwang and Lee's (33) Gaussian pyramid scheme. Although not exhaustive, the tests are designed to evaluate how well the proposed method can be expected to perform on real x-ray images.

4.1.1 Image Preparation. A small mammogram region possessing significant texture variation was selected to be the source image. The image patch is presmoothed using the Gaussian filter described in Chapter III with a 4 x 4 kernel and a standard deviation of 1.5 pixels. Image intensities were then quantized to fall in the range 0 to 255.

4.1.2 Test Case Generation. Seven different tests were conducted on image pairs having known differences. The first two test cases evaluate the ability of the optical flow module to recover translational motion. Two target images are tested: one shifted down by five pixels relative to the source image, and another shifted to the right again by five pixels. For the third test, the source image is rotated about the center pixel. Since the registration method will be required to perform nonlinear mapping, the ability to detect rotational deformations is critical to the success of this system. A similar test assesses how well the system can track movement of a

edge contour. This test will simulate matching dissimilar skin edges separated by short distances. Finally, the reaction to finding an object on the target image not present on the source image is investigated. This capability is important to both image mapping and subsequent tumor detection.

A final test was constructed to evaluate how well the system can capture the actual optical flow between two images. This test was designed to mimic the degree of complexity the system would be expected to handle in an operational setting. The source image in this case was an actual mammogram downsampled by a factor of 16 to simplify analysis. This source image was then subjected to a known affine transformation using the technique discussed in the global alignment section. The system then had to compute the flow between the original image (source) and the warped image (target). Ideally, the computed flow would be very similar to the flow defined under the known affine transformation.

4.1.3 Test Case Execution. The regularization parameter α was set to 10, and the target error rate for convergence was set to 0.05, for all test cases. The title of each velocity flow diagram includes the total number of iterations required for convergence.

Test Case Specifications		
Test Case	Description	Parameters
Horizontal Translation	shift of target relative to source	5 pixels
Vertical Translation	shift of target relative to source	5 pixels
Rotation	rotation of source about the center	10 degrees
Translation and Rotation	horizontal shift and rotation	5 pixels; 10 degrees
Contour Tracking	shift of curved target boundary	5 pixels
Foreign Object Insertion	superposition of a box onto source	10 X 10 pixels

Table 5 Specifications for the six validation test cases.

4.1.4 Test Evaluation. The results of the six tests are displayed in Figures 19 through 24. The most apparent difference

In general, the two methods produced remarkably similar results. Two main observations can be made about the comparative performance of the two methods. First, Horn and Schunck's gradient-based method invariably requires almost twice as many iterations to converge as Hwang and Lee's multiresolution approach. Second, the Horn and Schunck method is not quite as consistent as Hwang and Lee's when compared to the expected outcome. For example, almost all vector arrows in the translation cases are parallel in the Hwang and Lee method, whereas a significant percentage show distinct deviation in the Horn and Schunck method. In the contour tracking test, Horn and Schunck's method provided good estimates at boundary regions only, while its competitor generated a consistent velocity field across the entire image. The combined accuracy and efficiency favor a multiresolution approach for a system as computationally intensive as the one proposed in this thesis.

The preferred multiresolution method was used in executing the last test case more closely simulating actual operating conditions. Figure 25 presents the results of this test. The computed optical flow is very similar to the true flow. The main differences occur in regions of high homogeneity. Gradient-based methods, such as the one used here, generally find such homogeneous areas ambiguous and difficult to compute accurately.

4.2 Mammogram Registration

4.2.1 Experimental Format. The primary focus of this thesis is on the registration of mammograms taken of the same breast at different times. Therefore, registration experiments conducted in this section are restricted to available temporal sequences of images. To keep the analysis focused and easy to follow, this section adopts a case study approach. The two cases presented register a time sequence of four mammograms for the same women. The first case (see Figure 26) aligns four craniocaudal views for the right breast, while the second case (see Figure 35) aligns four mediolateral oblique views for the same breast. The mammograms for

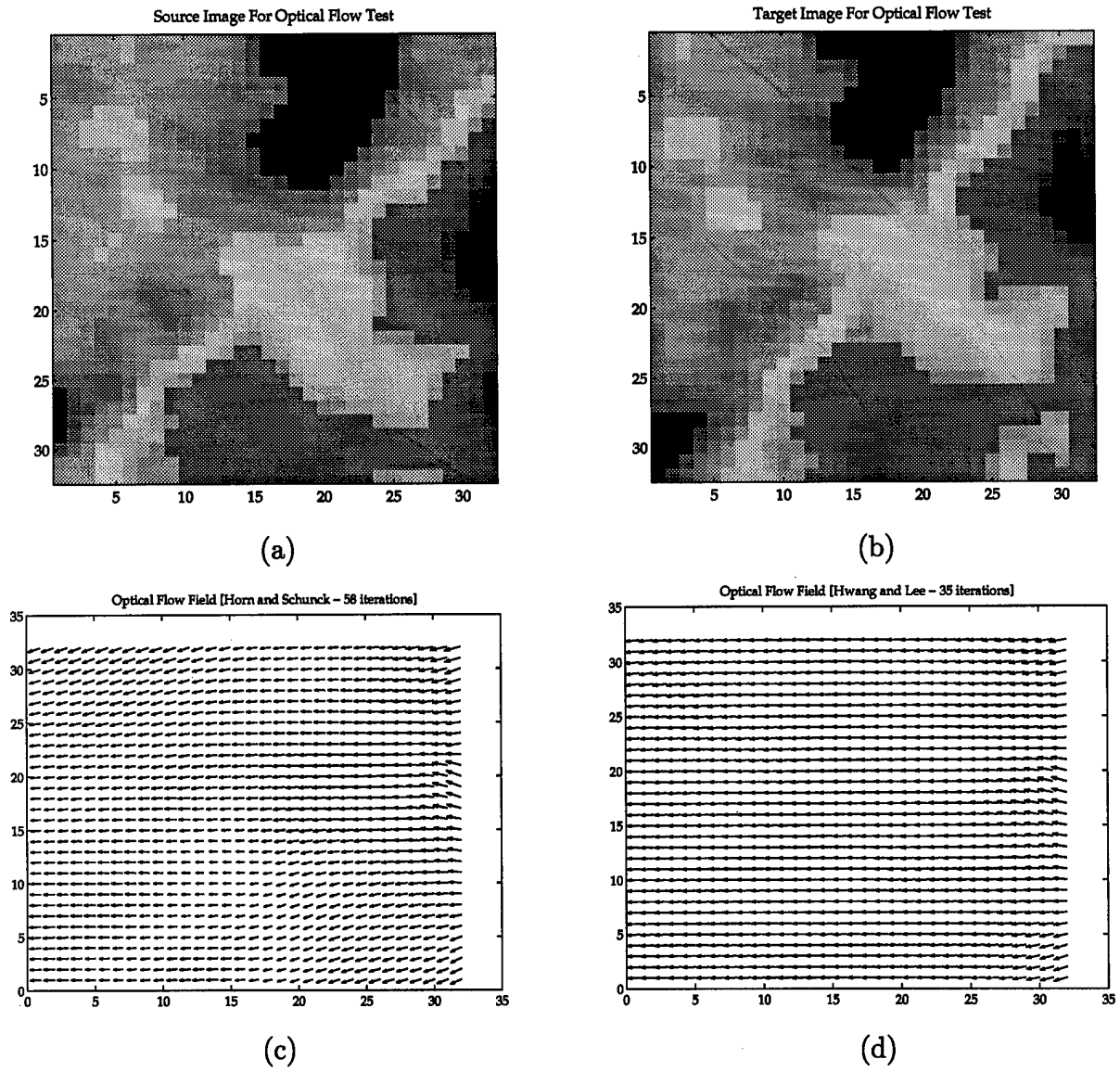

Figure 19 Comparison of two optical flow computation methods for image translation test case. (a) Original image (b) original image shifted to the right by 5 pixels (c) Horn and Schunck gradient method (d) Hwang and Lee multiresolution method.

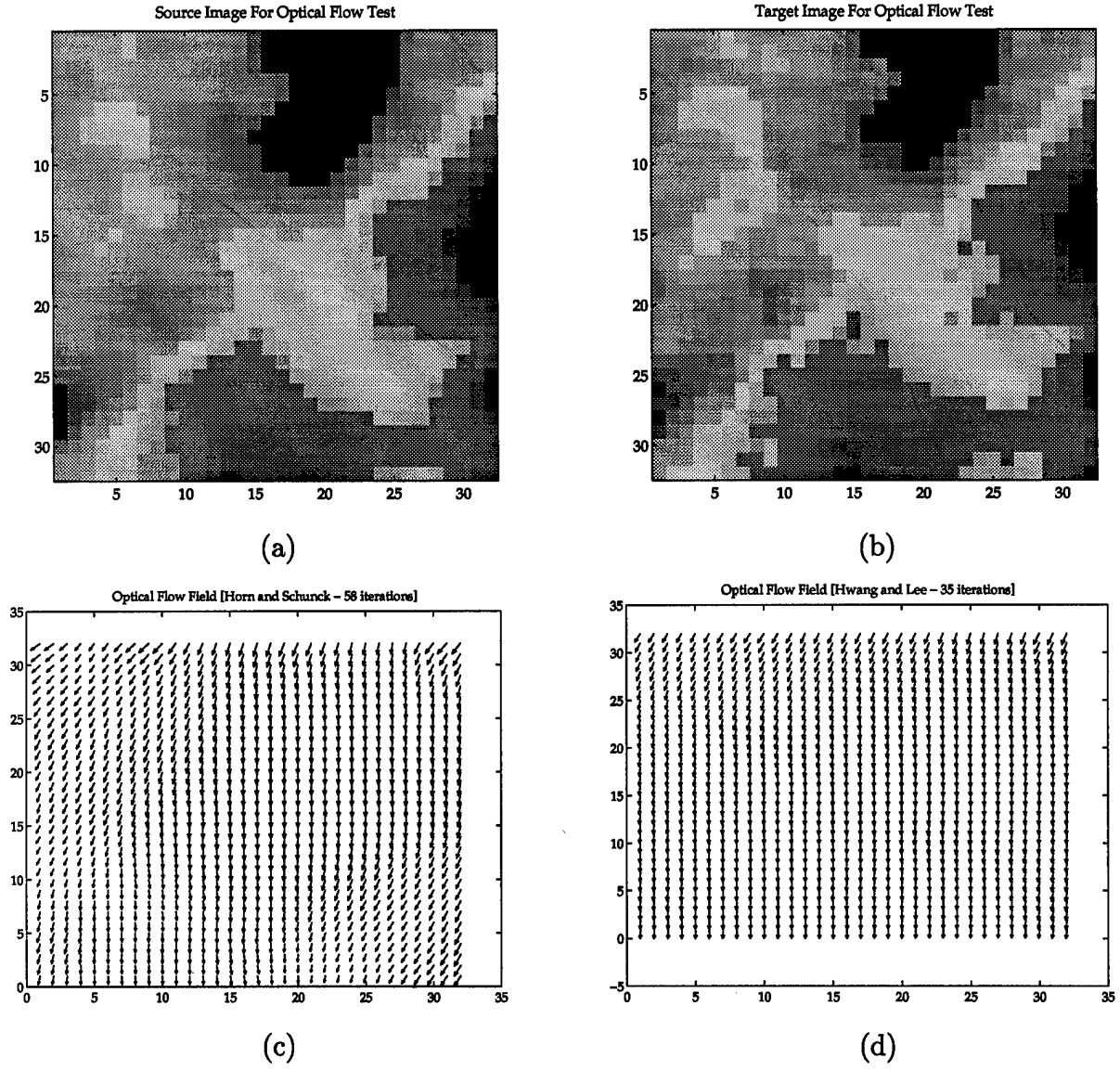

Figure 20 Comparison of two optical flow computation methods for image translation test case. (a) Original image (b) original image shifted down by 5 pixels (c) Horn and Schunck gradient method (d) Hwang and Lee multiresolution method.

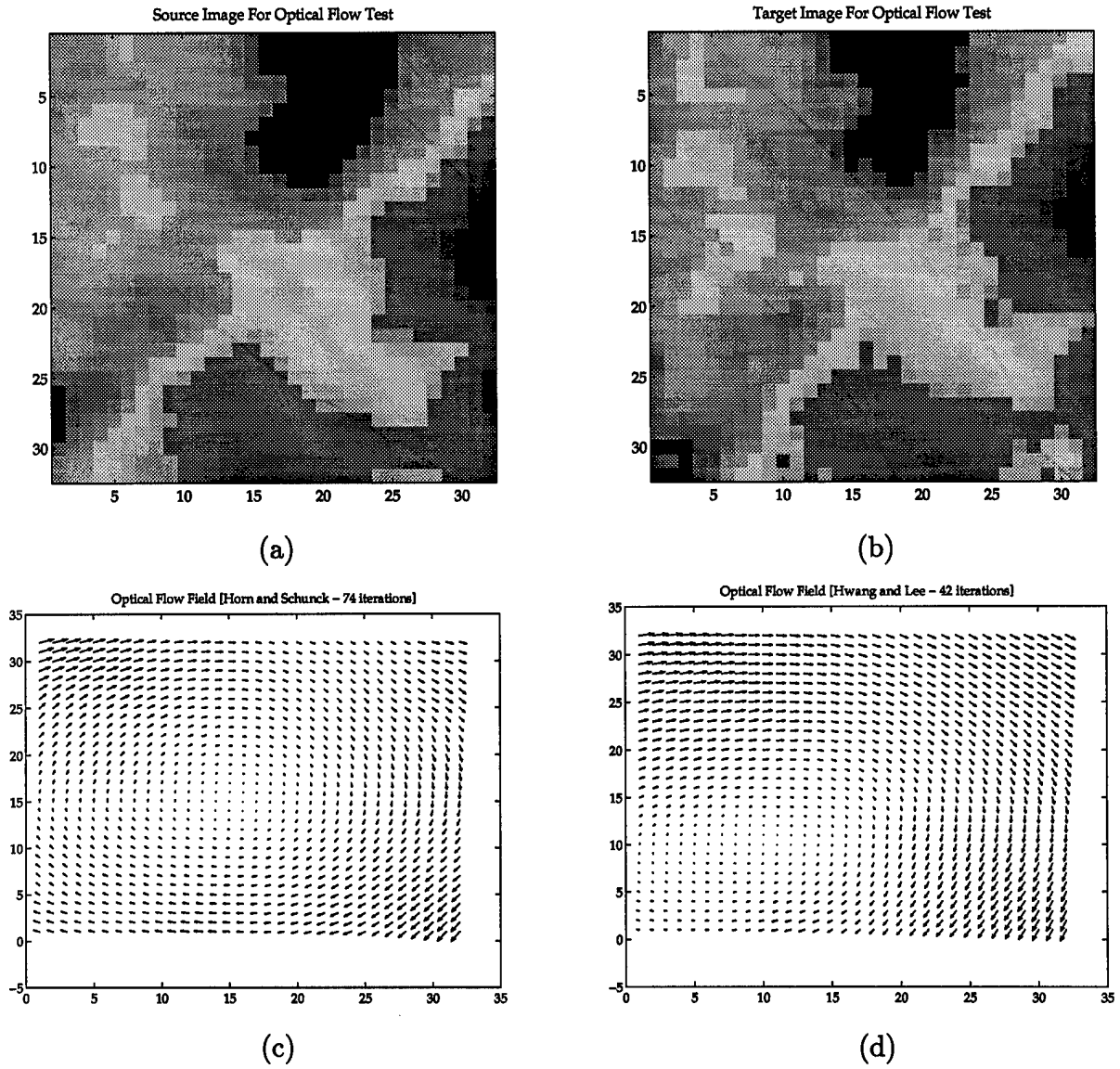

Figure 21 Comparison of two optical flow computation methods for image rotation test case. (a) Original image (b) original image rotated counterclockwise by 10 degrees (c) Horn and Schunck gradient method (d) Hwang and Lee multiresolution method.

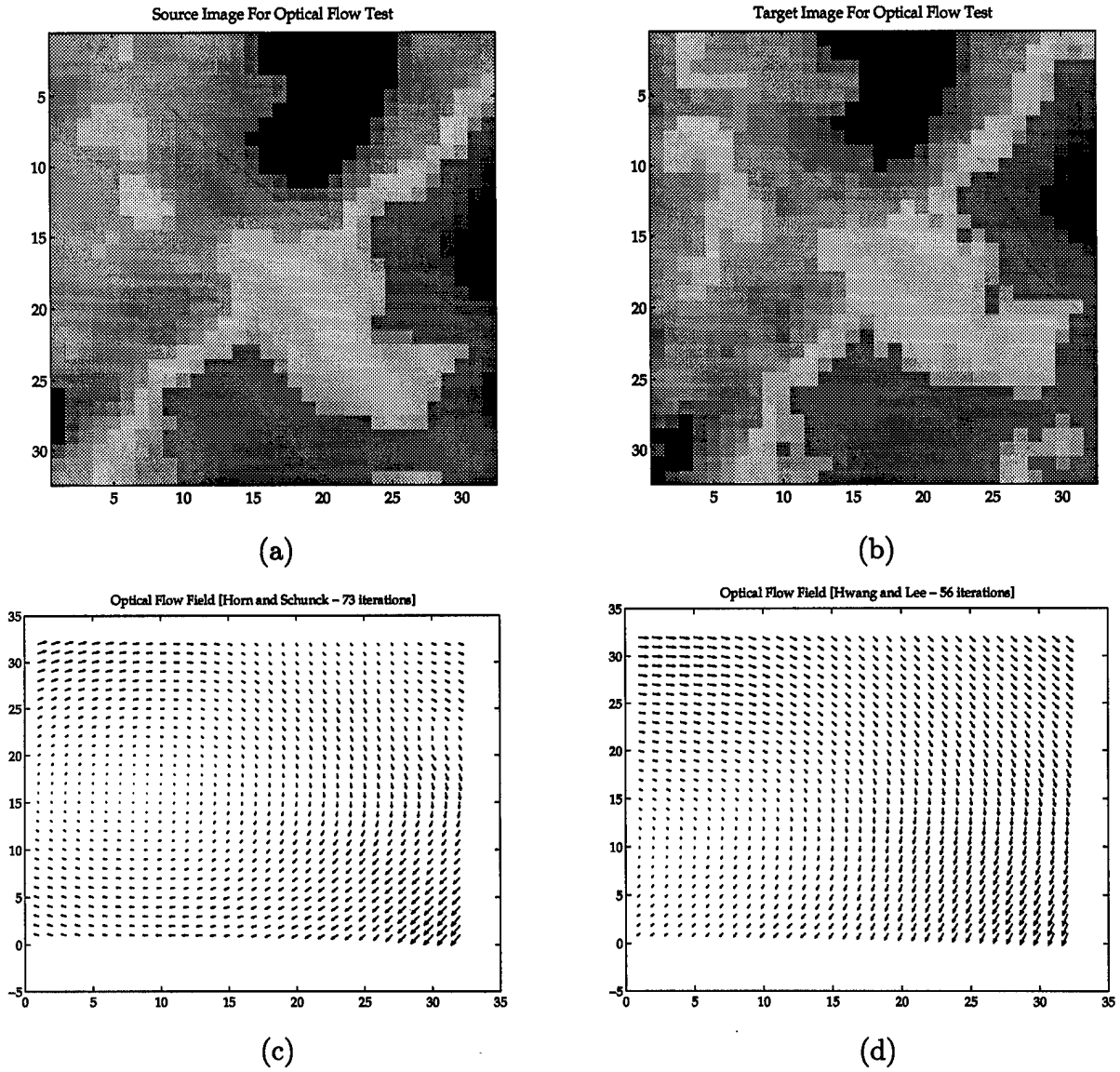

Figure 22 Comparison of two optical flow computation methods for image translation and rotation test case. (a) Original image (b) original image shifted down by 5 pixels (c) Horn and Schunck gradient method (d) Hwang and Lee multiresolution method.

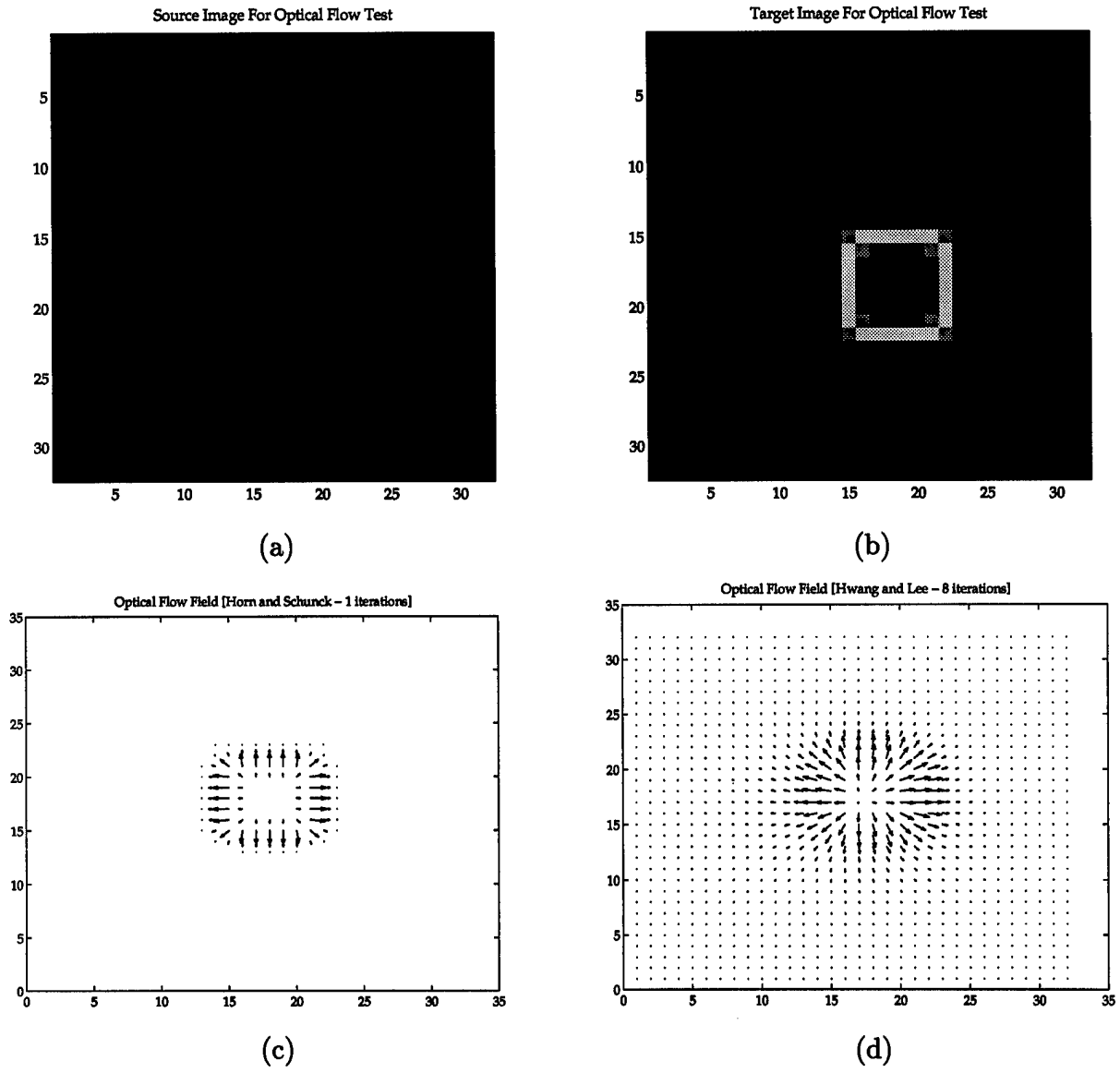

Figure 23 Comparison of two optical flow computation methods for image with box superimposed. (a) Original image (b) original image shifted down by 5 pixels (c) Horn and Schunck gradient method (d) Hwang and Lee multiresolution method.

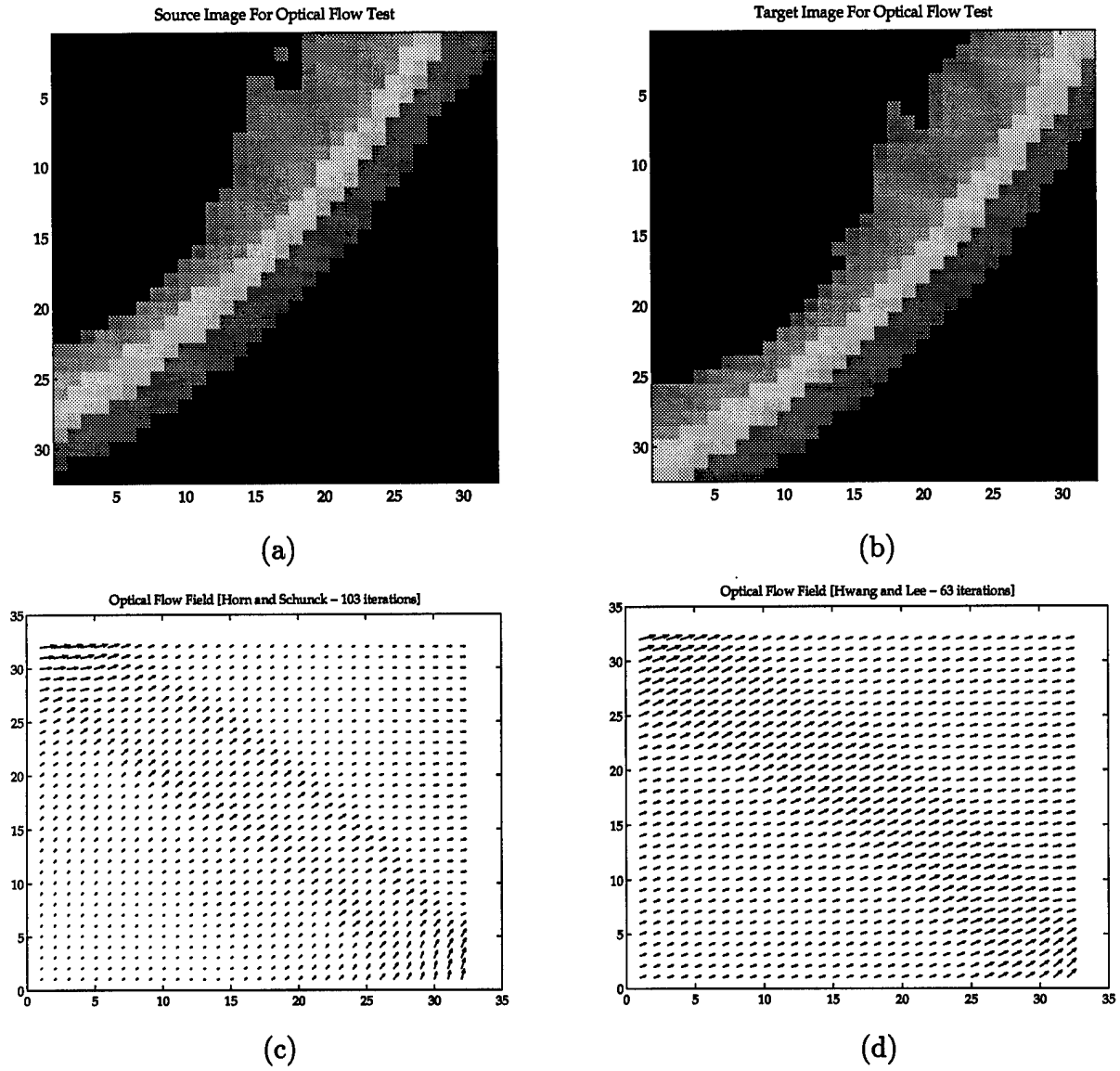

Figure 24 Comparison of two optical flow computation methods for image contour tracking. (a) Original image (b) original image shifted down and to the right by 10 pixels (c) Horn and Schunck gradient method (d) Hwang and Lee multiresolution method.

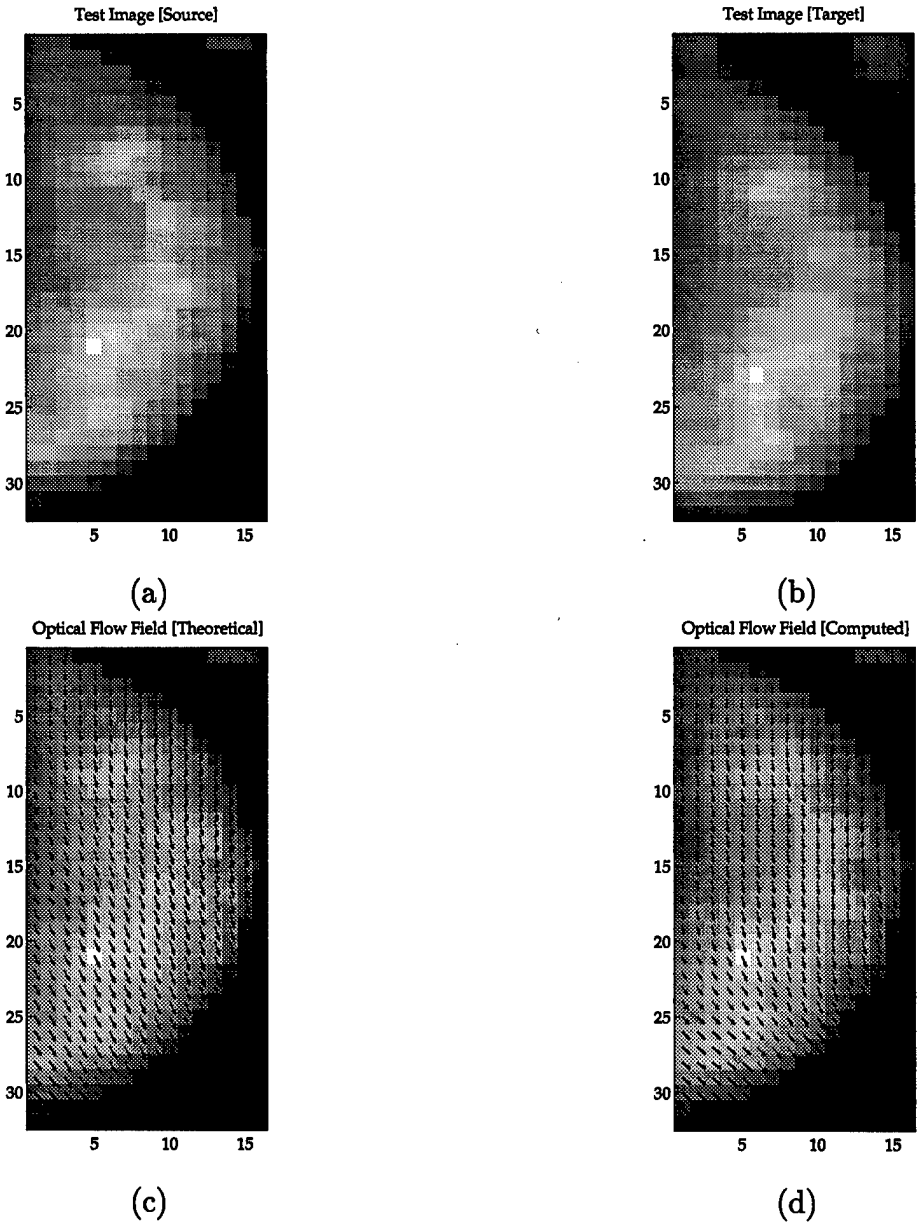

Figure 25 Comparison of computed optical flow with true optical flow. (a) Source image (b) target image (c) actual optical flow field (d) computed optical flow field using Hwang and Lee multiresolution method.

each registration case are arranged from (a) to (d) by date of screening in ascending order. Figures 27 and 28 are examples of the Gaussian and Laplacian pyramids constructed for each of the images in preparation for the alignment process. All images have been enhanced using histogram equalization to make internal structure easier to identify.

4.2.2 Results Format. The results of each registration set are displayed in a four-panel graphic. The upper left and right panels show the source and target images, respectively. The bottom left panel shows the final optical flow field for level three of the Gaussian pyramid. This level was chosen primarily because it is easy to visualize on the printed page. Figure 17 shows what all four optical flow levels look like for an example registration session. The Laplacian image for the first pyramid level is included to help validate the results of the alignment. Since Laplacian images typically enhance structural features at the appropriate scale, they are useful in matching features between two images and thus evaluating registration performance.

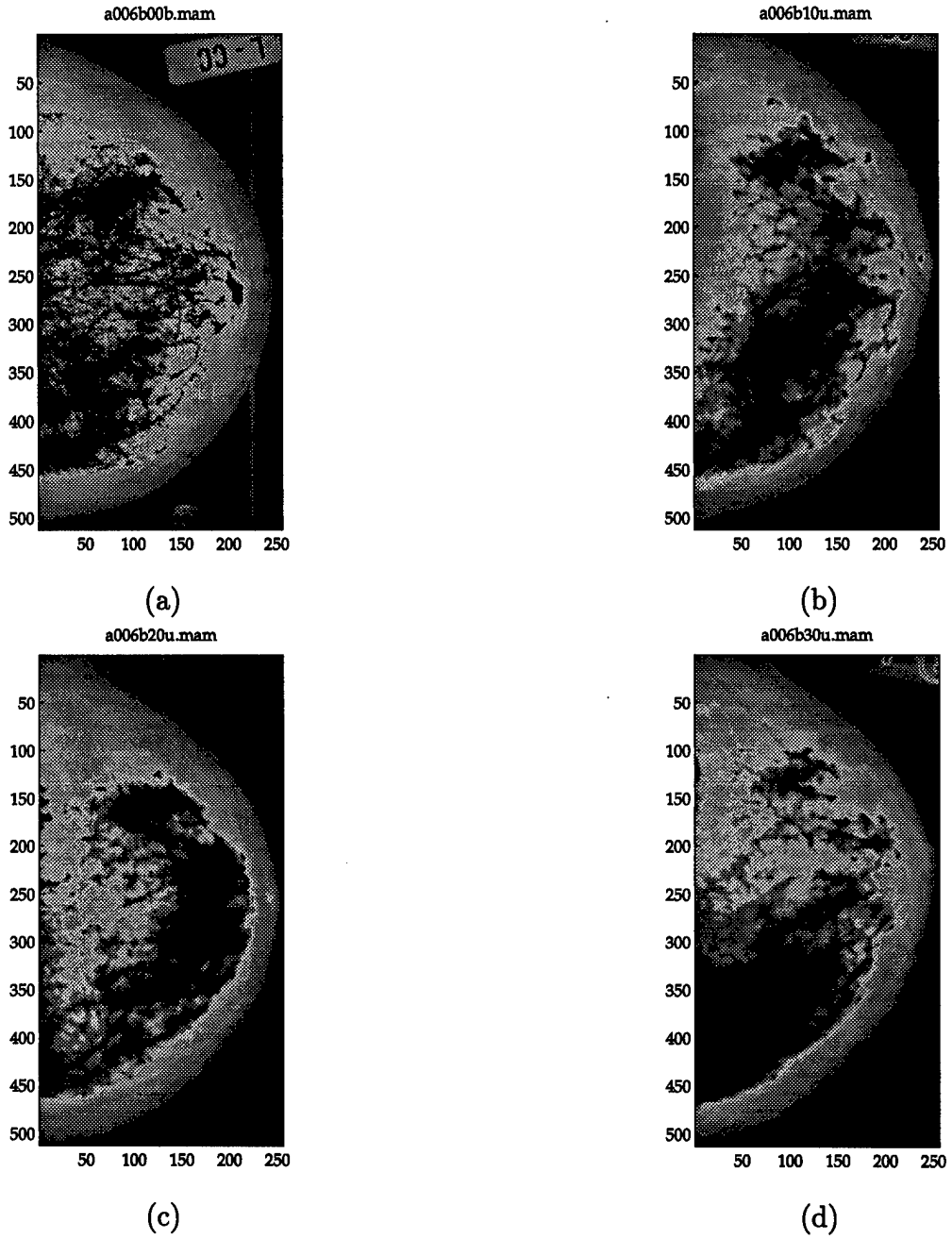

Figure 26 Temporal sequence of four mammograms taken during different screenings. These images are used for individual two-image matches in the next three case studies. All images are craniocaudal views of the left breast. The sequence (a)-(d) represents the order in which the mammograms were taken, with (a) being the earliest and (d) being the latest.

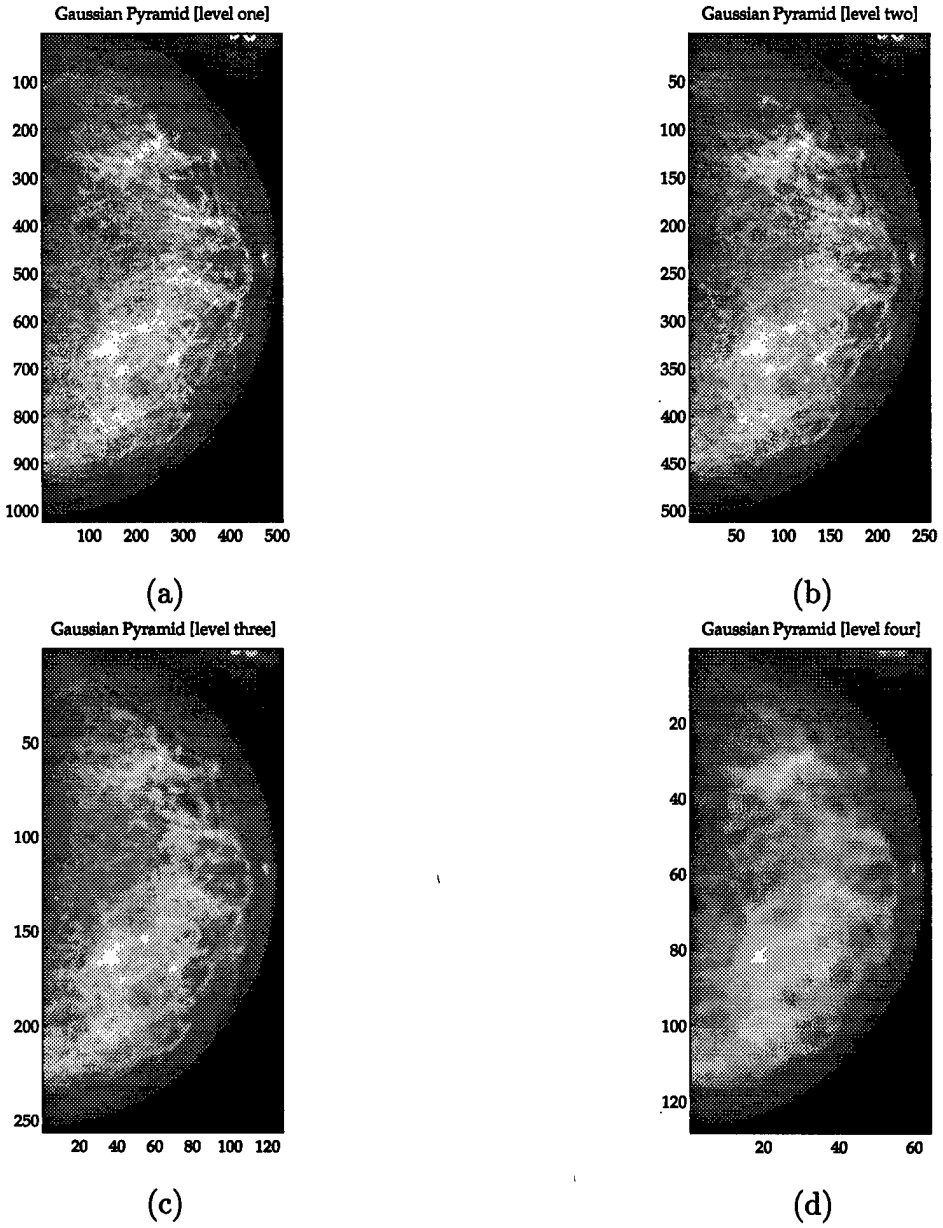

Figure 27 Gaussian pyramid constructed from original mammogram [σ=1.5]. (a) Base image decimated X 4 (b) second tier decimated X 8 (c) third tier decimated X 16 (d) fourth tier decimated X 32.

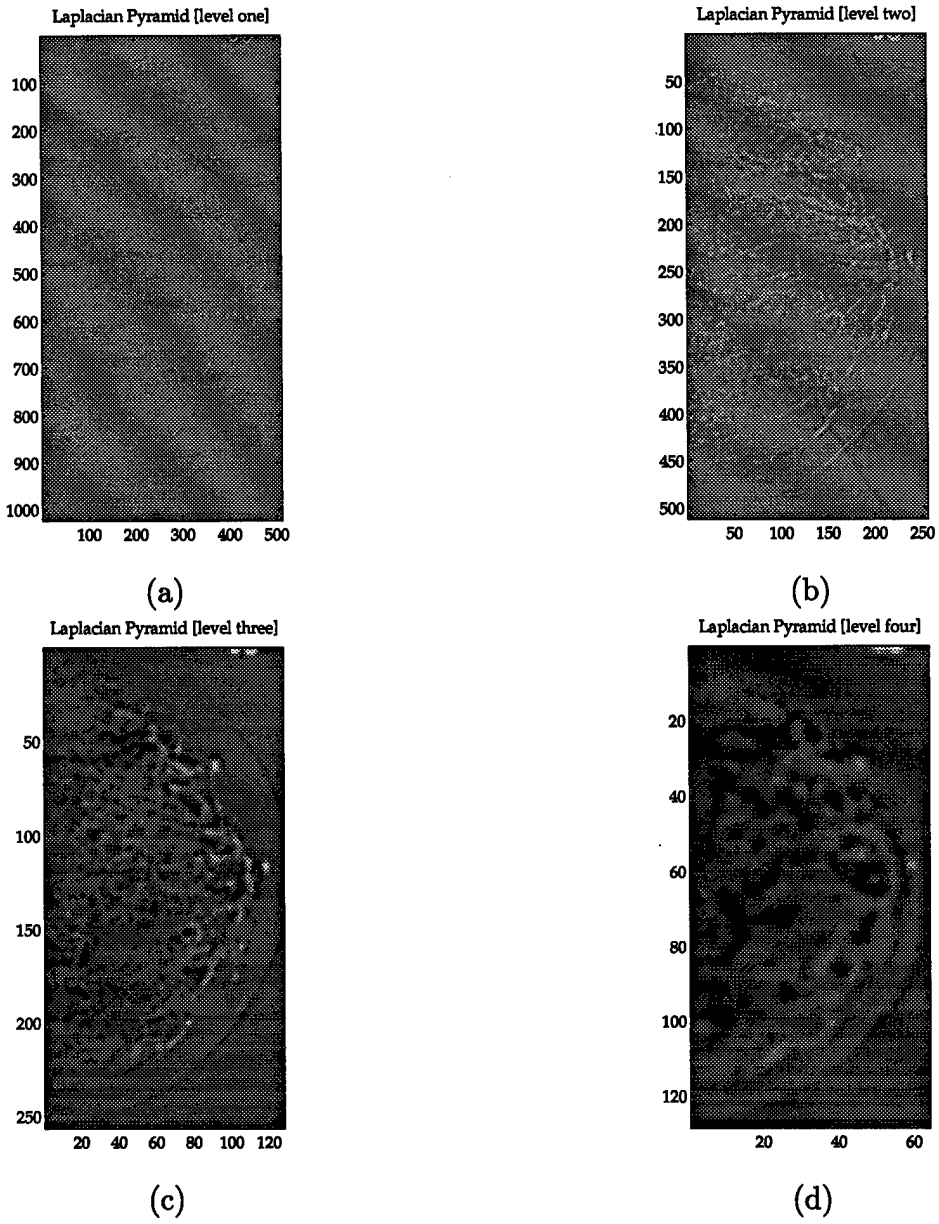

Figure 28 Laplacian pyramid constructed from original mammogram [σ=1.5]. (a) Base image decimated X 4 (b) second tier decimated X 8 (c) third tier decimated X 16 (d) fourth tier decimated X 32.

4.2.3 Registration Case 1.

4.2.3.1 Key Factors. Figure 26 displays the four mammograms comprising registration case 1. All images are craniocaudal (CC) views. The global alignment stage is not required for these four images due to the absence of any significant translation or rotation difference between them.

4.2.3.2 Registration Results. The registration system has no difficulty lining up the breast outline in any of the three image sets. Also, the internal structures (based on intensity characteristics only) correspond well between images. Case 1.1 shows the most difference in the upper third of the images. The computed optical flow field is particularly prominent in that region and weak everywhere else. The flow field in case 1.2 clearly demonstrates the ability of the system to detect translational motion between two images. The smooth vertical flow is consistent with a downward shift in the target image as can be readily by comparing the two breast outlines. Case 1.2 presents a challenge because it is not at all clear whether the dark patch in the lower left quadrant is due to tissue compression of an artifact of poor imaging. Since the registration procedure cannot differentiate either, it attempts to map the dark region in the source and target images. The resulting warped image displayed in panel (d) matches up well in the upper half of the images. In each case, the system computed flow fields consisting of both linear (translational) and non-linear (distortion) components. It is precisely this ability to deal with regional distortion differences, such as compression and expansion, that makes the approach so appealing and potentially useful.

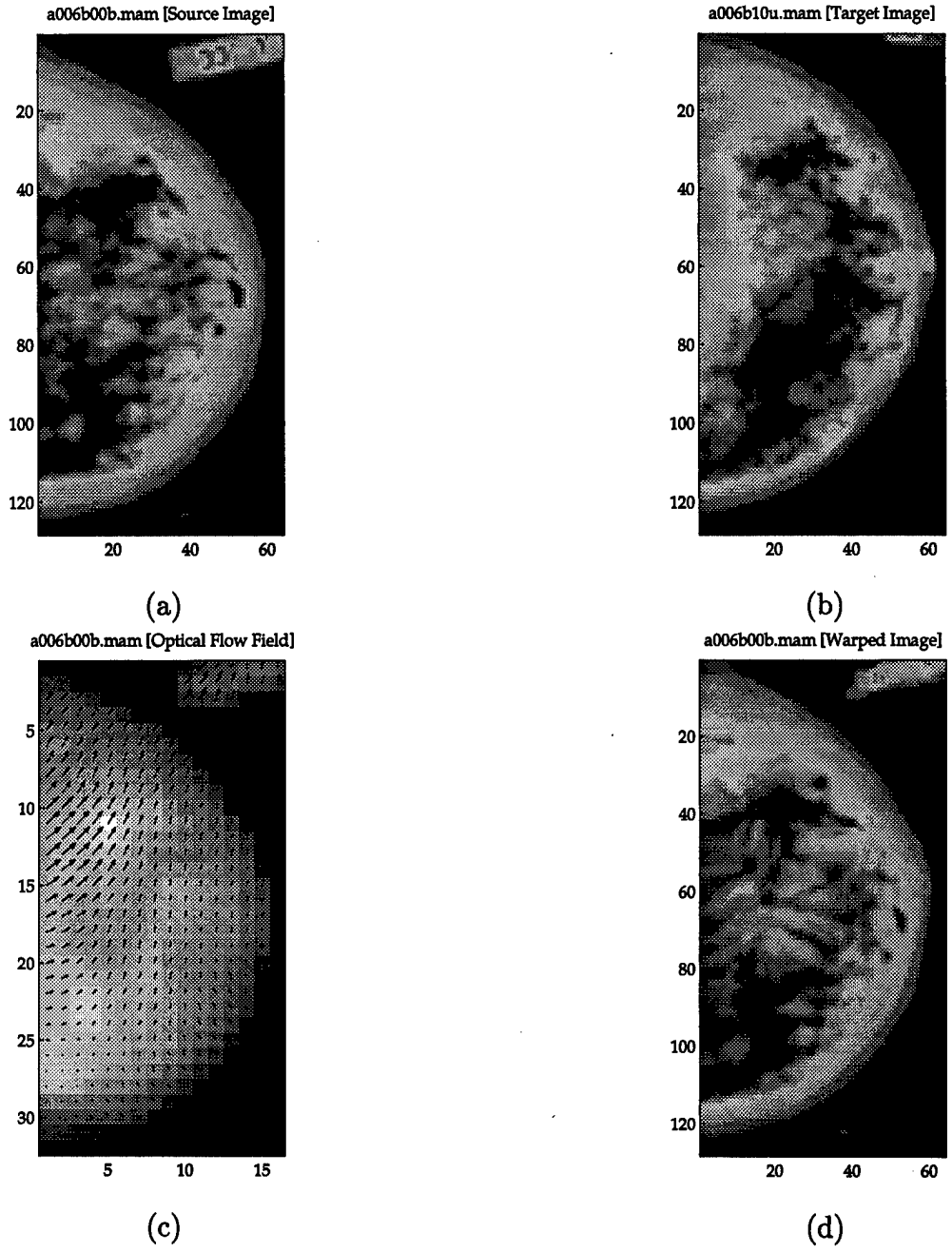

Figure 29 Case 1.1 Registration of two mammograms taken at different times [craniocaudal view]. The optical flow field shown corresponds to level 2 of the Gaussian pyramid to facilitate viewing (a) Mammogram from previous screening (b) mammogram from current screening (c) optical flow field calculated from source image [in upper left panel] to target image [upper right panel] (d) mammogram from current screening.

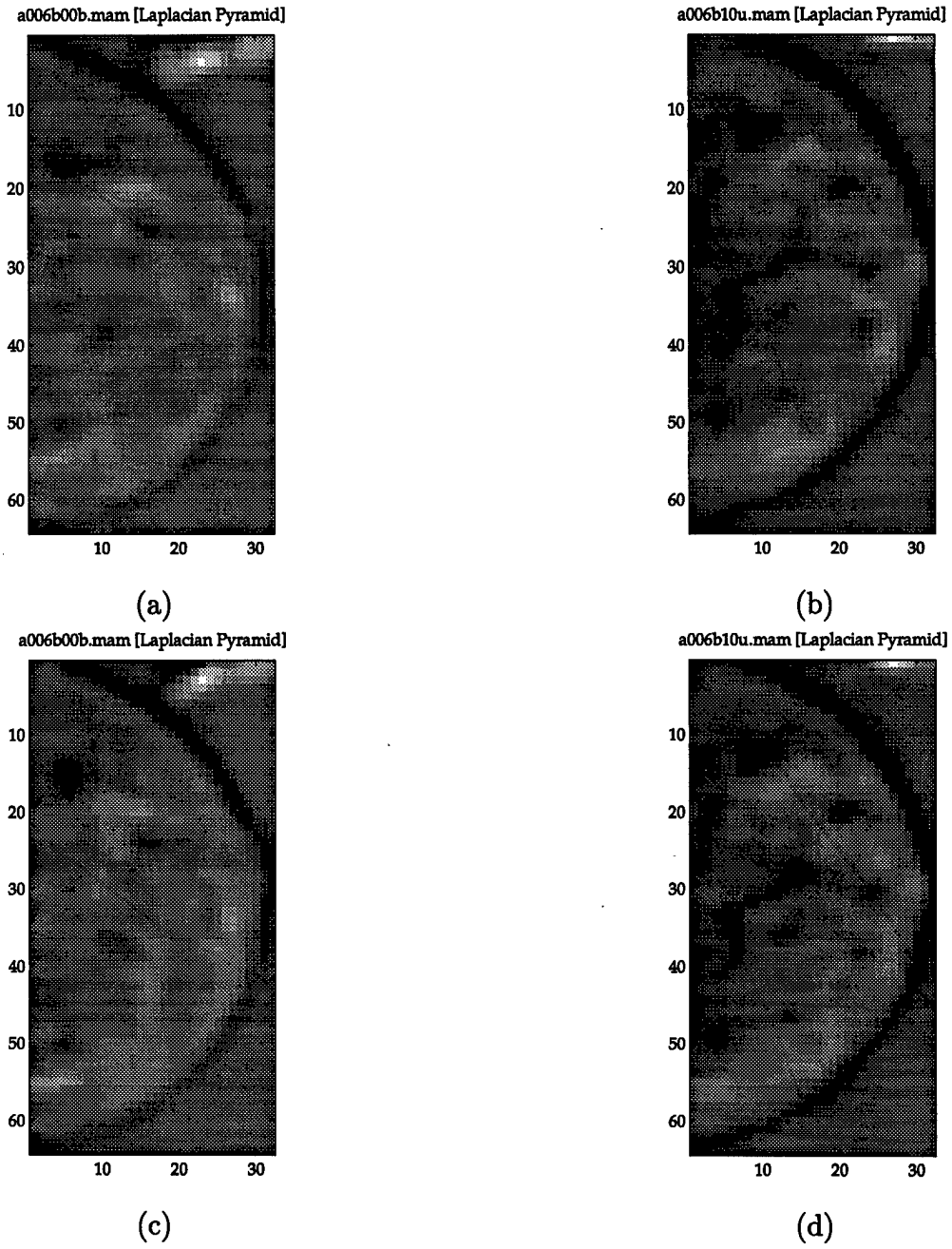

Figure 30 Case 1.1 Laplacian images of the warped and target images. (a) Source image (b) target image (a) warped image from source (b) target image.

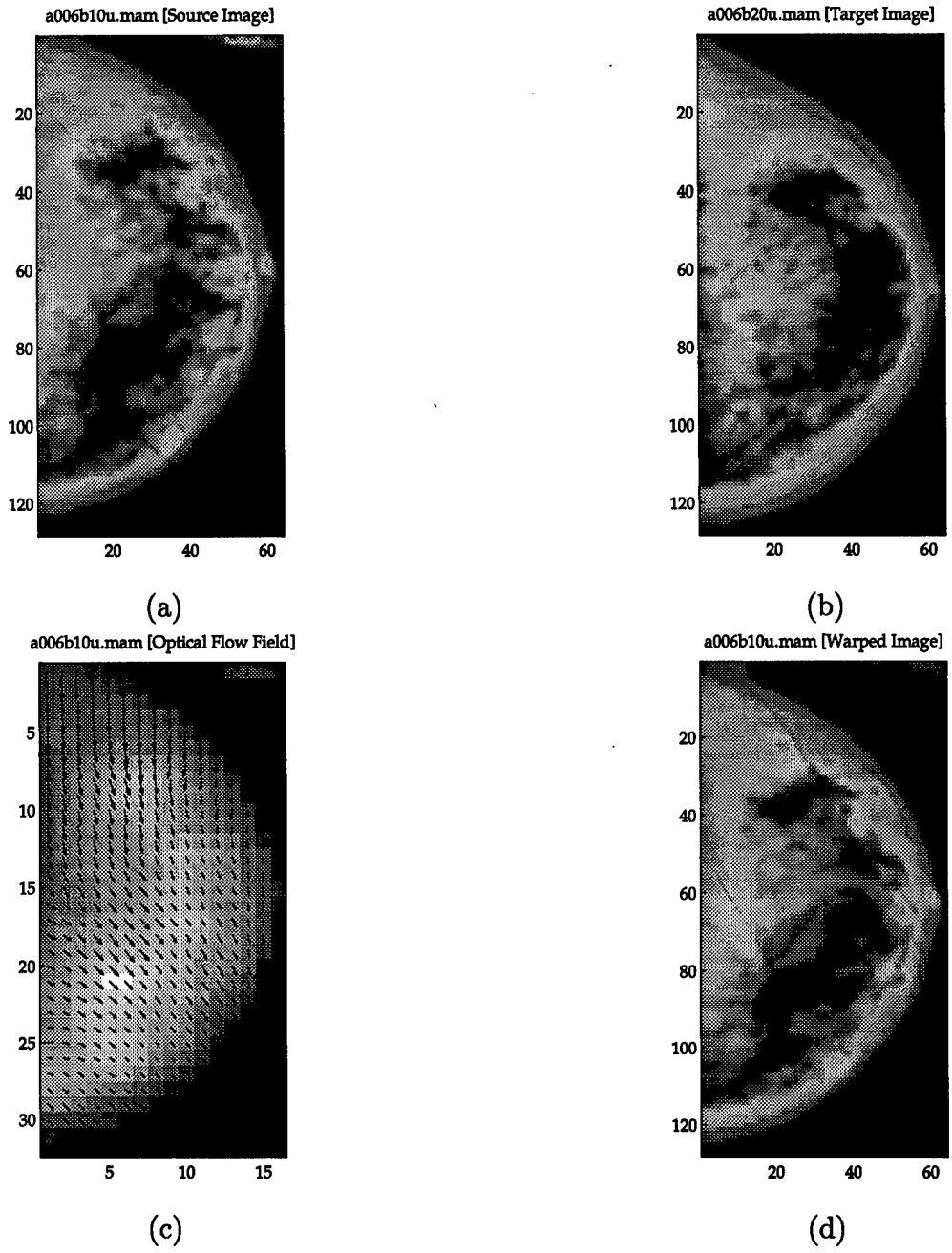

Figure 31 Case 1.2 Registration of two mammograms taken at different times [craniocaudal view]. The optical flow field shown corresponds to level 2 of the Gaussian pyramid to facilitate viewing (a) Mammogram from previous screening (b) mammogram from current screening (c) optical flow field calculated from source image [in upper left panel] to target image [upper right panel] (d) mammogram from current screening.

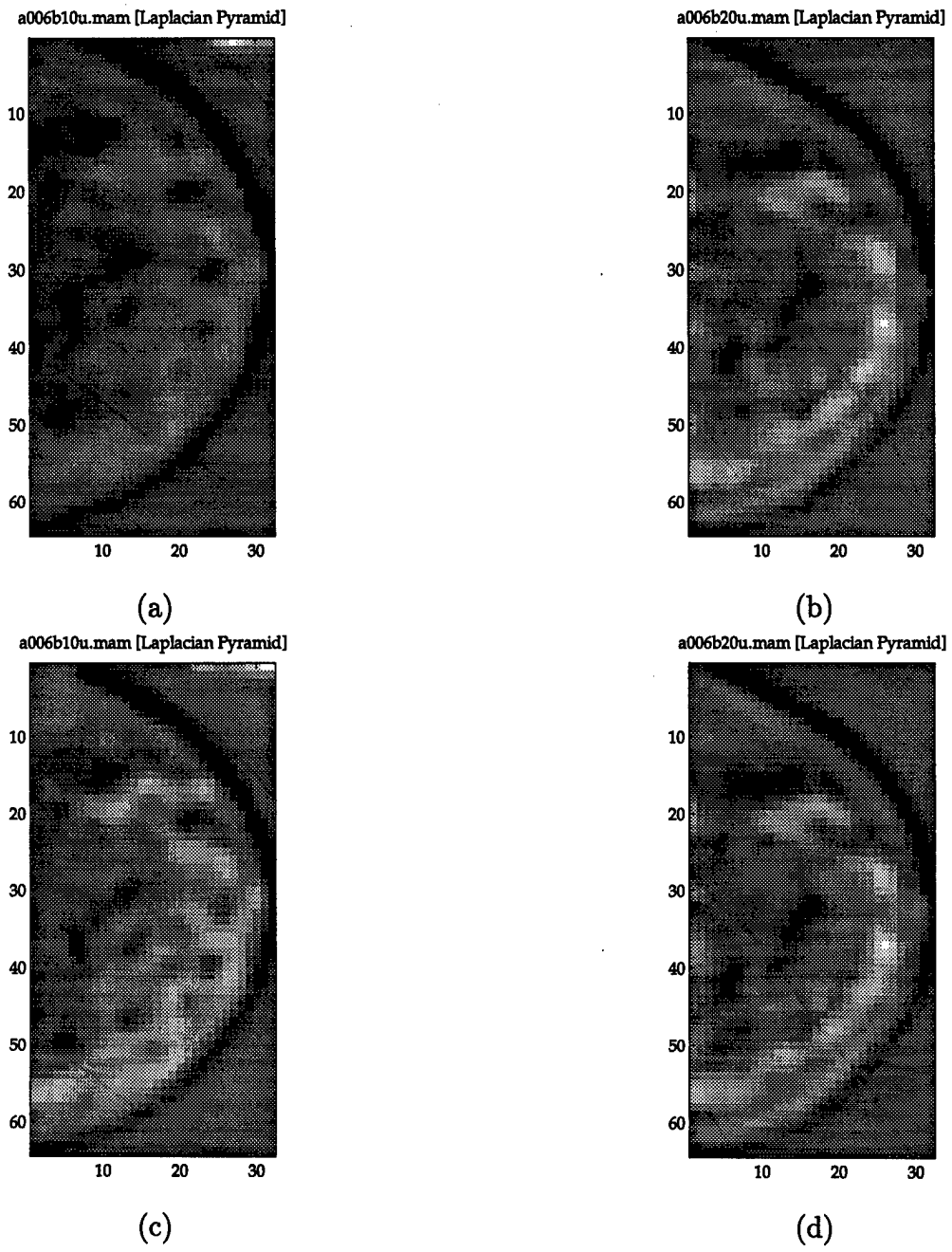

Figure 32 Case 1.2 Laplacian images of the warped and target images. (a) Source image (b) target image (a) warped image from source (b) target image.

4.2.4 Registration Case 2.

4.2.4.1 Key Factors. Figure 35 portrays the four mammograms used for registration case 2. Whereas the previous sets involved the craniocaudal view, case 2 deals with images taken from the medial-lateral oblique (MLO) view. In most MLO views, the pectoral wall can be clearly seen and can serve as an excellent registration landmark. A significant vertical shift is noticeable between the source and target images. This translation was not adjusted by the alignment module in order to assess the ability of the system to include such a shift in the computed optical flow field.

4.2.4.2 Registration Results. In case 2.1, the pectoral wall protrudes deeper in the target image than it does in the source image. The computed flow field easily detects this strong intensity shift as seen in the strong translational response in the upper left of the flow field. The obvious global misalignment in case 2.1 was purposely not handled by the alignment module to demonstrate the ability of the multiresolution algorithm to resolve large intensity shifts between images. The computed flow displays a strong vertical component in an attempt to compensate for the significant downward translation from source to target image. Closer inspection of the flow field shows that the algorithm is able to deal with both the relative vertical shift and inward compression as seen in the center right portion of the flow field.

Case 2.2 is instructive because it shows how the system reacts when a significant portion of the source-target pair exhibit only minor differences, while elsewhere large differences are visible. As expected, the computed flow field is weak between the highly similar regions and strong between the regions exhibiting large intensity differences. Case 2.3 requires a large vertical downward shift and displacement of the pectoral wall to the left.

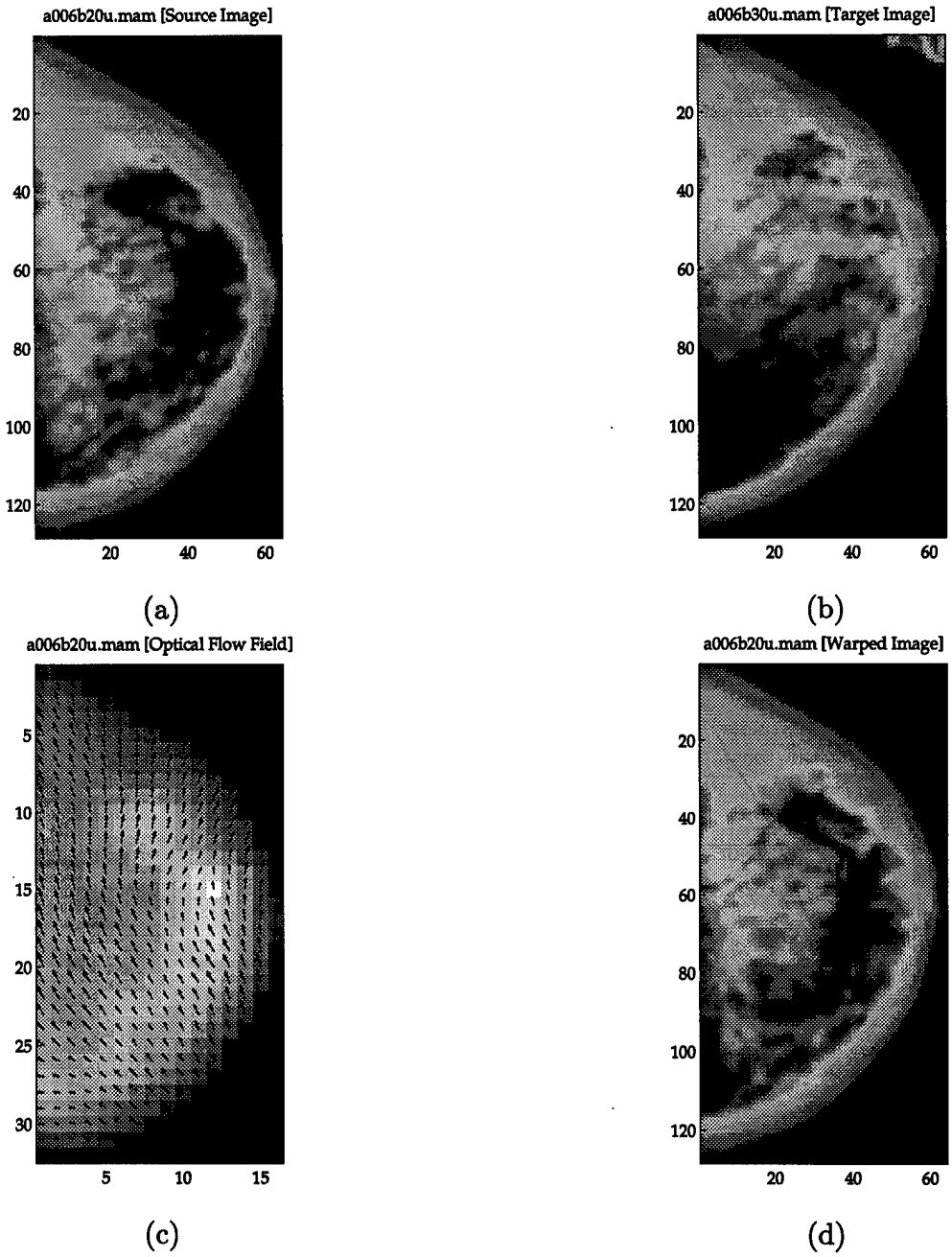

Figure 33 Case 1.3 Registration of two mammograms taken at different times [craniocaudal view]. The optical flow field shown corresponds to level 2 of the Gaussian pyramid to facilitate viewing (a) Mammogram from previous screening (b) mammogram from current screening (c) optical flow field calculated from source image [in upper left panel] to target image [upper right panel] (d) mammogram from current screening.

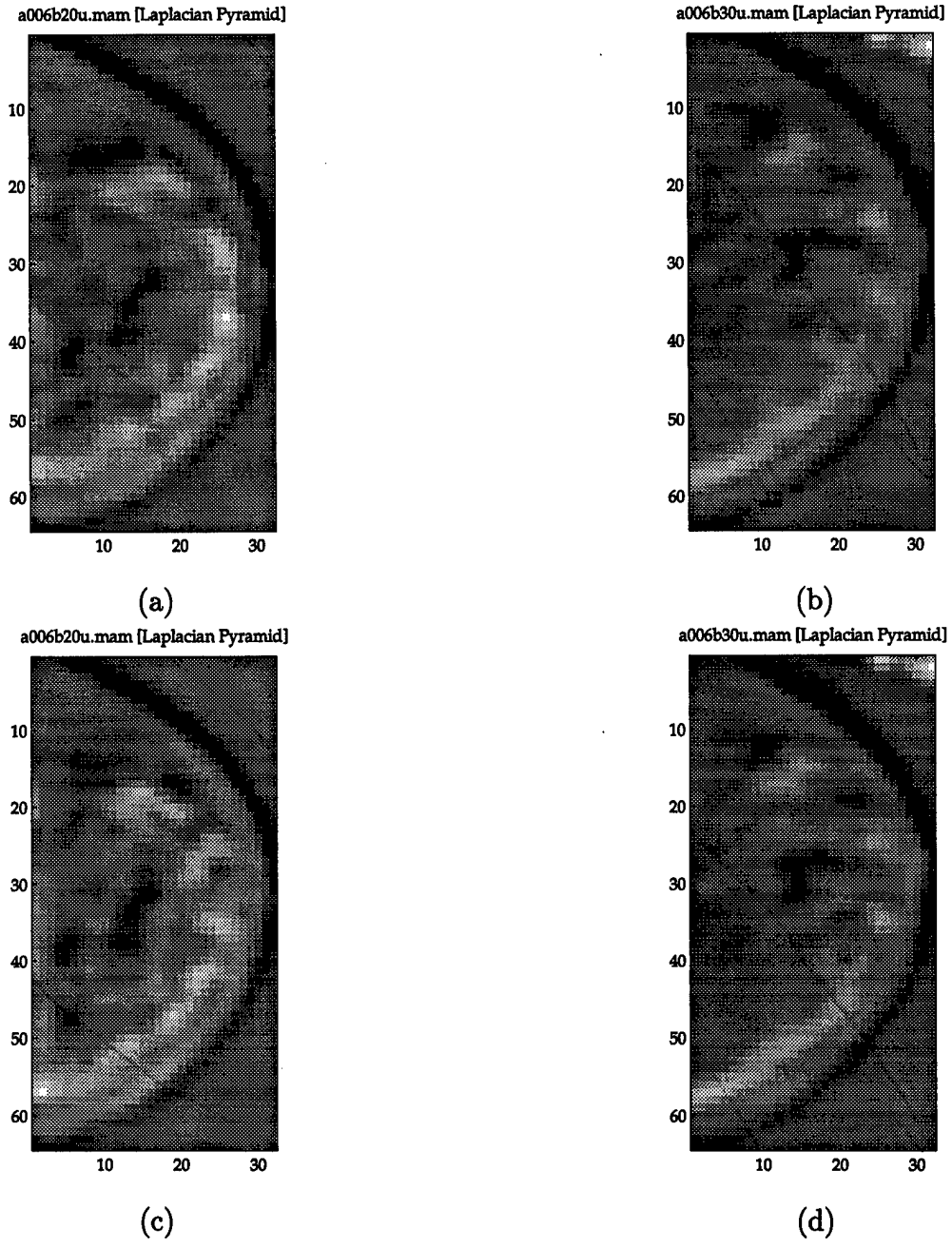

Figure 34 Case 1.3 Laplacian images of the warped and target images. (a) Source image (b) target image (a) warped image from source (b) target image.

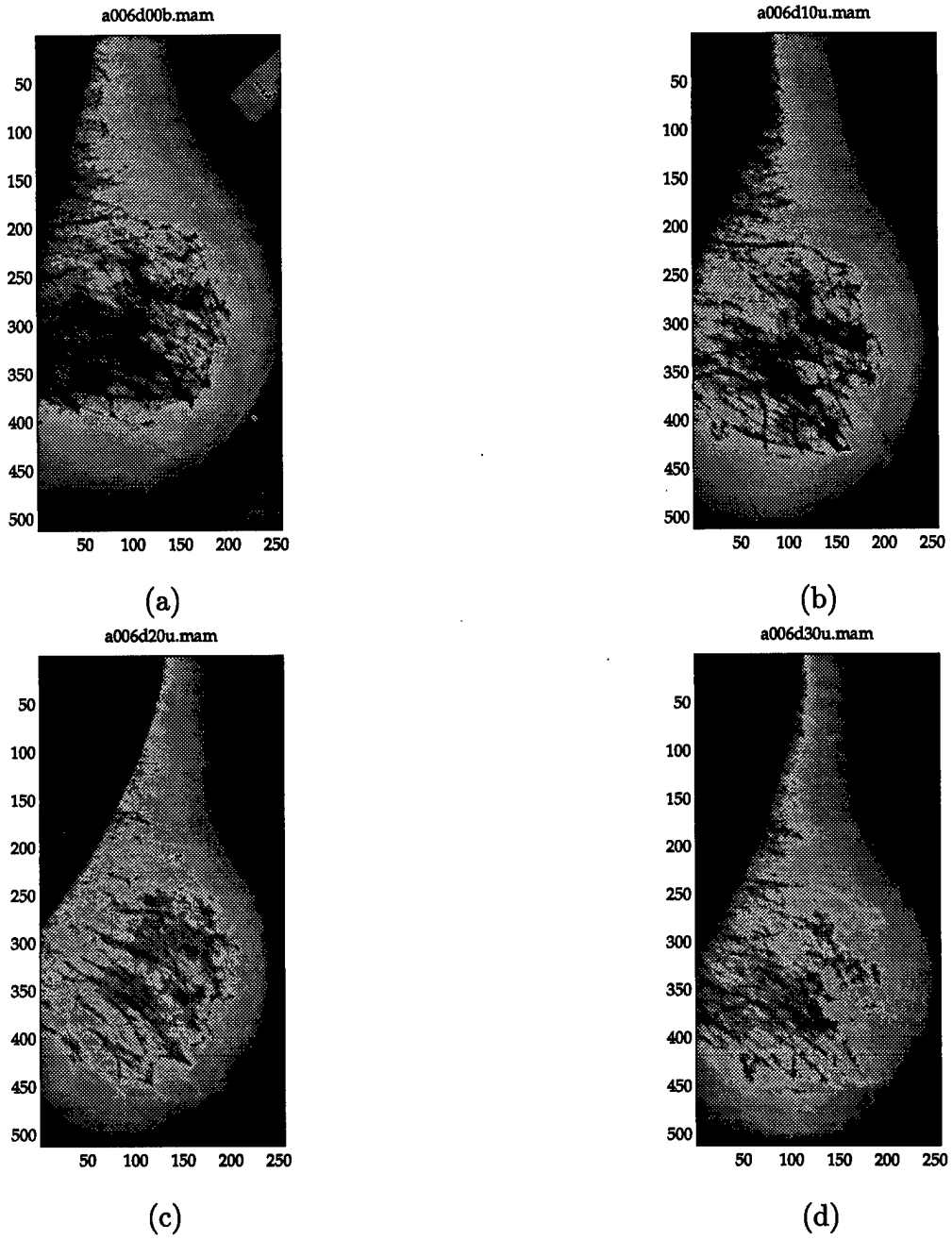

Figure 35 Temporal sequence of four mammograms taken during different screenings. These images are used for individual two-image matches in the next three case studies. All images are medial-lateral oblique views of the left breast. The sequence (a)-(d) represents the order in which the mammograms were taken, with (a) being the earliest and (d) being the latest.

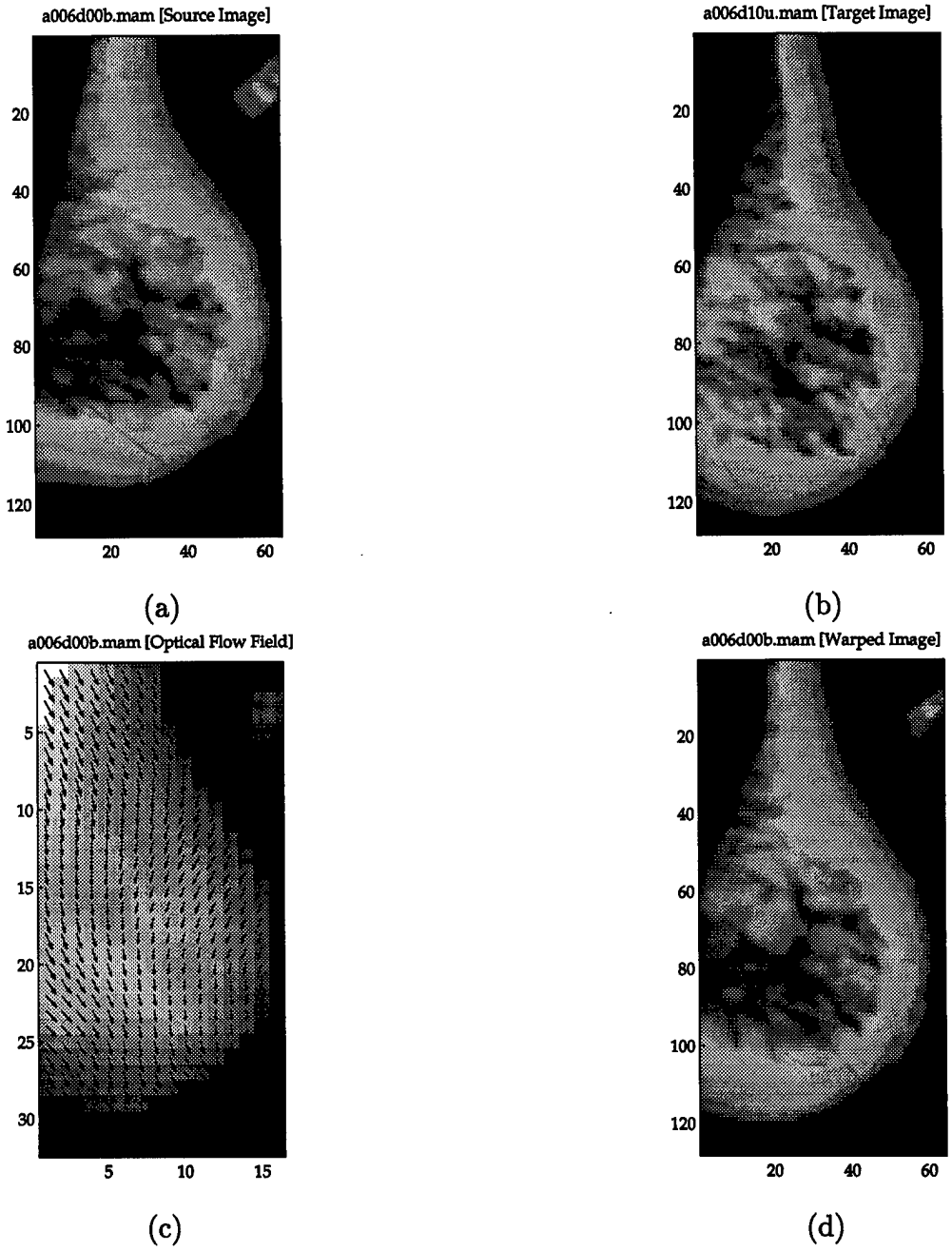

Figure 36 Case 2.1 Registration of two mammograms taken at different times [mediolateral oblique view]. The optical flow field shown corresponds to level 2 of the Gaussian pyramid to facilitate viewing (a) Mammogram from previous screening (b) mammogram from current screening (c) optical flow field calculated from source image [in upper left panel] to target image [upper right panel] (d) mammogram from current screening.

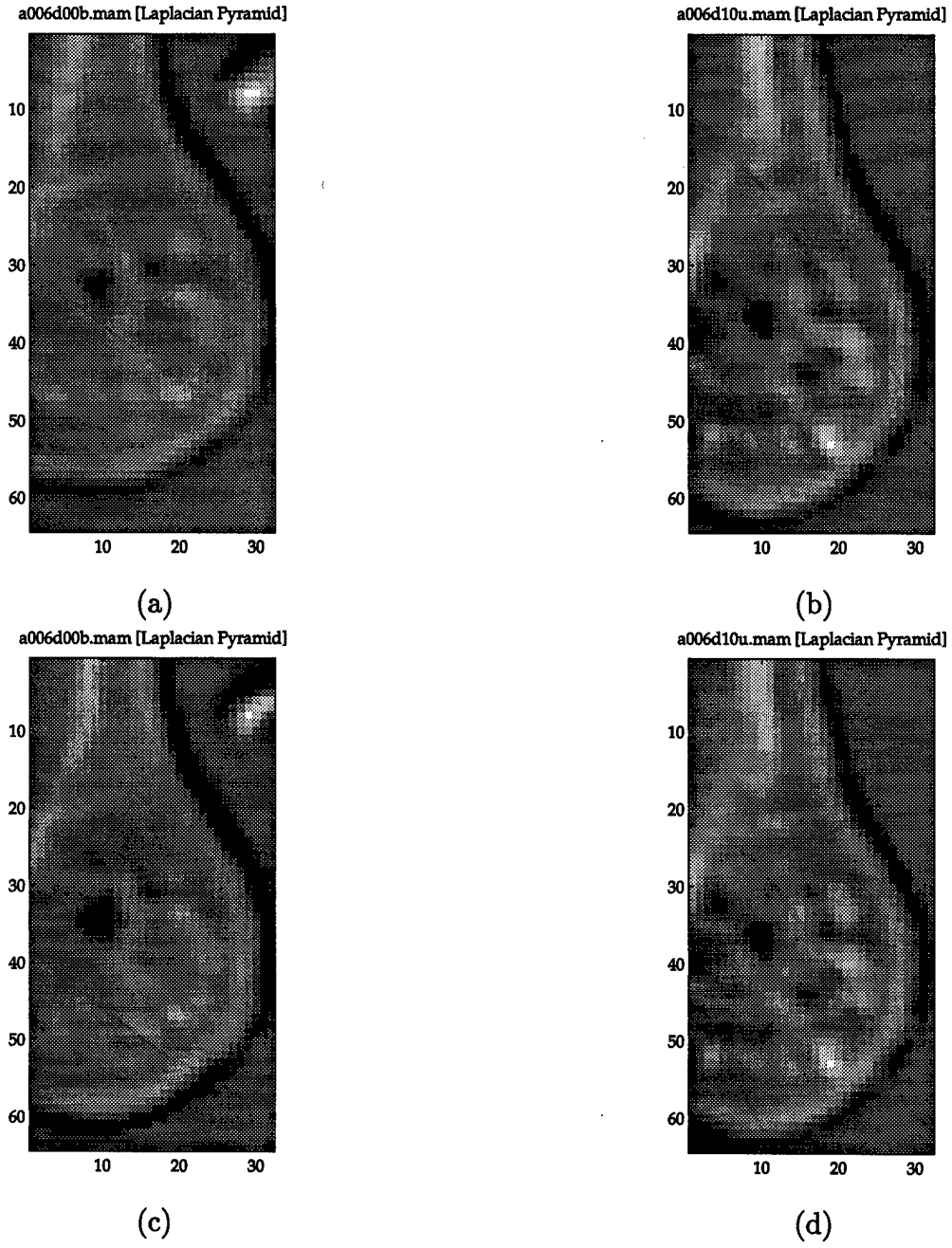

Figure 37 Case 2.1 Laplacian images of the warped and target images. (a) Source image (b) target image (a) warped image from source (b) target image.

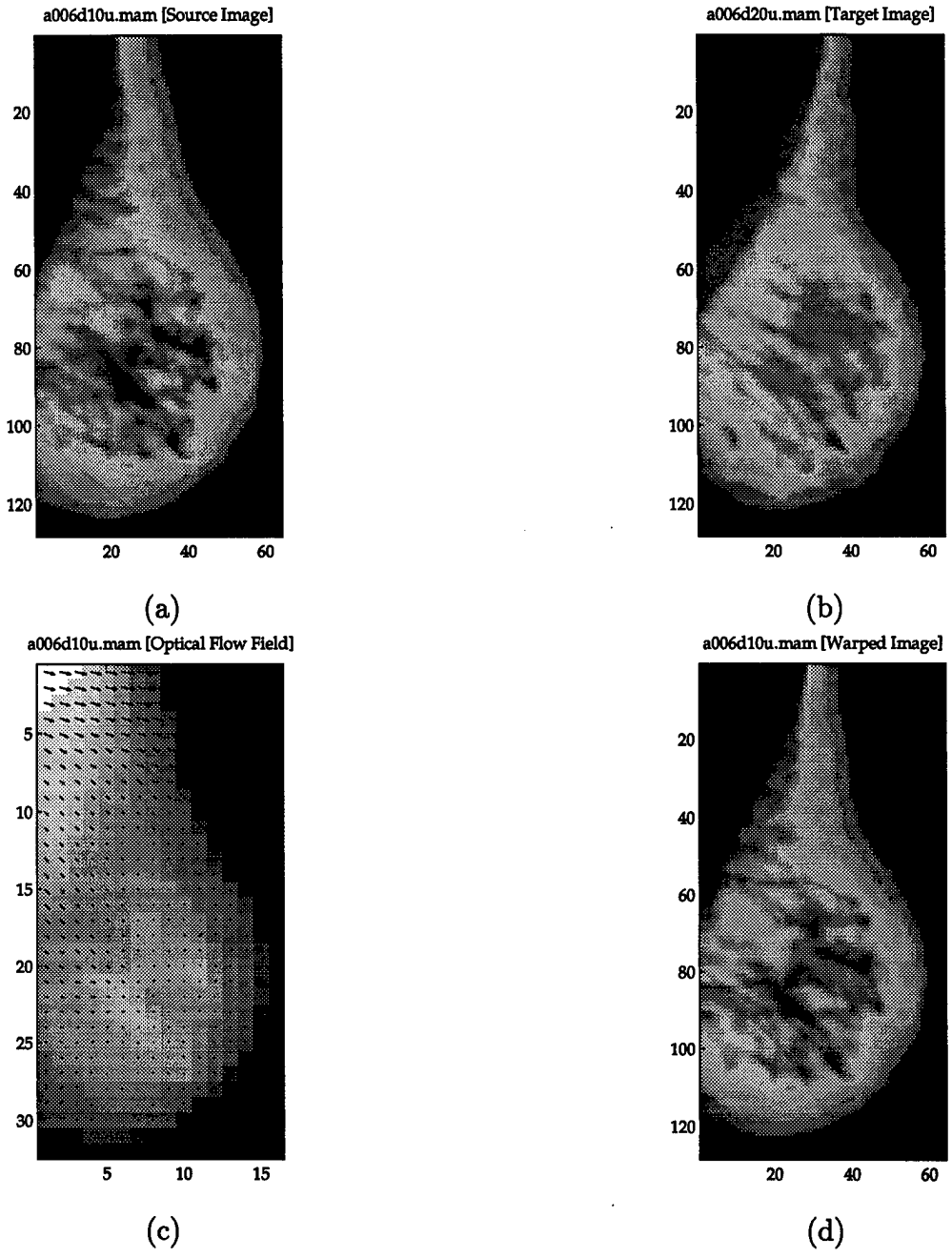

Figure 38 Case 2.2 Registration of two mammograms taken at different times [mediolateral oblique view]. The optical flow field shown corresponds to level 2 of the Gaussian pyramid to facilitate viewing (a) Mammogram from previous screening (b) mammogram from current screening (c) optical flow field calculated from source image [in upper left panel] to target image [upper right panel] (d) mammogram from current screening.

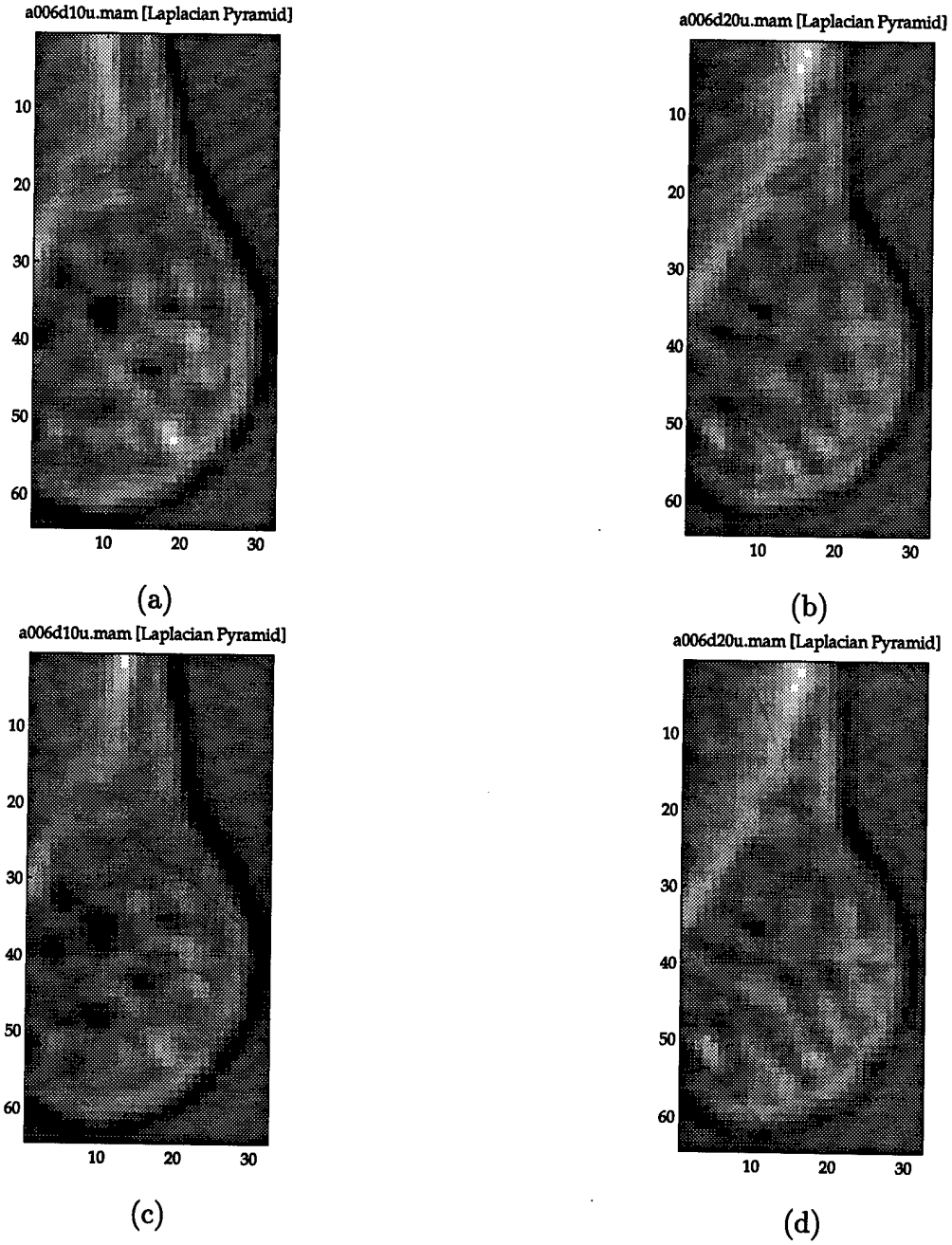

Figure 39 Case 2.2 Laplacian images of the warped and target images. (a) Source image (b) target image (a) warped image from source (b) target image.

Table 6 summarizes results for both case 1 and case 2 registration sets. The similarity metric between images is a sum of squared difference taken between each pixel intensity value in the first image and the corresponding pixel intensity value in the second image. Difference 1 measures the total intensity difference between the source and target image pair. The second measures the difference between the source and the warped image obtained from the source image, while the third measures the difference between the warped and target images. The pattern is clear: in each case, the difference between warped and target image is less than half the difference between source and target image pairs. This result shows that the match between warped and target images is better than between the original source-target image pair.

4.3 Summary

This chapter presents results obtained from test case simulations and the registration of historical mammogram sets. The optical flow produced during the testing phase corresponded very well with expected test results. The multiresolution approach in general proved superior to the single image method by achieving a higher degree of consistency and executing much faster. Acceptable optical flow estimates were obtained after one relaxation sweep (approximately 50 iterations).

Results obtained from registering actual mammogram images were consistent with expected results.

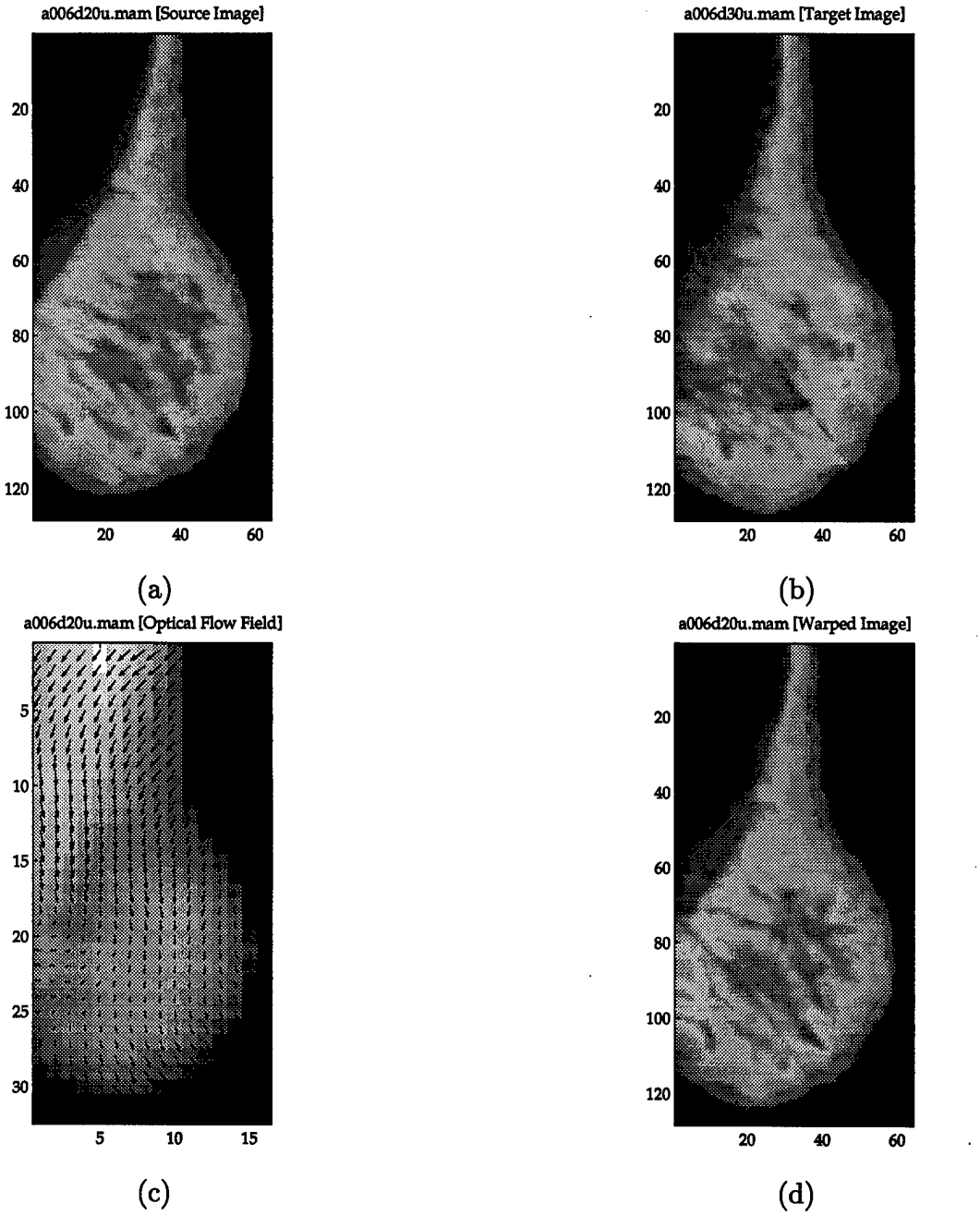

Figure 40 Case 2.3 Registration of two mammograms taken at different times [mediolateral oblique view]. The optical flow field shown corresponds to level 2 of the Gaussian pyramid to facilitate viewing (a) Mammogram from previous screening (b) mammogram from current screening (c) optical flow field calculated from source image [in upper left panel] to target image [upper right panel] (d) mammogram from current screening.

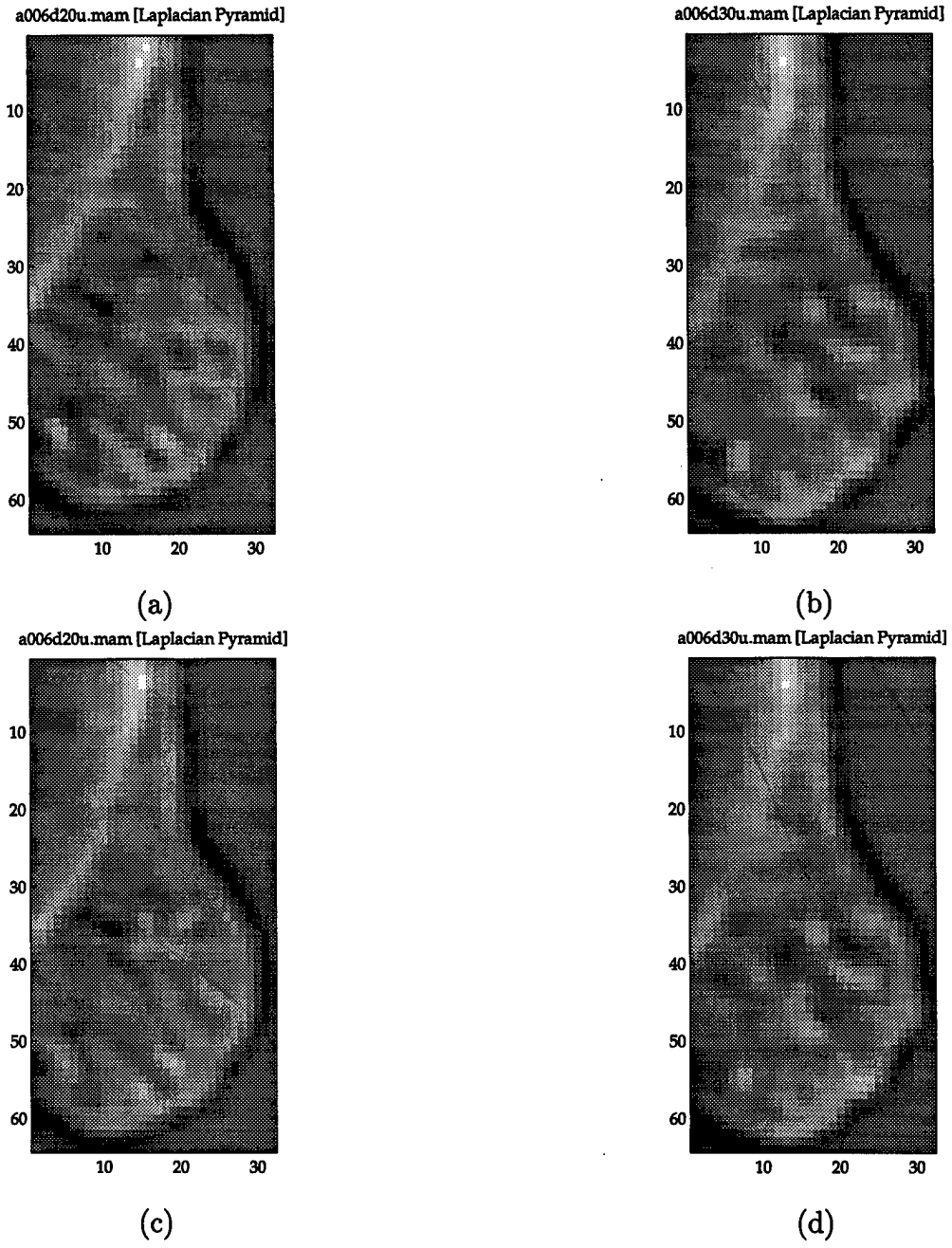

Figure 41 Case 2.3 Laplacian images of the warped and target images. (a) Source image (b) target image (a) warped image from source (b) target image.

Registration Results Summary				
Case/Set	Iterations	Difference 1	Difference 2	Difference 3
1.1	55	6.04	4.04	2.9
1.2	56	4.85	3.63	2.01
1.3	51	5.25	3.81	2.17
2.1	38	5.00	3.04	2.30
2.2	34	3.31	2.15	1.40
2.3	50	3.54	2.70	1.33

Table 6 Summary of registration statistics. The first the difference between original image pair. The second is the between source image and warped image. The third is the difference between warped image and target image. All difference measures are sum of squares.

V. Conclusion

This chapter summarizes the proposed registration method, discusses contributions, and suggests possible avenues for future research.

5.1 Summary

Breast cancer is lethal disease, indiscriminately afflicting nearly two hundred thousand women in this country each year. Early detection of suspected cancerous growth is an important weapon in the fight against this deadly killer. Today's mammography screening procedures provide an effective means toward this end but in general fail to achieve the desired level of detection accuracy. Radiologists typically compare mammograms taken at different times to improve the likelihood that a cancer will be noticed. Although computer-aided detection (CADx) are being developed to help the radiologist make a more informed decision, current systems are generally limited to single-image analysis.

The image registration system developed in this thesis attempts to bridge the gap between the needs of the radiologist during a mammography screening and the capabilities of an automated assistant. Its primary purpose is to align two mammograms of the same breast so that the radiologist can make a direct comparison between a time sequence of images. Since it is often very difficult to establish structural features in the image pair to facilitate a mapping between them, this system is designed not to rely on the availability of such landmarks. Instead, the proposed system compares regional intensity values and calculates the apparent motion between source and target image. This computed optical flow field then forms the basis for a non-linear mapping between the two images. This transformation results in a warped version of the original source image which can be directly compared with the target image. Finally, the underlying architecture of the registration system is

based on a multiresolution computational model, significantly enhancing both the accuracy and efficiency of the matching process.

The proposed system incorporates features to provide a robust registration result. Since many image pairs exhibit significant differences in the positioning and orientation of the breast structure, a global alignment module is included to correct for such differences prior to computing the mapping between the images. This module relies on a genetic algorithm to quickly and accurately search for an optimal global alignment. It requires no user intervention to perform the alignment task. A second module is provided to perform critical segmentation duties. This segmentation subsystem uses a neural network to partition each image into regions of high homogeneity. The module is designed to carry out two different segmentation tasks: 1) extraction of the breast structure from the surrounding background, and 2) partitioning on the breast structure itself into regions of similar intensity. The segmented image can often help the radiologist interpret an image and facilitate identification of different tissue types.

The initial performance of the system was evaluated on two sets of images taken of the same breast. Each set of images represented a historical sequence of mammograms taken at four different screenings. One set consisted of four craniocaudal views, while the other presented the complementary mediolateral oblique views. Several test cases where constructed and executed to evaluate system performance. Then a mapping between pairs of images (source and target) in each set was computed to obtain a warped source image. The system performed well even in the face of major differences between images. In all cases the breast contour of the warped and target images matched up very closely. The system demonstrated its proficiency at coping with distortion such as compression and expansion by generating a non-linear optical flow field. In all cases, the sum-squared intensity difference between warped and target image pairs was always considerably less than the original difference between source and target images.

5.2 Contributions

As a part of the effort to develop the mammogram registration system, three specific contributions can be highlighted:

1. Application of optical flow and multiresolution computation to solve the mammogram correspondence problem
2. Application of a genetic algorithm to find an optimal set of parameters for an affine transformation
3. Development of a segmentation method based on the Kohonen neural network and multiresolution image decomposition

5.3 Recommendations

The research conducted in preparing this thesis does not purport to solve the mammogram correspondence problem. The task of bringing two images into common alignment—especially images having significant differences—is a complex and perhaps unsolvable problem. The work presented here attempts only to provide some fresh ideas that might stimulate even better approaches. The system developed in this thesis should be improved and expanded to directly address cancer detection. Further insight into the problem might lead to a system capable of flagging potential tissue abnormalities as its computes the optical flow field between two images. Much creative work remains toward the development of an intelligent, comprehensive approach to image comparison and abnormality detection.

Bibliography

1. Anandan, P. "A computational Framework and an Algorithm for the Measurement of Visual Motion," *International Journal of Computer Vision*, *2*(3):283–310 (January 1989).
2. Babaud, Jean, et al. "Uniqueness of the Gaussian Kernel for Scale-Space Filtering," *IEEE Transactions on Pattern Analysis and Machine Intelligence*, *8*(1) (January 1986).
3. Barron, J. L., et al. "Performance of Optical Flow Techniques," *International Journal of Computer Vision*, *12*(1):43–77 (1994).
4. Battiti, Roberto, et al. "Computing Optical Flow Across Multiple Scales: An Adaptive Coarse-to-Fine Strategy," *International Journal of Computer Vision*, *6*(2):133–145 (1991).
5. Bick, Ulrich, et al. "Automated Segmentation of Digitized Mammograms," *Acad Radiology*, *2*(1):1–9 (1995).
6. Black, Michael J. and P. Anandan. "The Robust Estimation of Multiple Motions: Parametric and Piecewise-Smooth Flow Fields," *Computer Vision and Image Understanding*, *63*(1) (January 1996).
7. Black, Michael J. and Allan D. Jepson. "Estimating Optical Flow in Segmented Images Using Variable-Order Parametric Models with Local Deformations," *IEEE Transactions on Pattern Analysis and Machine Intelligence*, *18*(10) (October 1996).
8. Bookstein, Fred. "Principal Warps: Thin-Plate Splines and the Decomposition of Deformations," *IEEE Transactions on Pattern Analysis and Machine Intelligence*, *11*(6):567–585 (June 1989).
9. Brown, Lisa. "A Survey of Image Registration Techniques," *ACM Computing Surveys*, *24*(4) (December 1992).
10. Burt, P. J. and E. H. Adelson. "The Laplacian pyramid as a Compact Image Code," *IEEE Transactions on Communications*, *31*(4):532–540 (April 1983).
11. Calway, A. D. and S. A. Krueger. "Estimating Disparity and Motion Using Multiresolution Fourier Analysis." *IEE Colloquium on Multiresolution Modelling and Analysis in image Processing and Computer Vision.* 1995.
12. Caves, R. G., et al. "Matching map features to synthetic aperture radar (SAR) images using template matching," *IEEE Transactions on Geoscience and Remote Sensing*, *13*(401-414) (1992).

13. Cheng, Kuo-Sheng, et al. "The Application of Competitive Hopfield Neural Network to Medical Image Segmentation," *IEEE Transactions on Medical Imaging*, *15*(4):560–567 (August 1996).

14. Cohen, Laurent D. and Isaac Cohen. "Finite-Element Methods for Active Contour Models and Balloons for 2-D and 3-D Images," *IEEE Transactions on Pattern Analysis and Machine Intelligence*, *15*(11):1131–1147 (November 1993).

15. Coppini, Giuseppe, et al. "Recovery of the 3-D Shape of the Left Ventricle from Echocardiographic Images," *IEEE Transactions on Medical Imaging*, *14*(2):301–317 (June 1995).

16. Davatzikos, Chris A. and Jerry L. Prince. "An active contour model for mapping the cortex," *IEEE Transactions on Medical Imaging*, *14*(1) (March 1995).

17. Dayhoff, Judith. *Neural Network Architectures*. International Thompson Computer Press, 1996.

18. Dinten, J. M., et al. "Opacities detection and characterization in mammograms using a bilateral comparison and local characteristics." *SPIE3034*. 1997.

19. Douglas, Craig C. "Multigrid Methods in Science and Engineering," *IEEE Computational Science and Engineering*, 55–68 (1996).

20. Durbin, Richard and David Willshaw. "An analogue approach to the travelling salesman problem using an elastic net method," *Nature*, *326*(14):689–691 (April 1987).

21. Enkelmann, W. "Investigations of Multigrid Algorithms for Estimation of Optical Flow Fields in Image Sequences," *Computer, Vision, Graphics, and Image Processing*, 150–177 (1988).

22. Fan, C. M., et al. "A New Image Motion Estimation Algorithm Based on the EM Technique," *IEEE Transactions on Pattern Analysis and Machine Intelligence*, *18*(3):348–352 (1996).

23. Fleet, D. and A. Jepson. "Computation of Component Image Velocity from Local Phase Information," *International Journal of Computer Vision*, *5*:77–104 (1990).

24. Friedland, N. and D.Adam. "Automatic Ventricular Cavity Boundary Detection from Sequential Ultrasound Images Using Simulated Annealing," *IEEE Transactions on Medical Imaging*, *8*(4):344–353 (December 1989).

25. Fuh, C. S. and P. Maragos. "Motion Displacement Estimation Using an Affine Model for Image Matching," *Optical Engineering*, *30*(7):881–887 (July 1991).

26. Geman, Stuart and Donald Geman. "Stochastic Relaxation , Gibbs Distributions, and the Bayesian Restoration of Images," *IEEE Transactions on Pattern Analysis and Machine Intelligence*, *6*(6):721–741 (November 1984).

27. Goldberg, David E. *Genetic Algorithms in Search, Optimization, and Machine Learning*. Addison-Wesley, 1989.

28. Gonzalez, Rafael C. and Richard E. Woods. *Digital Image Processing*. Addison-Wesley Publishing Company, 1992.

29. Hall, E. L. "A survey of preprocessing and feature extraction techniques for radiographic images," *IEEE Transactions on Computers* (September 1971).

30. Holland, John H. "Genetic Algorithms," *Scientific American*, 66–72 (July 1992).

31. Horn, Berthold K.P. and Brian G. Schunck. "Determining Optical Flow," *Artificial Intelligence, 17* (1981).

32. Hummel, R. A. and S. W. Zucker. "On the foundations of relaxation labeling processes," *IEEE Transactions on Pattern Analysis and Machine Intelligence, 5*:267–287 (1983).

33. Hwang, Shin H. and Sang U. Lee. "A Hierarchical Optical Flow Estimation Algorithm Based on the Interlevel Motion Smoothness Constraint," *Pattern Recognition, 26*(6) (1993).

34. Kallergi, Maria, et al. "Image Segmentation in Digital Mammography: Comparison of Local Thresholding and Region Grpwong Algorithms," *Computerized Medical Imaging and Graphics, 16*(5):323–331 (1992).

35. Kamel, M. S. and Shokri Z. Selim. "A Thresholded Fuzzy C-Means Algorithm For Semi-Fuzzy Clustering," *Pattern Recognition, 24*(9):825–833 (1991).

36. Kass, Michael, et al. "Snakes: Active Contour Models," *International Journal of Computer Vision*, 321–331 (1988).

37. Kobatake, Hidefumi, et al. "CAD system for full-digital mammography and its evaluation." *Proceedings of the SPIE3034*.

38. Kohonen, T. *Self-Organization and Associative Memory* (2 Edition). Springer-Verlag, 1988.

39. Kundel, Harold L. and George Revesz. "Lesion Conspicuity, Structured Noise, and Film Reader Error," *American Journal of Roentgenology, 126* (1976).

40. Lau, Tin-Kit and Walter F. Bischof. "Automated Detection of Breast Tumors Using the Asymmetry Approach," *Computers and Biomdical Research, 24*:273–295 (1991).

41. Lee, Jiann-Shu, et al. "Occluded Objects REcognition Using Multiscale Features and Hopfield Neural Network," *Pattern Recognition, 30*(1):113–122 (1997).

42. Lee, Kevin A. "Segmentation of Mammography Images Using Kohonen Self-Organizing Feature Maps." *Proceedings Eigth Midwest Artificial Intelligence and Cognitie Science Conference*, CF-97-01, edited by Jr. Eugene Santos. 41–46. May 1997.

43. Lin, Wei-Chung, et al. "Constraint Satisfaction Neural Networks for Image Segmentation," *Pattern Recognition*, *25*(7):679–691 (1992).

44. LLacer, Jorge, et al. "Representation of Medical Images By Visual Response Functions," *IEEE Engineering in Medicine and Biology*, 40–47 (March 1993).

45. Lobregt, Steven and Max A. Viergever. "A Discrete Dynamic Contour Model," *IEEE Transactions on Medical Imaging*, *14*(1):12–24 (March 1995).

46. Luettgen, Mark R., et al. "Efficient Multiscale Regularization with Applications to the Computation of Optical Flow," *IEEE Transactions on Image Processing*, *3*(1):41–63 (July 1994).

47. Mathews, John H. *Numerical Methods for Mathematics, Science, and Engineering*. Prentice Hall, 1992.

48. Mendez, Arturo J., et al. "Automatic detection of breast border and nipple in digital mammograms," *Computer Methods and Programs in Biomedicine*, *49*:253–262 (1996).

49. Meyer, Francois, et al. "Tracking Myocardial Deformation Using Phase Contrast MR Velocity Fields: A Stochastic Approach," *IEEE Transactions in Medical Imaging*, *15*(4):453–465 (August 1996).

50. M.L.Giger, et al. "Investigation of methods for the computerized detection and analysis of mammographic masses." *Proceedings of the SPIE1233*. 183–184. 1990.

51. Nagel, H. H. and W. Enkelmann. "An investigation of smoothness constraints for the estimation of displacement vector fields from image sequences," *IEEE Transactions on Pattern Analysis and Machine Intelligence*, *8*(5):565–593 (1986).

52. Poggio, Tomaso, et al. "Computational vision and regularization theory," *Nature*, *317*(26):314–319 (September 1985).

53. P.P.Raghu and B.Yegnanarayana. "Segmentation of Gabor-Filtered Textures Using Deterministic Relaxation," *IEEE Transactions on Image Processing*, *5*(12):1625–1635 (December 1996).

54. Ranade, S. and A. Rosenfeld. "Point pattern matching by relaxation," *Pattern Recognition*, *12*:269–275 (1980).

55. Ranganath, Surendra. "Contour Extraction from Cardiac MRI Studies Using Snakes," *IEEE Transactions on Medical Imaging*, *14*(2) (June 1995).

56. Rogowska, Jadwiga, et al. "Applications of Similarity Mapping in Dynamic MRI," *IEEE TRansactions on Medical Imaging*, *14*(3):480–486 (September 1995).

57. Rosenfeld, A., et al. "Scene labeling by relaxation operations," *IEEE Transactions on Systems, Man, and Cybernetics*, *6*:420–433 (1976).

58. Rosenfeld, Ariel and G. Vanderfrug. "Coarse-fine template matching," *IEEE Transactions on Systems, Man, and Cybernetics* (February 1977).

59. Russ, John C. *The Image Processing Handbook*. CRC Press, 1992.

60. Saint-Marc, Philippe, et al. "Adaptive Smoothing: A General Tool for Early Vision," *IEEE Transactions on Pattern Analysis and Machine Intelligence*, *13*(6) (June 1991).

61. Schmidt, Robert A., et al. "Computer-Aided Diagnosis in Mammography." *A Categorical Course in Breast Imaging*, edited by Daniel B. Kopans and Ellen Mendelson. 1995.

62. Simchony, T., et al. "Pyramid Implementation of Optimal-Step Conjugate-Search Algorithms for Some Low-Level Vision Problems," *IEEE Transactions on Systems, Man, and Cybernetics*, *19*(6):1408–1425 (November 1989).

63. Smith, Robert A. "The Epidemiology of Breast Cancer." *A Categorical Course in Breast Imaging*, edited by Daniel B. Kopans and Ellen b. Mendelson. 7–20. 1995.

64. Szeliski, R. and J. Coughlan. "Hierarchical Spline-Based Image Registration," *International Journal of Computer Vision*

65. Szeliski, R. and S. Lavallee. "Matching 3-D Anatomical Surfaces with Non-Rigid Deformations Using Octree-Splines," *International Journal of Computer Vision*, *18*(2):171–186 (May 1996).

66. Szeliski, Richard and Heung-Yeung Shum. "Motion Estimation with Quadtree Splines," *IEEE Transactions on Pattern Analysis and Machine Intelligence*, *18*(12) (December 1996).

67. Terzopoulos, Demetri. "Image analysis using multigrid relaxation methods," *IEEE Transactions on Pattern Analysis and Machine Intelligence*, *8*(2) (March 1986).

68. Thirumalai, Srikanth and Narendra Ahuja. "Parallel Distributed Detection of Feature Trajectories in Multiple Discontinuous Motion Image Sequences," *IEEE Transactions on Neural Networks*, *7*(3):594–603 (May 1996).

69. Toennies, Klaus D. and Daniel Rueckert. "Image segmentation by stochastically relaxing contour fitting." *Proceedings of the SPIE (Medical Imaging 1994: Image Processing)*. 1994.

70. van den Elsen, Petra A., et al. "Medical Image Matching-A Review with Classification," *IEEE Engineering in Medicine and Biology*, 26–38 (March 1993).

71. Verri, A. and T. Poggio. "Motion Field and Optical Flow," *IEEE Transactions on Pattern Analysis and Machine Intelligence*, *11*:490–498 (1989).

72. Vujovic, Nenad and Dragana Brzakovic. "Establishing the Correspondence Between Control Points in Pairs of Mammographic Images," *IEEE Transactions on Image Processing*, *6*(10) (October 1997).

73. Wilson, Terry A. *Perceptual Based Image Fusion with Applications to Hyspectral Image Data*. MS thesis, Air Force Institute of Technology, 1994.

74. Witkin, A., et al. "Signal Matching Through Scale Space," *International Journal of Computer Vision*, *1*:133–144 (1987).

75. Yue, Zhanjun, et al. "Automatic Detection of Rib Borders in Chest Radiographs," *IEEE Transactions on Medical Imaging*, *14*(3):525–536 (September 1995).

76. Zhang, Jun and Gerald G. Hanauer. "The Application of Mean Field Theory to Image Motion Estimation," *IEEE Transactions on Image Processing*, *4*(1):19–33 (January 1995).

77. Zheng, Bin, et al. "Computerized Detection of Masses from Digitized Mammograms: Comparison of Single-Image Segmentation and Bilateral-Image Subtraction," *Acad Radiology*, *2*:1056–1061 (1995).

78. Zhu, Yan and Hong Yan. "Computerized Tumor Boundary Detection Using a Hopfield Neural Network," *IEEE Transactions on Medical Imaging*, *16*(1):55–67 (February 1997).

Vita

Major Kevin A. Lee obtained a bachelor of science degree from the University of Colorado in 1983 and a commission as a second lieutenant in the United States Air Force in 1985. From March 1985 to April 1990 he served as communications control and combat crew communications officer at March AFB, CA. During this period he was awarded a master of science degree in systems management from the University of Southern California. From April 1990 to May 1993 he served as a software engineer and process improvement lead at US Strategic Command, Offutt AFB, NE. From June 1993 to May 1996 he served as director of the Basic Communications-Computer Training course and chief of joint training for the Global Command and Control System at Keesler AFB, MS. From June 1996 to December 1997 he has been pursuing a masters degree in computer systems at the Air Force Institute of Technology, Wright-Patterson AFB, OH. From January 1998 on he may be reached at the College of Aerospace Doctrine Research and Education located at Maxwell AFB, AL.

Permanent address: 113 Buckeye Cir
WPAFB, OH 45433

REPORT DOCUMENTATION PAGE

Form Approved
OMB No. 0704-0188

1. AGENCY USE ONLY *(Leave blank)*	2. REPORT DATE	3. REPORT TYPE AND DATES COVERED
	December 1997	Master's Thesis

4. TITLE AND SUBTITLE

A MAMMOGRAPHIC REGISTRATION METHOD BASED ON OPTICAL FLOW AND MULTIRESOLUTION COMPUTING

5. FUNDING NUMBERS

6. AUTHOR(S)

Kevin A. Lee
Major USAF

7. PERFORMING ORGANIZATION NAME(S) AND ADDRESS(ES)

Air Force Institute of Technology, WPAFB OH 45433-6583

8. PERFORMING ORGANIZATION REPORT NUMBER

AFIT/GE/ENG/97D-14

9. SPONSORING/MONITORING AGENCY NAME(S) AND ADDRESS(ES)

Major Jeff Hoffmeister
AL/CFHV Bldg 248A, 2255 H Street, WPAFB, OH 45433-7022

10. SPONSORING/MONITORING AGENCY REPORT NUMBER

11. SUPPLEMENTARY NOTES

12a. DISTRIBUTION AVAILABILITY STATEMENT

Distribution Unlimited

12b. DISTRIBUTION CODE

13. ABSTRACT *(Maximum 200 words)*

Breast cancer is second only to lung cancer as the most prevalent form of cancer to afflict women—remaining the leading cause of cancer death in women between the ages of 40 and 55. Mammography is a potent weapon in the fight against this lethal disease, due in large part to its widespread availability and low cost. Despite the fact that mammography can detect small lesions as early as two years before they become palpable on physical exam, between 10 and 30 percent of cancerous lesions go undetected during evaluation by the radiologist. One approach to improving detection rates involves comparing mammograms of the same breast from successive years. Since most forms of breast cancer develop slowly, multiple-view techniques might be able to detect subtle changes indicative of cancerous growth. This thesis proposes a computer-aided system designed to bring two images into correspondence, or alignment, so that they can be compared and evaluated for possible abnormalities. The system estimates a mapping between two images by calculating the optical flow, or apparent intensity change, between a source and target mammogram. The efficiency of the proposed registration system is enhanced by utilizing a multiresolution approach whereby images are compared at more than one scale. In contrast to other registration attempts which match sets of morphological features, this system does not require the identification of any control points at all. This advantage permits the system to perform well even when the two images differ significantly from one another. Preliminary results suggest the potential usefulness of this system as part of a clinical computer-aided detection (CADx) system.

14. SUBJECT TERMS

Breast Cancer, Genetic Algorithms, Image Registration, Medical Imaging, Multiresolution Computing, Neural Networks, Optical Flow, Pattern Recognition

15. NUMBER OF PAGES

106

16. PRICE CODE

17. SECURITY CLASSIFICATION OF REPORT	18. SECURITY CLASSIFICATION OF THIS PAGE	19. SECURITY CLASSIFICATION OF ABSTRACT	20. LIMITATION OF ABSTRACT
UNCLASSIFIED	UNCLASSIFIED	UNCLASSIFIED	UL